BASIC REQUIREMENTS FOR MANUSCRIPTS

This Journal represents an effort by the Society to achieve high standards of quality with the greatest possible speed. To this end, the editorial burden on authors of technical papers has been kept to a minimum. Papers that require extensive editorial work will be returned to the author for revision before publication.

Original papers and discussions of current papers should be addressed to the Manager of Technical Publications, ASCE. The final decision on whether discussion should reach the Society is governed by agreement with each paper's author. Those planning to submit material should study the review and publication procedures by complying with the following basic requirements:

1. Titles should have a length not exceeding 50 characters and spaces.

2. A 50-word summary should accompany the paper.

3. The manuscript (an original copy and two copies) should be double-spaced on one side of 8½-in. by 11-in. paper. Papers that were originally prepared for oral presentation must be retyped into the above format before submitting them.

4. The author's full name, Society membership grade, and author's professional affiliation (present employment) should appear on the first page of the paper.

5. Mathematics are sometimes the most troublesome part of a paper. Authors should realize that it is necessary that capital letters be drawn in black ink, that subscripts and superscripts be clearly shown, that Greek letters be identified in the margin, and that special symbols (such as those for summation, integration, and partial derivatives) be explained. Authors should also bear in mind that proportions dictated by aesthetic considerations must often be altered to meet publication requirements. Maximum use should be made of the built-in characters of standard typewriters (avoiding the use of italics, boldface, and Greek characters, wherever possible, in favor of the standard lettering practice) and fractions in the text should usually be written with a solidus (/) and negative exponents rather than with a fraction bar. Where a long or complicated fraction must be displayed, it should be typed on a separate line and centered. Only the briefest mathematical derivations should be included in papers submitted for publication. Authors should recognize that every character and every line of mathematics in a paper must be set by hand, and complex mathematical derivations will greatly increase the costs of publication. Two copies of typed equations may be used but they will be proportionately smaller than the printed version.

6. Tables should be typed (ribbon copies) on one side of 8½-in. by 11-in. paper within a 6½-in. by 10½-in. invisible frame. Small tables should be grouped within this frame. Spacing, references, and explanations should be adequate to make each table self-explanatory.

7. Illustrations should be drawn in black ink on one side of 8½-in. by 11-in. paper within a 6½-in. by 10½-in. invisible frame that is ruled lightly in blue. All lettering should also be included within this frame. Because illustrations will be reduced to 60% of the original size, the capital letters should be at least ⅛ in. high. Consideration should be given to the clarity of the illustration after it has been reduced to the size it will appear in the publication. Explanations and descriptions should be made within the illustration rather than in the text. Photographs should be submitted as glossy prints in a size that will not require more than 50% reduction.

8. Papers should usually be limited to about 12,000 words in length and should rarely be longer than 18,000 words. An illustration approximately equivalent to a full page of typed text, or a table, or illustration is the equivalent of 250 words.

Further information concerning the preparation of technical papers is contained in "Publication Procedure for Technical Papers" (Proc. Paper 1901), which can be obtained from the Society.

Reprints from this Journal may be made on condition that the full title of the paper, name of author, page, and year of publication (or paper number), and date of publication by the Society are given. The Society is not responsible for any statement made or opinion expressed in its publications.

This Journal is published quarterly by the American Society of Civil Engineers. Publication office is at 2500 South State Street, Ann Arbor, Michigan. Editorial and General Offices are at 33 West 39th Street, New York 18, New York. $10.00 of a member's dues is assigned as a subscription to this Journal. Second-class mail privileges are authorized at Ann Arbor, Michigan.

Journal of the
ENGINEERING MECHANICS DIVISION
Proceedings of the American Society of Civil Engineers

ENGINEERING MECHANICS DIVISION

Executive Committee

Clayton O. Donhrenwend, Chairman
Harry N. Hill, Vice Chairman
John S. McNown
George W. Housner
Daniel C. Drucker
Merit P. White, Secretary

West Coast Committee

Egor P. Popov, Chairman
John F. P. Brahtz
Boris Bresler
George W. Housner
Harry A. Williams

CONTENTS

July, 1956

Papers

	Number
Creep Relaxation of Plexiglas IIA for Simple Stresses by Joseph Marin and J. E. Griffith	1029
Suppression of the Fluid-Induced Vibration of Circular Cylinders by Peter Price	1030
Some Observations on Open Channel Flow at Small Reynolds Numbers by Lorenz G. Straub, Edward Silberman and Herbert C. Nelson	1031
Lateral Bracing Forces on Beams and Columns by William Zuk	1032
Discussion	1033

DIVISION ACTIVITES

Newsletter 1956-16

Copyright 1956 by the American Society of Civil Engineers.

Paper 1029 EM 3

Journal of the
ENGINEERING MECHANICS DIVISION
Proceedings of the American Society of Civil Engineers

CREEP RELAXATION OF PLEXIGLAS IIA FOR SIMPLE STRESSES

Joseph Marin[1] and J. E. Griffith[2]

SUMMARY

Many investigations have been conducted to determine the creep strain-stress-time relations for materials subjected to simple tension and constant stress. However, in a number of applications where creep occurs the stresses do not remain constant and the so-called condition of stress-relaxation occurs. To the authors' knowledge, the only stress-relaxation creep studies conducted in the past have been for the case of simple tension. In this paper, experimental creep-relaxation results for a plastic designated as Plexiglas IIA are obtained for simple tension, simple compression, and pure bending. Based on constant-stress tension and compression creep data and creep-stress-time relations obtained from such constant stress data, creep relaxation relations for simple tension, compression and bending are derived. These creep relations are then compared with the actual creep relaxation relations obtained in tension, compression and bending. The agreement between experimental and derived relations is considered to be satisfactory.

INTRODUCTION

In evaluating the suitability of a plastic for certain products and structural parts, the creep properties may sometimes become an important consideration. That is, for certain stress values, the creep deformations may become so large that the member becomes unserviceable or they may approach such magnitudes as to produce fracture and failure of the material. To avoid these possibilities, the designer must select a working strain of such magnitude as to prevent excessive deformation or fracture. The selection of an appropriate design stress requires a consideration of both the creep properties and mechanics of creep. For example, for a member subjected to bending and creep, the designer would like to have a method of determining the creep deflection, using creep constants obtained from the usual simple tension creep test.

Note: Discussion open until December 1, 1956. Paper 1029 is part of the copyrighted Journal of the Engineering Mechanics Division of the American Society of Civil Engineers, Vol. 82, No. EM 3, July, 1956.

1. Prof. and Head, Dept. of Eng. Mechanics, Pennsylvania State Univ., University Park, Pa.
2. Asst. Prof., Dept. of Civ. Eng., Yale Univ., New Haven, Conn.

In some applications the stresses do not remain fixed but decrease with time. That is, a condition of stress relaxation occurs. In this investigation, the condition of stress relaxation is considered for simple tension, compression and bending. Methods are also developed for predicting the creep relaxation relations for these simple stresses from the usual constant tension creep stress relations.

Material Tested

The tests reported herein were made on a plastic designated as plexiglas IIA and manufactured by the Rohm and Haas Company. The average mechanical properties of this material are given in Table I. All the creep tests were conducted under conditions of constant relative humidity of 50% (± 2%) and constant temperature of 78°F. (± 2°). The initial loads in all cases were applied at such a rate as to prevent any time-dependent strain taking place before the total load was applied.

Constant Tension and Compression Stress Creep Test Results

The creep testing equipment for the tension, constant stress creep tests is illustrated in Fig. 1(a). Fig. 1(b) shows the compression fixture used for obtaining compression creep with the tension creep testing machine. The dimensions of the specimen used for the creep tests are shown in Fig. 2. The creep strains in both the tension and compression tests were measured by SR-4 electric strain gages, Type A-3, having a 3/4 in. gage length. These strain gages had a sensitivity of 5×10^{-6} in. per in. and a range of 0.02 in. per in.

Table I

Mechanical Properties of Plexiglas IIA

Average Mechanical Properties of Plexiglas IIA	
Ultimate Tensile Strength	10,500 psi
Ultimate Compressive Strength	17,600 psi
Ultimate Shear Strength	8,680 psi
Initial Tangent Modulus of Elasticity	530,000 psi
Secant Modulus of Elasticity (0-2500 psi offset)	477,000 psi
Rockwell Number	94 M
Impact Strength	3.1 ft-lbs 1/2 in. x 1/2 in.
Flexural Strength	17,000 psi
Elongation at Rupture in Tension	4.8%

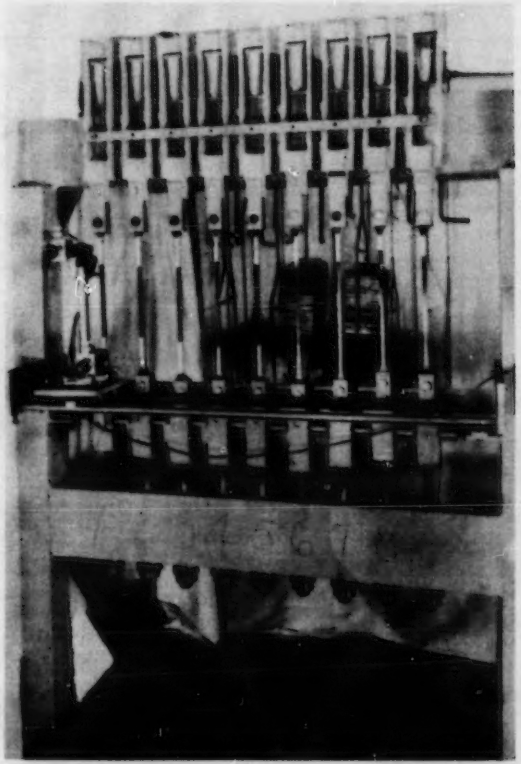

(a) TENSION CREEP MACHINE

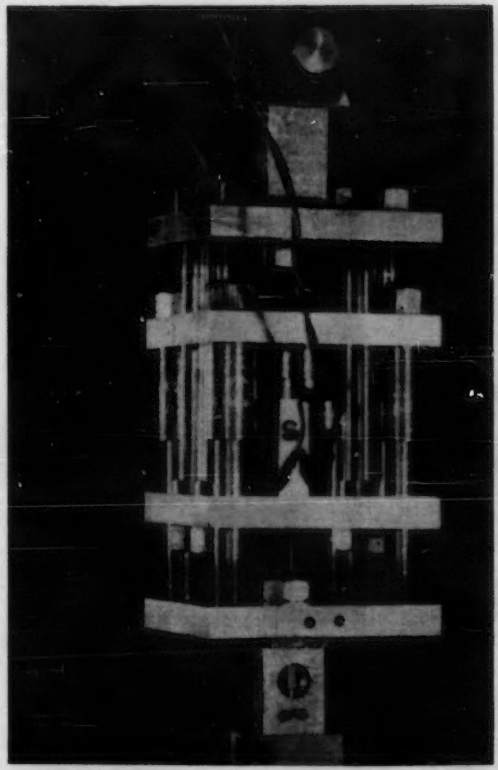

(b) COMPRESSION CREEP UNIT.

FIGURE 1.

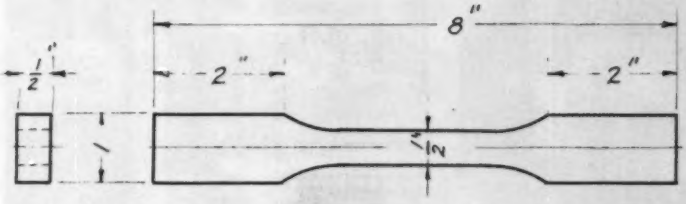

scale : half size

(a) TENSION & BENDING SPECIMEN

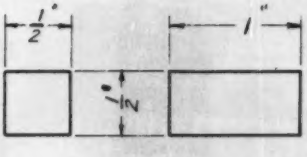

(b) COMPRESSION SPECIMEN

FIG. 2 DIMENSIONS OF SPECIMENS

Table II

Material Creep Constants in Tension and Compression

Note: The units for k_1, k_2 and k_3 are in $(in^2/lb)^n$; while q is in (1/hr) if t is measured in hours. The constant n in Table II is dimensionless.

Tension Constants	Compression Constants
$k_1 = 0$	$k_1 = 0$
$k_2 = 6.07 \times 10^{-8}$	$k_2 = 4.04 \times 10^{-8}$
$k_3 = 9.78 \times 10^{-11}$	$k_3 = 6.27 \times 10^{-11}$
$q = 0.0658$	$q = 0.0658$
$E = 4.8 \times 10^5$ psi	$E = 5.3 \times 10^5$ psi
$n = 1.32$	$n = 1.36$

Two gages were bonded on each specimen, one on each side to eliminate the errors due to eccentricity. End effects were reduced in the compression test by lubricating the specimen ends.

The constant stress tension and compression creep-time results are shown in Figs. 3 and 4 for various stress values as indicated. The time of 250 hours was selected because of time limitations.

Interpretation of Constant Stress Creep Results

To obtain empirical equations which express the relation between the stress, creep strain and time, various methods of interpretation have been used, (2). A relation which has been found to give a good representation of tension creep data is one similar to that proposed by Pao and Marin (3). By this relation, the strain in terms of the stress is made up of four parts - that is

$$\varepsilon = \varepsilon_e + \varepsilon'_p + \varepsilon''_p + \varepsilon'''_p \qquad (1)$$

where

ε_e = the elastic strain

ε'_p = the plastic strain

ε''_p = the transient creep strain

ε'''_p = the "minimum rate" or steady state creep strain

Separating the strains obtained in creep tests according to the components indicated in eq. (1), it is found that each of the components may be approximately expressed by the following relations:

$$\varepsilon_e = \frac{\sigma}{E}, \quad \varepsilon'_p = k_1 \sigma^n, \quad \varepsilon''_p = k_2 \sigma^n (1 - e^{-qt}), \quad \varepsilon'''_p = k_3 \sigma^n t \qquad (2)$$

where

σ = the stress

t = the time

e = base of natural logarithms

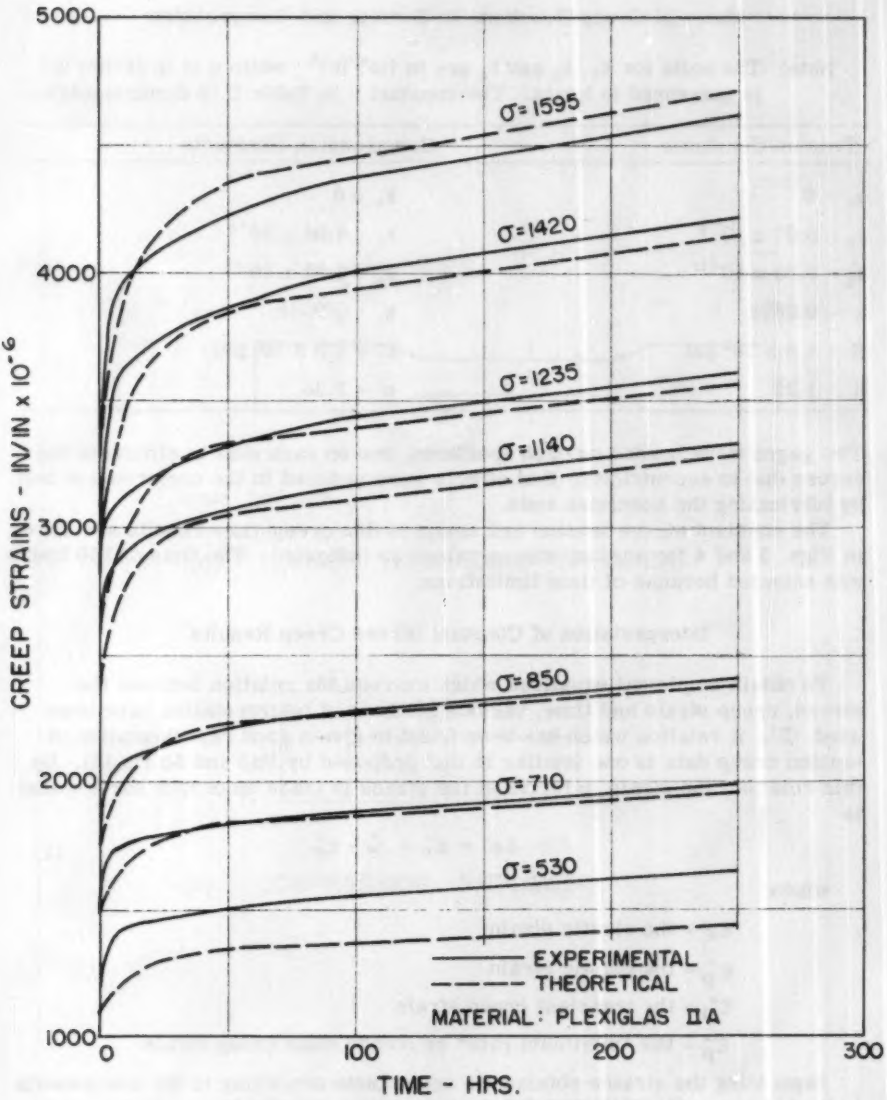

FIG. 3 TENSION CREEP CURVES.

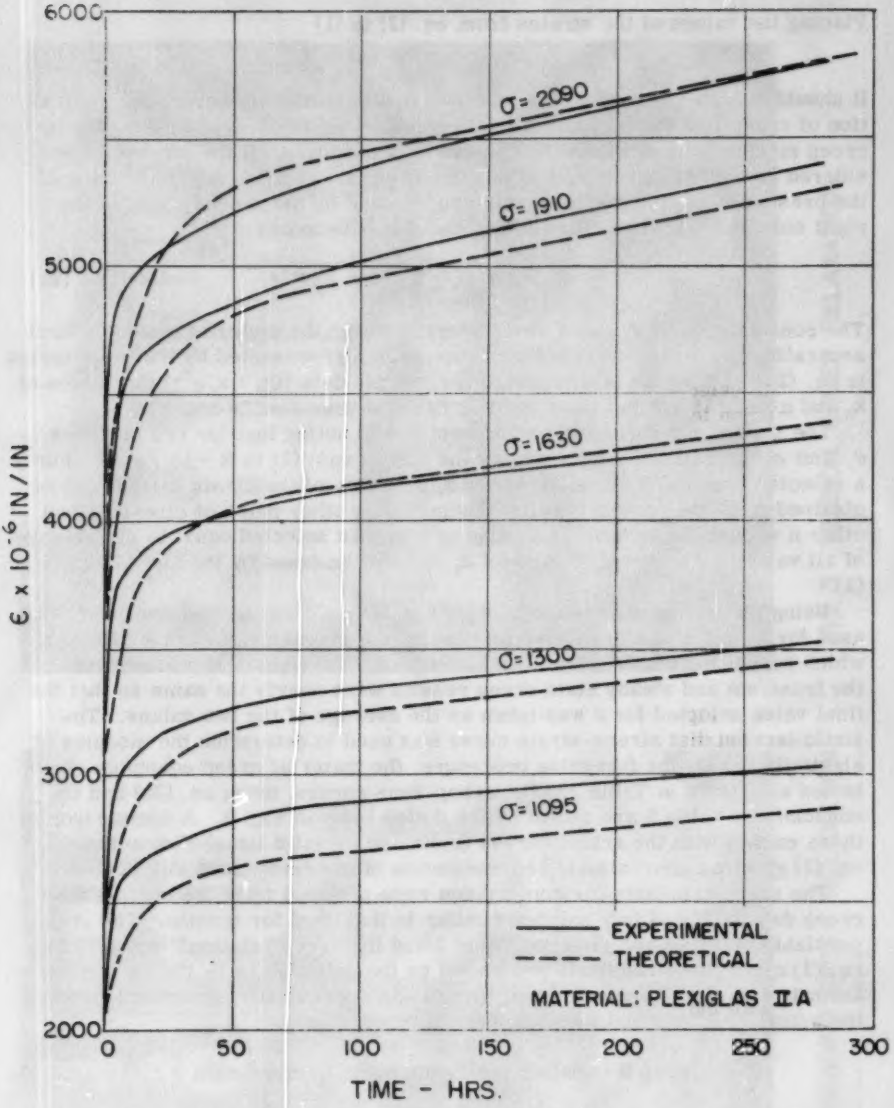

FIG. 4 COMPRESSION CREEP CURVES.

E, k_1, k_2, k_3, q and n = experimental constants

Placing the values of the strains from eq. (2) in (1)

$$\varepsilon = \frac{\sigma}{E} + k_1\sigma^n + k_2\sigma^n(1-e^{-qt}) + k_3\sigma^n t \qquad (3)$$

It should be noted that eq. (3) is an empirical relation. However, the separation of creep into the component parts represented in eq. (3) is supported by creep mechanisms proposed by Orowan (5) and others. If the stresses considered are in the linear part of the stress-strain relation (as in the case of the present tests) the plastic strain represented by the second term on the right side of eq. (3) is negligible and the strain becomes

$$\varepsilon = \frac{\sigma}{E} + k_2\sigma^n(1-e^{-qt}) + k_3\sigma^n t \qquad (3a)$$

The constants k_2, q, k_3 and n were determined for the material tested by first separating the strain into the three components represented by the three terms in eq. (3a). Using the steady state creep strain data ($\varepsilon_p'' \equiv k_3\sigma^n t$) the values of k_3 and n were found that gave the best fit for a time t = 250 hours.

The method for finding k_3 and n consisted in noting that for two stresses σ_1 and σ_2 the ratio of the strains by the last of eqs. (2) is $R = (\sigma_1/\sigma_2)^n$. For a selected time t and stresses σ_1 and σ_2 the value of the strain ratio R can be obtained from the plotted results. By selecting other pairs of stress values other n values can be found. A value of n is then selected equal to the average of all values. The average value of k_3 can now be found by the last of eqs. (2).

Using the transient creep data, $e_p'' = k_2\sigma^n(1 - e^{-qt})$ a method similar to that used for k_3 and n was developed for finding the average values of k_2, n and q which best fitted the data for all the stresses. The values of n found from the transient and steady state creep results were nearly the same so that the final value selected for n was taken as the average of the two values. The static tension test stress-strain curve was used to determine the modulus of elasticity E. By the foregoing procedure, the material creep constants obtained are listed in Table 2. The creep-time curves, using eq. (3a) and the constants of Table 2 are shown by the dotted lines in Fig. 3. A comparison of these curves with the actual curves (indicated by solid lines) shows that eq. (3) gives an approximate representation of the creep-time relation.

The creep constants for comparison were obtained from the compression creep data in Fig. 4 in a manner similar to that used for tension. The creep constants obtained are given on Table 2 and the creep relations expressed by eq. (3) using these constants are shown by the dotted lines in Fig. 4. An examination of Fig. 4 indicates that there is an approximate agreement between the actual relations and those expressed by eq. (3).

Creep Relaxation for Tension and Compression

To determine the accuracy of the creep-stress time (eq. 3) in predicting the creep relaxation relation for tension and compression, a number of creep relaxation tests were conducted for a series of initial stress values in both tension and compression. The equipment used for these experiments is shown in Fig. 5. The tension and compression specimens had the same dimensions as those used for the constant stress creep tests. In the relaxation creep tests, the specimens were loaded rapidly to a predetermined strain

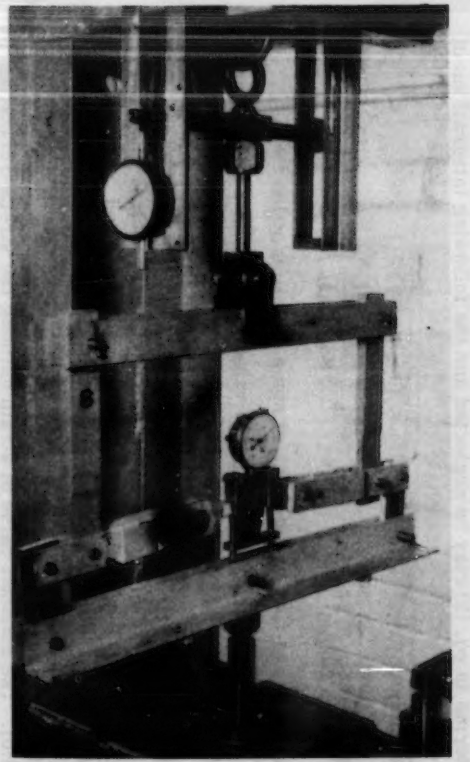

FIG. 9 BENDING CREEP RELAXATION UNIT.

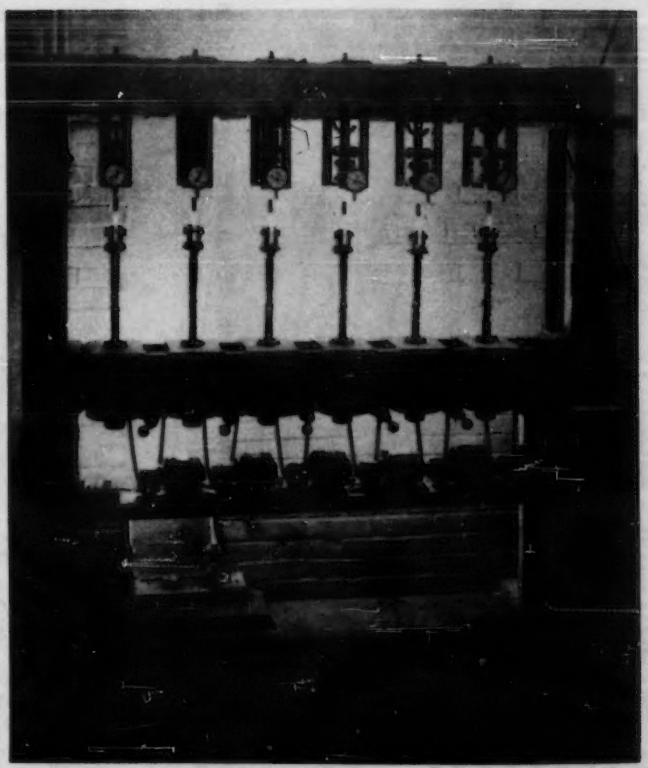

FIG. 5 TENSION CREEP RELAXATION.

corresponding to a selected initial stress value. The loads were applied at a uniform load rate and the maximum loading time for the largest strain was 2 minutes. This strain was then maintained constant by unloading the specimen gradually. The operation of the equipment is described in reference (4). The strains were measured using SR = 4 gages with 3/4 in. gage lengths.

The stress-time relaxation relations using various initial stress values are shown in Figs. 6 and 7 for tension and compression.

From eq. (3a) the creep stress-time relaxation relation for simple tension or compression may be determined analytically by expressing the condition of constant strain. To do this, the change in strain with change in time and stress will be expressed. That is,

$$d\varepsilon = \left(\frac{\partial \varepsilon}{\partial \sigma}\right) d\sigma + \left(\frac{\partial \varepsilon}{\partial t}\right) dt \tag{4}$$

For the condition of relaxation considered herein, $d\varepsilon = 0$. Placing $d\varepsilon = 0$ and the value of ε from eq. (3a) in eq. (4),

$$d\sigma\left[\frac{1}{E} + n\sigma^{n-1}\left\{k_2(1-e^{-q_1 t}) + k_3 t\right\}\right] + \sigma^n\left[k_2 q_1 e^{-q_1 t} + k_3\right] dt = 0 \tag{5}$$

The solution of eq. (5) for the stress-time relation is not simple. For all values of t a solution using series could be used. For short and long times, certain terms in eq. (5) may be neglected and the following integrations of eq. (5) result:

For short times: $$\sigma^{1-n} = \sigma_0^{1-n} - E(1-n)(k_2 q_1 + k_3)t \tag{6}$$

For long times: $$\log_e \frac{\sigma}{\sigma_A} = \frac{-k_3}{n} \log_e \left(\frac{k_2 + k_3 t}{k_2 + k_3 t_A}\right) \tag{7}$$

where $\sigma = \sigma_0$ at $t = 0$ and $\sigma = \sigma_A$ at some long time value $t = t_A$.

Another method of solving eq. (5) for all values of time is to use a graphical procedure. This procedure will be explained by referring to Fig. 8. Using eq. (3a), a family of tensile creep-time curves are first plotted as shown in Fig. 8a for various stress values. After subtracting the plastic strains, the creep strain-time curves are obtained as shown by the dotted lines in Fig. 8(a). With these creep strain-time relations and a selected time t, a series of values of stress and creep strains can be obtained. These may then be used to plot a creep strain-stress curve as shown in Fig. 8(b). For other values of time, other creep strain-stress relations can be plotted as indicated in Fig. 8(b). The constant value of strain defining the stress-relaxation condition is determined from Fig. 8(b) by the point on the t = 0 curve corresponding to $\sigma = \sigma_0$ (the initial stress value.) The intersection of the constant strain line with other curves in Fig. 8(b) defines stress values corresponding to various times. These stress and time values may then be used to obtain the

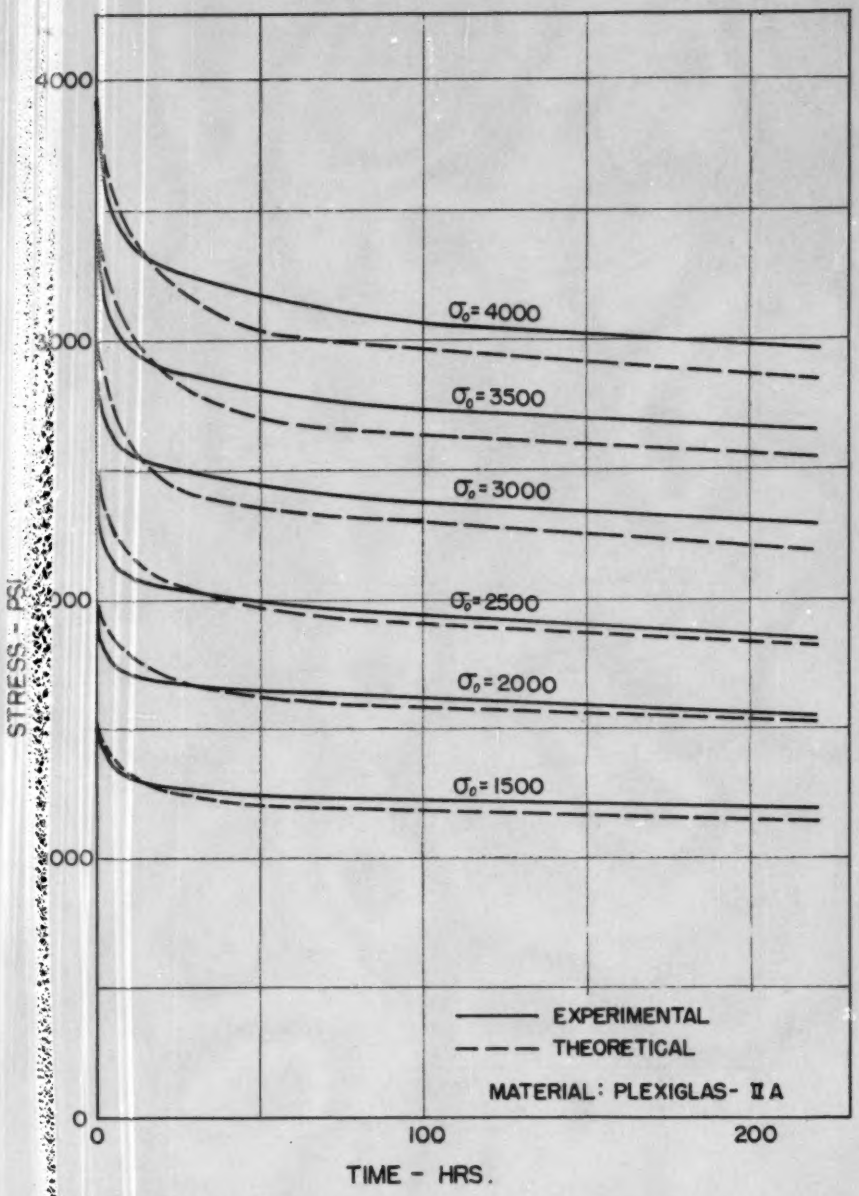

FIG. 6 TENSION RELAXATION CURVES

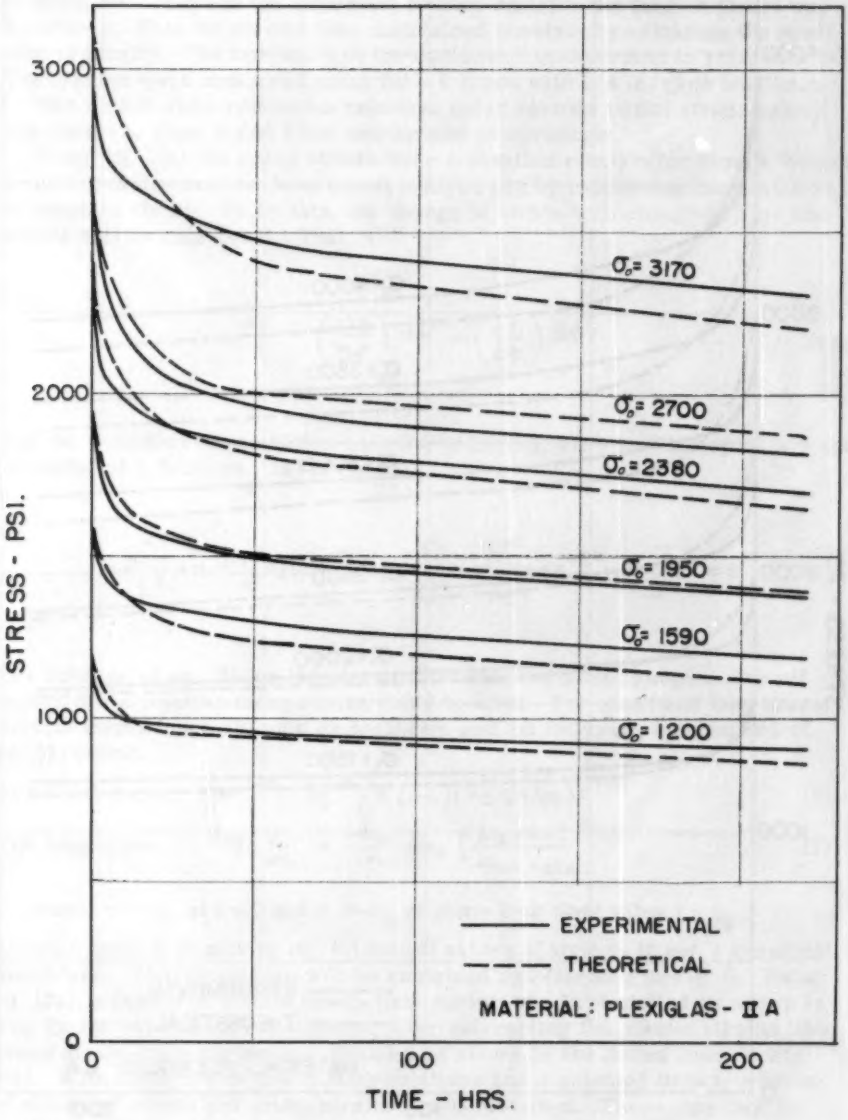

FIG. 7 COMPRESSION RELAXATION CURVES

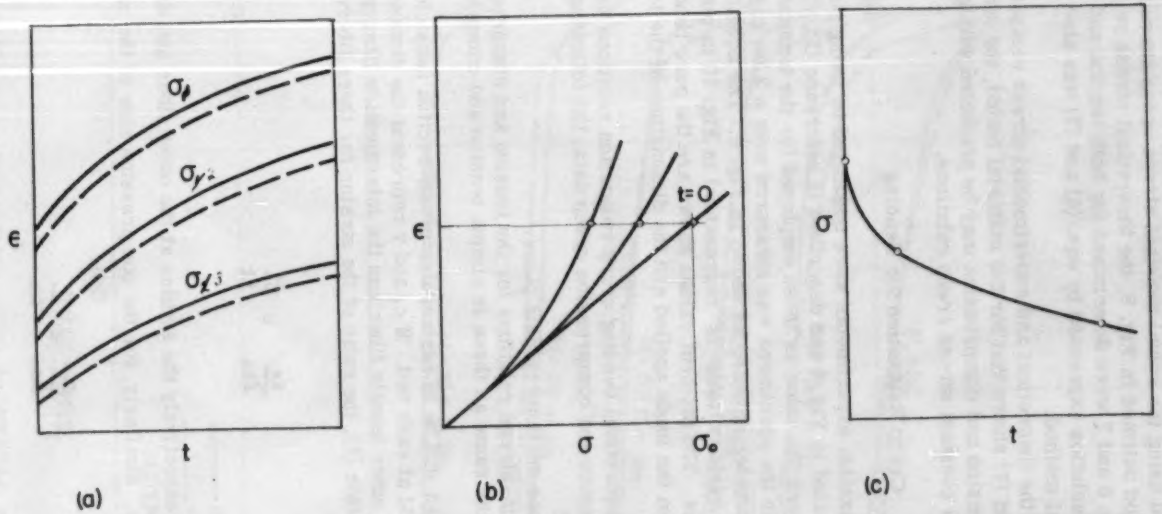

FIG. 8 GRAPHICAL SOLUTION OF STRESS-TIME RELATION FOR UNIAXIAL STRESS.

stress relaxation curve shown in Fig. 8(c). It should be noted that the foregoing procedure for finding the stress-relaxation relation need not use the approximate creep-time relation expressed by eq. (3), since the same procedure may be applied using the actual constant stress creep curves.

Based on the method outlined in Fig. 8, the theoretical stress relaxation curves shown in Figs. 6 and 7 were determined for both tension and compression. The analytical solution expressed by eqs. (6) and (7) was also used as a check on the graphical method.

An examination of the theoretical and experimental stress relaxation curves in Figs. (6) and (7) shows that for the material tested, the stress relaxation relation in tension and compression may be predicted with good accuracy from the usual constant stress creep relations.

Creep Relaxation for Bending

Creep bending relaxation experiments were conducted by using pure bending fixtures as illustrated in Fig. 9 and described in reference (1). The bending specimens used were the same as those employed for the tension tests. The creep deflection in the specimens was measured over a 2 in. gage length by means of a deflectometer mounted as shown in Fig. 9. The actual relaxation-time relation for various loads is represented in Fig. 10 in terms of moment-time relations. The moment values shown are the pure bending moments determined from the loads applied and the dimensions of the loading fixture.

To determine the theoretical bending creep relaxation relations based on the constant stress tension and compression creep data, the following assumptions were made:

(1) Transverse plane sections remain plane.

(2) The creep strain-stress relations for the tension and compression fibers in bending are the same as those in simple tension and compression creep.

The member considered will be of rectangular cross-section subjected to a pure bending moment M at each end. If c_t and y represent the distances from the neutral axis to the outer tensile fiber and the intermediate fiber respectively, then by assumption (1), the ratio of the strains for these fibers is

$$\frac{\varepsilon_t}{\varepsilon_{t_0}} = \frac{y}{c_t} \qquad \text{(a)}$$

where ε_{t_0} and ε_t are respectively the strains at the outer fiber and distance y from the neutral axis. Similarly, for the compression side of the member

$$\frac{\varepsilon_c}{\varepsilon_{c_0}} = \frac{y}{c_c} \qquad \text{(b)}$$

For equilibrium of internal stresses

$$\Sigma F = 0, \quad \Sigma M = M \qquad \text{(c)}$$

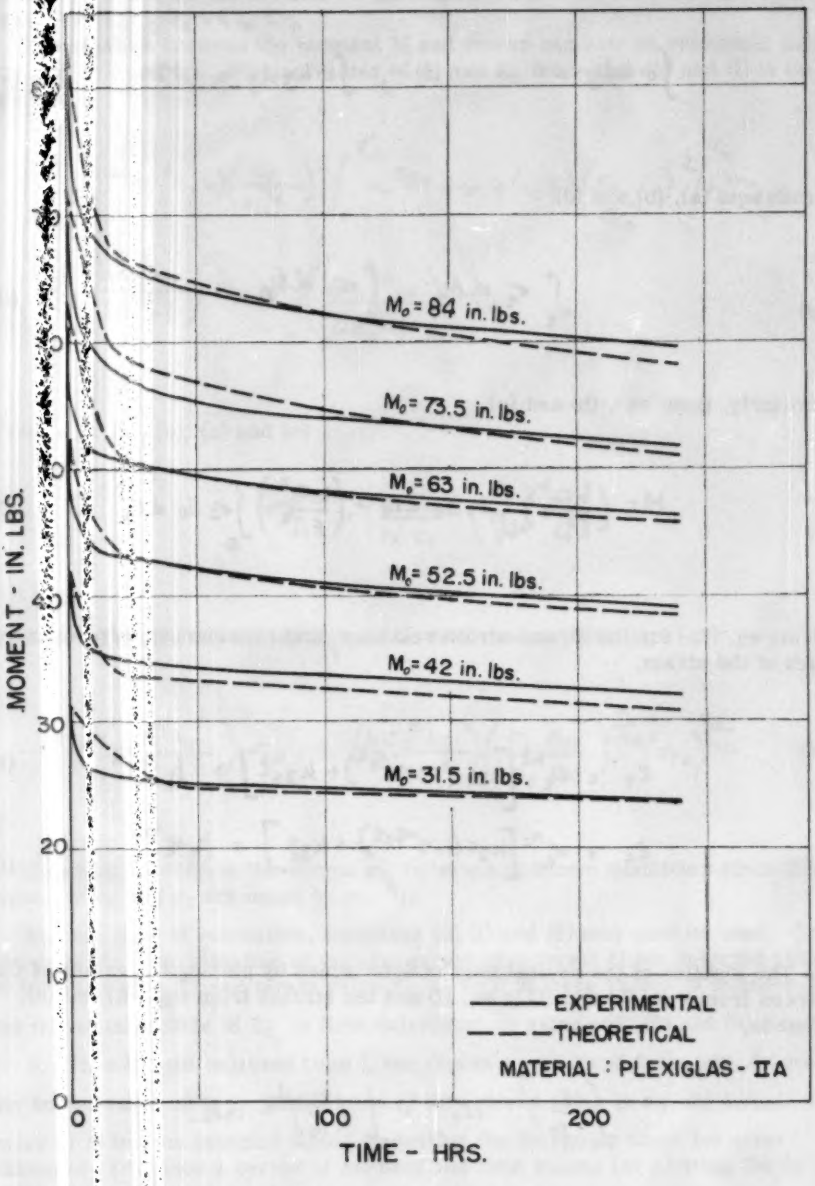

FIG. 10 BENDING RELAXATION CURVES.

For a rectangular cross section, equation (c) may be written

$$\int \sigma b\,dy = 0 \text{ ---- (d)} \quad , \quad \int \sigma b y\,dy = M \tag{e}$$

From eqs. (a), (b) and (d)

$$\int_t \sigma_t\, d\varepsilon_b = \int_c \sigma_c\, d\varepsilon_b \tag{f}$$

Similarly, from eqs. (b) and (c)

$$M = \left(\frac{b c_t^2}{\varepsilon_{to}^2}\right)\int_t \sigma_t\, \varepsilon_t\, d\varepsilon_t + \left(\frac{b c_c^2}{\varepsilon_{co}^2}\right)\int_c \sigma_c\, \varepsilon_c\, d\varepsilon_c \tag{g}$$

Using eq. (3a) for the stress-strain relations, and considering only the creep part of the strain,

$$\varepsilon_t = \sigma_t^{n_t}\left[k_{2t}\left(1-e^{-q_t t}\right) + k_{3t}t\right] = p_t\,\sigma_t^{n_t} \tag{h}$$

$$\varepsilon_c = \sigma_c^{n_c}\left[k_{2c}\left(1-e^{-q_c t}\right) + k_{3c}t\right] = p_c\,\sigma_c^{n_c} \tag{i}$$

The location of the neutral axis is determined by placing the values of the stress from eqs. (h) and (i) in eq. (f) and the strains from eqs. (a) and (b). That is,

$$\int_t \left(\frac{\varepsilon_t}{p_t}\right)^{\frac{1}{n_t}} d\varepsilon_t = \int_c \left(\frac{\varepsilon_c}{p_c}\right)^{\frac{1}{n_c}} d\varepsilon_c$$

or

$$\left(\varepsilon_{to}\right)^{\frac{1}{n_t}+1}\left(\frac{1}{p_t}\right)^{\frac{1}{n_t}}\left(\frac{n_t}{1+n_t}\right) = \left(\varepsilon_{co}\right)^{\frac{1}{n_c}+1}\left(\frac{1}{p_c}\right)^{\frac{1}{n_c}}\left(\frac{n_c}{1+n_c}\right) \tag{j}$$

Equation (j) defines the location of the neutral axis since with known, by assumption (1), $c_t/c_o = \varepsilon_{t_o}/\varepsilon_{c_o}$.

The relation between the moment M and stress can now be evaluated, using eqs. (h), (i), and (g). Placing values of ε_t and ε_c from eqs. (h) and (i) in eq. (g),

$$M = (n_t b)\left(\frac{c_t}{\sigma_{t_o}^{n_t}}\right)^2 \int_0^{\sigma_{t_o}} \sigma_t^{2n_t}\, d\sigma_t + (n_c b)\left(\frac{c_c}{\sigma_{c_o}^{n_c}}\right)^2 \int_0^{\sigma_{c_o}} \sigma_c^{2n_c}\, d\sigma_c$$

$$M = \left(\frac{b c_t^2 n_t}{2n_t+1}\right)\sigma_{t_o} + \left(\frac{b c_c^2 n_c}{2n_c+1}\right)\sigma_{c_o} \qquad (k)$$

From eqs. (a), (b), (h) and (c)

$$\sigma_{c_o}^{n_c} = \left(\frac{p_t c_c}{p_c c_t}\right)\left(\sigma_{t_o}^{n_t}\right) \qquad (l)$$

By eqs. (k) and (l) the stress σ_{t_o} can be determined. That is,

$$M = \left(\frac{b c_t^2 n_t}{2n_t+1}\right)\sigma_{t_o} + \left(\frac{b c_c^2 n_c}{2n_c+1}\right)\left(\frac{p_t c_c}{b_c c_t}\right)^{\frac{1}{n_c}}\left(\sigma_{t_o}\right)^{\frac{n_t}{n_c}} \qquad (8)$$

Equation (8) defines the stress σ_{t_o} in terms of known quantities since the values of c_c and c_t are found by eq. (j).

For the case of relaxation, equations (h), (i) and (8) may also be used. This requires the determination of various values of moment M for selected values of time t to give a fixed strain value ε_{t_o}. To find these values of moment M, the initial magnitude of ε_{t_o} is first calculated by using eqs. (8) and (h) for $t = 0$. Then for the selected time t, the stress σ_{t_o} is found from eqs. (h) for the known value of ε_{t_o}. Substitution of this stress value in eq. (8) defines the value of M for the selected time. Repeating the foregoing steps for other values of t provides a series of moment and time values for plotting the M-t relaxation relation.

A graphical procedure for finding the relaxation moment-time relation may also be used as illustrated in Fig. 11. The solid lines in Figs. 11(a) and (b) represent the creep strain-time relations for both tension and compression. The dotted lines in Fig. 11(a) and (b) are the creep strain-time relations with the initial strains subtracted. Using the dotted curves in Figs.

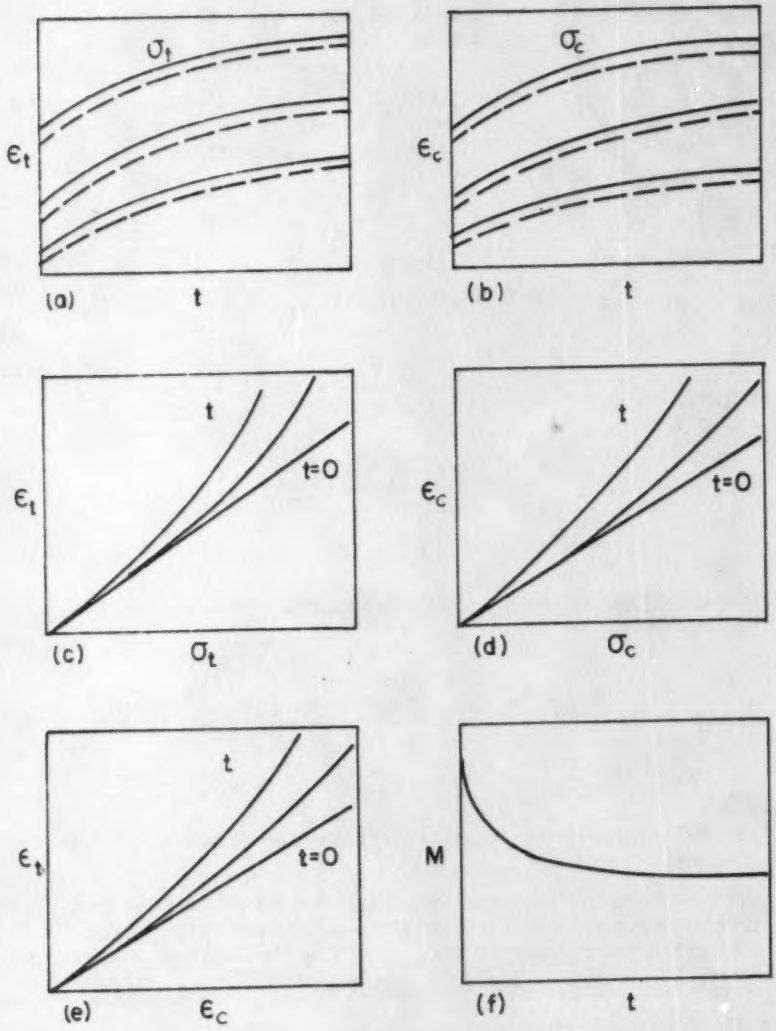

FIG. 11 GRAPHICAL SOLUTION FOR MOMENT-TIME RELATION IN BENDING.

1. (c) and (b), and selecting values of time t, curves relating the strain and stress are determined as illustrated in Figs. 11 (c) and (d). The position of the neutral axis is next determined graphically by using Figs. 11 (c) and (d) together with eq. (f). That is, from Figs. 11 (c) and (d) and a selected time t, the value of ε_o corresponding to ε_t is found by applying the condition expressed in eq. (f), namely, that the area of stress-strain diagrams in Figs. 11 (c) and 11 (d) must be equal for a selected time value. By this means, the strain relations of Fig. 11 (e) are found. The moment values for selected times can be obtained by noting that in eq. (g) the integrals represent moments under the stress-strain diagrams about the stress axis. These moments may be calculated by using Figs. 11 (c) and (d). The values of ε_{t_o} and ε_{c_o} in eq. (g) are found from Fig. 11 (e). Calculation of the moment M can then be made using eq. (g) for the particular time selected. For other values of time, the foregoing procedure may be repeated and in this way, the moment-time relaxation relation shown in Fig. 11 (f) is found.

The method outlined above was applied using the creep strain-time relations for the material tested. The resulting moment-time relaxation relations are indicated by the dotted lines in Fig. 10. A comparison of the actual and the theoretically predicted relaxation curves in Fig. 10 shows that they are in good agreement.

CONCLUSION

This paper develops theories for predicting creep relaxation relations for tension, compression and bending based on constant stress tension and compression creep relations. Creep relaxation experiments in tension, compression and bending were made on a Plexiglas IIA. The tests show that for the material tested, there is good agreement between theoretical predictions and the actual behavior.

ACKNOWLEDGMENTS

The authors appreciate the financial assistance provided by the National Science Foundation in making possible this investigation. The advice given in the course of this study by Dr. L. W. Hu, Assistant Professor of Engineering Research, is also gratefully acknowledged. The study herein reported represents a part of a Ph.D. thesis by John Griffith conducted under the supervision of Joseph Marin.

REFERENCES

1. Marin, Joseph; Pao, Yoh-Han and Cuff, George; "Creep Properties of Lucite and Plexiglas for Tension, Compression, Bending and Torsion," Trans. ASME, Vol. 73, No. 5, July 1951, p. 705.
2. Marin, Joseph, Engineering Materials, Prentice-Hall Book Company, 1952.
3. Pao, Yoh-Han and Marin, Joseph, "An Analytical Theory of the Creep Deformation of Materials," Journal of Applied Mechanics, Trans. ASME. Vol. [illegible] 1953, pp. 245-252.

4. Marin, Joseph and Pao, Yoh-Han, "Creep Relaxation Relations for Styrene and Aerylic Plastics," Proc. ASTM, Vol. 51, 1951.

5. Orowan, E., "Creep in Metallic and Non-Metallic Materials," Proc. First U.S. National Congress of Applied Mechanics, 1951.

Paper 1030 EM 3

Journal of the
ENGINEERING MECHANICS DIVISION
Proceedings of the American Society of Civil Engineers

SUPPRESSION OF THE FLUID-INDUCED VIBRATION OF CIRCULAR CYLINDERS[1]

Peter Price[2]
(Proc. Paper 1030)

SYNOPSIS

An investigation of the vibration of circular cylinders in fluid streams has been made in an effort to evolve a means of suppressing the dangerous, wind induced oscillation of tall steel smokestacks.

Exploratory vibration tests of plain and modified cylinders were made over a wide range of cylinder flexibility at subcritical Reynolds numbers in a water channel. These tests established that the enclosure of a cylinder within a concentric perforated shroud was the most effective vibration suppressor of the profile modifications investigated. Wind tunnel tests proved the shroud to be an effective vibration suppressor at transitional and supercritical Reynolds numbers.

The drag coefficient of the shrouded cylinder was found to be substantially immune to Reynolds number effects in the range explored and the value for a typical configuration was approximately 0.6.

SYMBOLS

V	Velocity (fps)
d	Cylinder diameter (ft)
I	Moment of inertia about axis of oscillation (in-lb-sec^2)
k	Torsional stiffness (in-lb/radian)
n	Frequency of vibration or of vortex discharge (cps)
S	Strouhal number (nd/V)
$\overline{f}$	Natural frequency of vibration (cps)
B	Double (tip) amplitude of vibration, water channel model (diameters)
Y_2	Double (tip) amplitude of vibration, wind tunnel model (diameters)

Note: Discussion open until December 1, 1956. Paper 1030 is part of the copyrighted Journal of the Engineering Mechanics Division of the American Society of Civil Engineers, Vol. 82, No. EM 3, July, 1956.

1. Based on the thesis submitted by Robert W. Thompson and the author for the Degree of Engineer, Stanford University, 1954.
2. Asst. Research Officer, Natl. Aeronautical Establishment, Ottawa, Canada.

ρ Fluid density (slugs/ft³)
ν Kinematic viscosity (ft²/sec)
q Dynamic pressure ($\rho V^2/2$ - psf)
R Reynolds number (Vd/ν)

S Transverse projected area of model - length x d(ft²)
D Drag (lb)
C_D Drag coefficient (D/qS)

INTRODUCTION

A problem common to many fields of engineering is that of suppressing the vibration caused by the motion of a circular cylindrical body relative to the surrounding fluid. Dangerously large vibrations of slender smokestacks, suspended pipelines, and electrical conductors, and the vibrational impairment of the usefulness of submarine periscopes are examples of this troublesome problem.

The basic phenomenon which causes these oscillations is the same one which produces the familiar rippling of a flag in the wake of a circular flag pole. The ripples are manifestations of a trail of vortices shed alternately from opposite sides of the pole in an arrangement similar to the ideal pattern shown below:

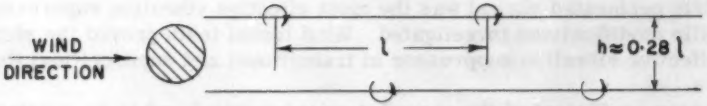

The formation and discharge of such a system of vortices produces alternating periodic asymmetry of the flow pattern and distribution of pressure around the cylinder. If the frequency of the resulting oscillating transverse force closely approximates the natural frequency of the cylinder, vibration of large amplitude is likely to occur.

The majority of vibrations caused by such periodic fluid forces are currently suppressed by stiffening the cylinder, providing external bracing or, when practical, installing damping devices. In the few problems which are characterized by unidirectional flow, enclosure of the cylinder within a fixed streamline fairing has proven effective. This solution is not applicable to smokestacks which may experience winds from all directions and serious consideration of proposals to provide omnidirectional effectiveness by building a stack fairing that would align itself with the wind is precluded by the considerations of size, weight, cost, and difficulty of maintenance.

Studies made by the Bechtel Corporation (Ref. 1) indicate that currently accepted means of suppressing vibration are inadequate. To provide the desired rigidity of tall stacks, guy wires may be excessively large and are themselves subject to wind induced vibration. Stack to stack trussing appears uneconomical and difficult because of the flexibility and complexity necessary to accommodate temperature changes. Friction damping is not only expensive but subject to impairment by icing.

In each case the approach to the problem has been directed towards minimizing the effects of the periodic aerodynamic forces, rather than towards

their suppression. The present investigation was initiated in the belief that the forces could be suppressed by so modifying the circular profile as to reduce the strength of the individual vortices or to inhibit their periodic discharge.

A review of previous work shows that the earliest study of the vibration of circular cylindrical bodies was made by Strouhal in 1878 (Ref. 2). He found that the vibration frequency (n) (and thus the frequency of vortex discharge) was directly proportional to the velocity of translation (V) and inversely proportional to the cylinder diameter (d). More specifically, the average value of the dimensionless ratio nd/V (now known as the Strouhal number, S) was found to be approximately 0.185.

In 1911, Von Karmàn (Ref. 3) proved theoretically that the only stable arrangement of periodically discharged vortex pairs is that shown on page 3. This configuration of vortices is usually referred to as the Karmàn street. Observation of streets in real flow (Ref. 4) indicate that they depart, often substantially, from this ideal pattern.

Tests conducted by Relf and Simmons in 1924 (Ref. 5) showed that, for a fixed (i.e. nonvibrating) circular cylinder, the Strouhal number had a constant value of approximately 0.19 throughout the range of Reynolds numbers between 500 and the value which corresponds to the lower limit of the critical regime. (The critical, or transitional, regime is identified by a radical reduction of the value of the drag coefficient with increase of Reynolds number; this decline is a consequence of the rearward movement of the points of flow separation and the associated narrowing of the wake.) It was also found that the Strouhal number increased in the critical regime and at supercritical Reynolds numbers vortex discharge became aperiodic. These results were later confirmed by Dryden and Heald (Ref. 6).

The first investigation of the vibration of a circular cylinder which was free to oscillate under elastic restraint and the action of fluid forces was made by Meier-Windhorst in 1939 (Ref. 7). These tests, made at subcritical Reynolds numbers in a water channel, explored the influence of damping, vibrating assembly moment of inertia, and restraining spring stiffness, on the amplitude and frequency of cylinder vibration over a range of water speeds.

The undamped cylinder, for all combinations of moment of inertia and spring stiffness, was found to reach a maximum amplitude at a water speed of approximately 5fd and the large amplitude continued to a water speed of approximately 7fd. Damping caused substantial reduction of amplitude at all water speeds. The rate of vortex discharge from the undamped cylinder, as indicated by the vibration frequency, was not proportional to velocity—as it is when the cylinder is fixed—but assumed values between the natural frequency of the vibrating assembly and those corresponding to the maintenance of a constant Strouhal number of 0.20. (Introduction of damping reduced vibration frequency slightly). This behavior is the result of the conflict between the tendency of a rigid cylinder to discharge vortices—and thus force oscillation of the cylinder—at a rate proportional to water speed, and the tendency of a flexible cylinder to vibrate at its natural frequency. This effect of transverse motion on the frequency of vortex discharge was previously noted by Frank (Ref. 8), who called it "steering". The effect has also been noted by Baird (Ref. 9), in studies made to find a method of suppressing the vibration of a suspended pipeline.

The results of Meier-Windhorst's work provided valuable guidance in the planning of the present investigation, but shed little light on the stack vibration problem because these experiments were characterized by small Reynolds numbers and highly flexible models. The Reynolds numbers were subcritical and such light restraining a springs were used that, in the absence of damping, all models attained maximum double amplitudes of at least two diameters. By way of contrast, the observations summarized in Table 4 of Ref. 10 indicate that a 224 ft. steel stack of 11 ft. 4 in. diameter vibrated so dangerously in a wind of approximately 30 mph that failure appeared imminent. The corresponding Reynolds number was 3,180,000 and the double amplitude was 0.25 diameter. The stack vibration problem is thus seen to be characterized by supercritical Reynolds numbers and relatively small amplitudes of vibration.

It was realized at the outset of this investigation that conclusive verification of the capability of any profile modification to suppress stack vibration could be accomplished only at supercritical Reynolds numbers. Nevertheless, exploratory tests were conducted in a small water channel to take advantage of the ease with which inexpensive models could be made, the simplicity of test technique, and the convenience of flow visualization. Moreover, it was believed that only such modifications as were found effective in the water channel would be likely to prove effective at the Reynolds numbers associated with full-scale stack vibration. It was therefore planned to verify the effectiveness of modifications which yielded promising results in the water channel by making wind tunnel tests of larger replicas at supercritical Reynolds numbers.

Apparatus and Technique

Water Channel

The exploratory phase of this investigation was conducted in a 9 by 15 inch water channel, capable of a maximum water velocity of 0.71 ft./sec. at a water depth of 10 inches.

The general arrangement of the apparatus is shown in Fig. A. This installation permitted statically balanced models to oscillate, under the action of fluid forces and the restraint of a torsion spring, about an axis parallel to, and above, the stream. The moment of inertia of the vibrating assembly and the stiffness of the restraining torsion spring were variable through a wide range, by movement of weights and spring clamp respectively. The forms and principle dimensions of the water channel models are illustrated and tabulated in Fig. 1. A plain cylinder model is shown in Fig. A and a photograph of modified models (and their components) is reproduced as Fig. B.

A solution of potassium permanganate was injected into the water just upstream of the model to facilitate flow visualization. The complete details of the water channel tests are given in the following section, entitled Test Program.

Preliminary experiments (test numbers 1 to 6) were made to explore the plain cylinder behaviour under the test conditions available and to verify, qualitatively, the results of Meier-Windhorst's work. These tests substantiated evidence found in Meier-Windhorst's results that the qualitative characteristics of the vibration were independent of flow velocity (for subcritical Reynolds numbers). For this reason all subsequent tests were conducted at a single convenient water speed.

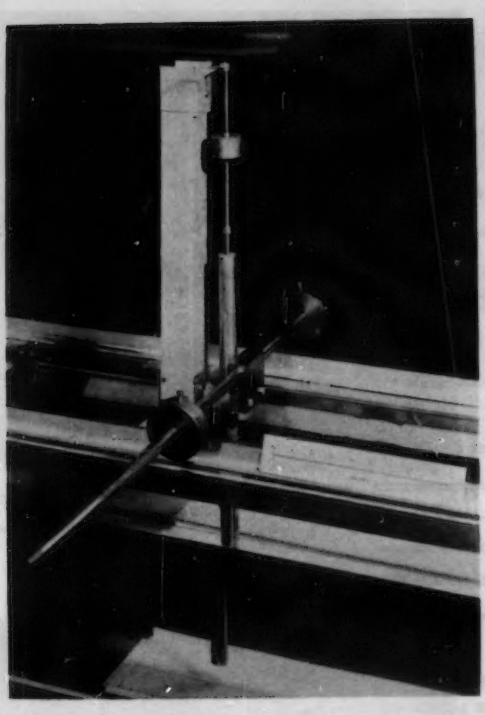

FIG. A
WATER CHANNEL APPARATUS

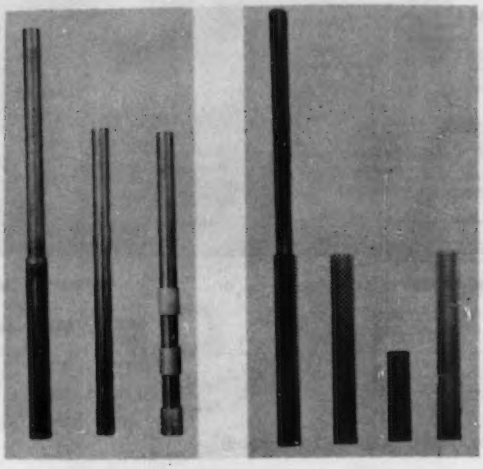

FIG. B
WATER CHANNEL MODELS

FIGURE 1

WATER CHANNEL MODELS

MODEL

1 PLAIN CYLINDER

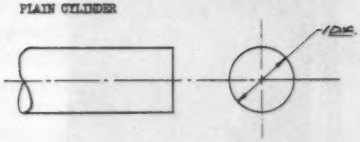

MODIFIED CYLINDER

2 CYLINDER & 3 WIRES PARALLEL TO CYL. AXIS

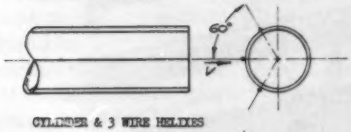

3 CYLINDER & 3 WIRE HELIXES

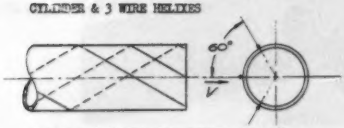

4 CYLINDER & 6 WIRE HELIXES(see Fig. B)

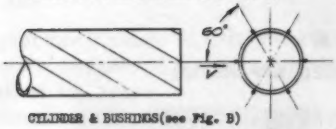

5 CYLINDER & BUSHINGS(see Fig. B)

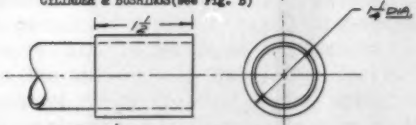

6 CYLINDER & RADIAL FINS(see Fig. B)

7 CYLINDER & PERFORATED FULL SHROUD(see Fig. C)

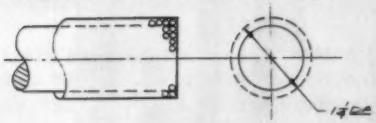

8 CYLINDER & PERFORATED HALF SHROUD(see Fig. C)

SEE MODEL 7

DETAILS & DIMENSIONS

WIRE DIAMETER(in.)

0.023

WIRE DIAMETER(in.)	PITCH(in.)
0.023	2

WIRE DIAMETER(in.)	PITCH(in.)
0.023	0.5, 4, 8, 16, 20
0.026	0.8
0.029	1
0.032	20

DISTANCE BETWEEN BUSHINGS - 1 ½

FIN THICKNESS - 0.020in.

POROSITY - 37%

SHROUD LENGTH	HOLE DIA.(in.)	ROW ORIENTATION WITH RESPECT TO CYL. AXIS
FULL	1/10	PARALLEL & PERPENDICULAR
FULL	1/8	" " "
FULL	1/10	INCLINED 45 DEG.
HALF	1/8	PARALLEL & PERPENDICULAR

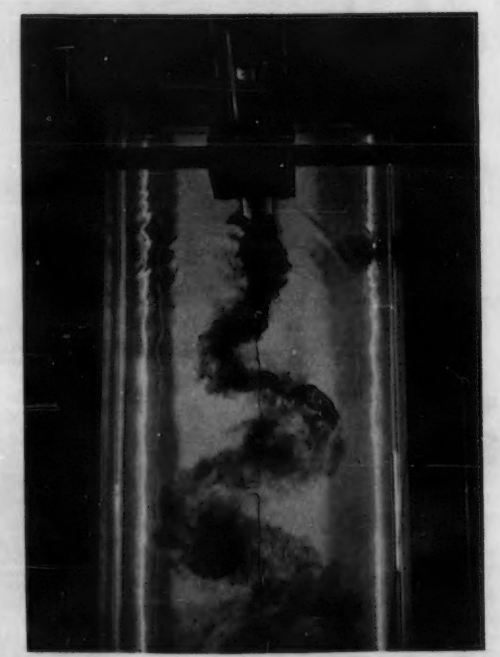

FIG. C
WAKE OF OSCILLATING PLAIN CYLINDER
k = 500 in lb/RAD.
n = 1·348 cps
B = 0·8 DIAM.

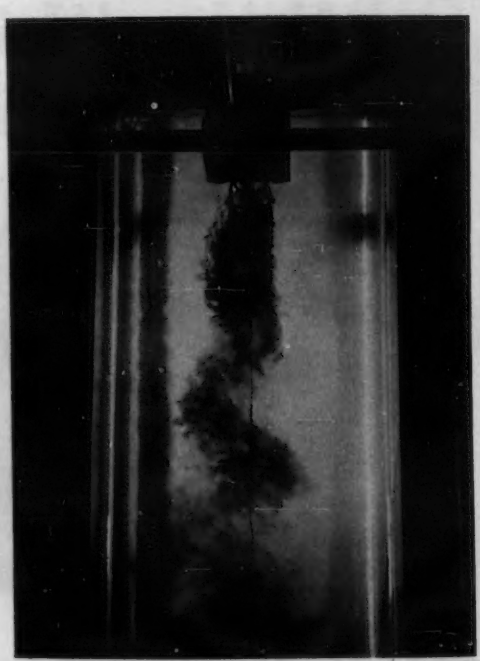

FIG. D
WAKE OF OSCILLATING SHROUDED CYLINDER
k = 500 in lb/RAD.
n = 1·381 cps
B = 0·04 DIAM.

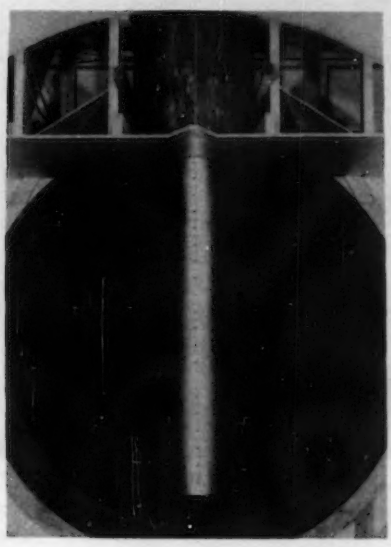

FIG. E
WIND TUNNEL DRAG TEST INSTALLATION
(AS VIEWED FROM DOWNSTREAM)

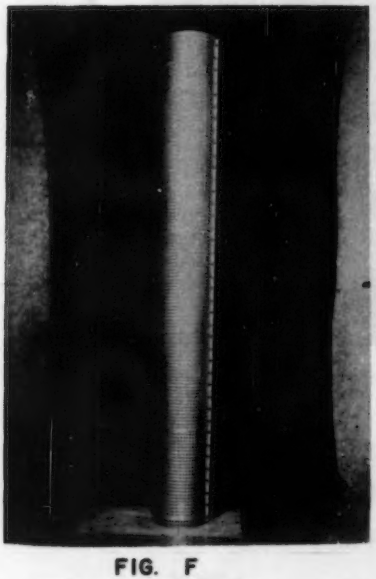

FIG. F
VIBRATION TEST INSTALLATION
(REFLECTING PLANE IN PLACE)

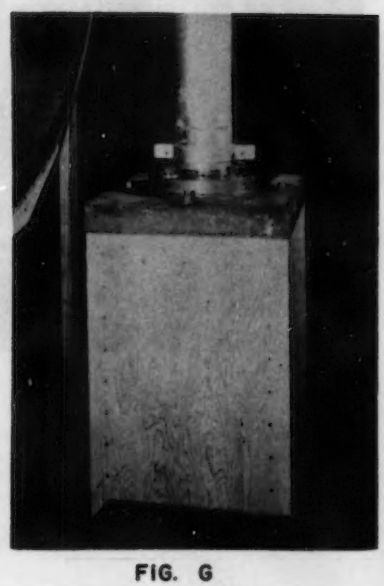

FIG. G
VIBRATION TEST INSTALLATION BASE
(REFLECTING PLANE REMOVED)

The final tests of the plain cylinder (test numbers 7 to 11) were made by progressively increasing the moment of inertia in successive tests until the spring stiffness required to produce maximum amplitude became so great that the maximum double amplitudes were reduced to less than one diameter. This technique served not only to extend the range previously covered by Meier-Windhorst, but enabled appraisal of the effectiveness of profile modifications (tests 12 to 18) in suppressing vibrations of the order of those encountered in actual stack vibration.

The moments of inertia of the various vibrating assembly configurations were determined by measuring the vibration frequency, in still water, for a known spring length and substituting this value in the formula

$$f = \frac{1}{2\pi}\sqrt{\frac{k}{I}}$$

where k was known for the chosen spring length from a bench calibration of the spring. Knowledge of this moment of inertia would then define the natural frequency of the assembly for any spring length using the above formula.

Wind Tunnel

The aerodynamic experiments were carried out in the 7.5 ft. diameter Eiffel type wind tunnel of Stanford University's Guggenheim Aeronautic Laboratory. The maximum speed of this tunnel is approximately 130 ft. per sec.

The plain cylinder wind tunnel model was a length of 6 inch outside diameter, 0.0625 inch wall, aluminum alloy tubing shrunk on, and clamped to, a cast iron base.

The only type of profile modification investigated in the wind tunnel was the perforated shroud. Shrouds were made from 24 gauge aluminum alloy sheet incorporating the same porosity (37 %) as that of the shrouds used in all water channel experiments. Spacing between shroud and cylinder (shroud gap) was maintained by six spacing rings. The shroud gaps and shroud hole diameters used in the wind tunnel tests are tabulated in the section entitled Test Program.

The first series of wind tunnel tests (test numbers 19-22—see Test Program) were drag measurements made to establish the transition range of Reynolds numbers for the plain cylinder, and to compare the drag coefficients of plain and shrouded cylinders at speeds ranging from the lowest at which reliable force measurements could be made to the highest obtainable with each model. For these drag tests the model was bolted to a shielded, stiff plywood pedestal attached to the floating frame of the overhead, six-component aerodynamic balance (see Fig. E). The ground at the base of a stack was simulated by a plywood reflecting plane which extended laterally beyond the limits of the airstream and had a length slightly greater than that of the free jet. The reflecting plane was so located that the exposed length of the model to its diameter was 10:1 and the midlength point was on the tunnel axis.

To study the effectiveness of the perforated shroud as a vibration suppressor at subcritical, transitional and supercritical Reynolds numbers the tests listed as test numbers 23 to 25 in the Test Program were made.

The vibration test installation is shown in Figs. F and G. The model was mounted, with tip upward, on a massive cast iron block surmounting a plywood pedestal bolted to the Eiffel chamber floor. The concentration of weight in the

cast iron base and the block gave an effective rigidity of support which was not obtainable from the relatively flexible floor structure of the Eiffel chamber. The reflection plane used in the drag tests was adapted to the vibration test installation. As may be seen in Fig. G, slots were cut in the base of the cylinder. The purpose of these slots was to reduce the model's natural frequency of transverse vibration. At the time vibration tests were begun, it was believed that this was essential to the attainment of maximum vibration amplitude. This belief had been fostered by the opinion expressed in several reports of observed vibration of large smokestacks, later found to be without foundation, that maximum vibration amplitude occurs as the result of "resonance" between the frequency of vortex discharge which corresponds to $S \approx 0.2$ and the natural frequency of the stack. To satisfy this condition, i.e. $V \approx 5fd$, with the unslotted model whose natural frequency was 57 cps would have required an airspeed of 142.5 ft. per sec., which could not be obtained in the Stanford tunnel. The slots were therefore cut and a weight added to the top of the plain cylinder to reduce the natural frequency of both the plain and shrouded models to 37.5 cps. The velocity required to satisfy the "resonance condition" was thus reduced to a value only slightly greater than the minimum for supercritical flow.

An inertia pickup rigidly mounted within the tip of the model was used to sense the vibratory motion. The voltage produced by the acceleration of the pickup was transmitted to a cathode ray oscillograph. Vibration amplitude was determined by multiplying the amplitude of the oscillograph trace by an appropriate calibration constant. Vibration frequency was evaluated by determining the sweep frequency which resulted in the production of a single standing wave on the oscillograph screen. Oscillograms were made to verify the visual observations of the oscillograph trace behaviour.

Test Program

A summary of the exploratory tests conducted in the water channel and the corresponding test parameters are presented below in tabular form. Dimensions and photographs of the various models are shown in Figures 1 and B, respectively.

Water Channel Vibration Tests - Preliminary

Test No.	Model No.	I (in.-lb-sec^2)	k (in.-lb/rad)	V (fps)	R
1	1	0.335	15.7 - 22.8	0.467	3370
2	1	.335	16.3 - 29.3	.527	3820
3	1	.335	16.3 - 36.2	.630	4560
4	1	.335	17.7 - 47.5	.650	4640
5	1	.335	17.7 - 47.5	.710	5150
6	1	.335	17.7	0.392-0.722	2840-5236

Water Channel Vibration Tests - Plain Cylinder

7	1	2.151	168 - 223	0.658	4640
8	1	2.810	186 - 384	0.658	4640
9	1	3.720	236 - 445	0.658	4640
10	1	4.893	301 - 423	0.658	4640
11	1	6.722	352 - 615	0.658	4640

Water Channel Vibration Tests - Modified Cylinder

V = 0.658 fps R = 4640

Test No.	Model No.	Configuration	I (in.-lb-sec²)	k (in.-lb/rad)
12	2	Cyl. + parallel wires	0.335	25 - 27
13	3	Cyl. + 3-wire helixes	0.335	25 - 48
14	4	Cyl. + 6-wire helixes[a]	0.335 & 6.313	25 - 615
15	5	Cyl. + bushings	0.405	16 - 41
16	6	Cyl. + radial fins[b]	6.803	168 - 615
17	7	Cyl. + perf. shroud[c]	0.482 - 6.537	25 - 725
18	8	Cyl. + perf. half shroud	6.711	423 - 725

The models used in the wind tunnel tests, which were made to determine the drag and vibration characteristics of plain and shrouded cylinders, are identified by the numbers and dimensions listed below.

Wind Tunnel - Drag Tests

Test No.	Model No.	Shroud Hole Dia. (in.)	Shroud Gap (in.)
Plain Cylinder			
19	9	---	---
Shrouded Cylinder			
20	10	3/4	3/4
21	11	1/4	3/4
22	12	1/4	1/4

Wind Tunnel - Vibration Tests

Plain Cylinder			
23	9	---	---
Shrouded Cylinder[d]			
24	12	1/4	1/4

RESULTS AND DISCUSSION

Water Channel

Plain Cylinder Tests.

The results of the preliminary tests, in which water speed was varied and model moment of inertia and restraining spring stiffness held constant, are presented in Fig. 2. The vibration characteristics of this model are substantially those observed by Meier-Windhorst (see Introduction) for a relatively flexible, undamped model in subcritical flow.

a Wire diameter and helix pitch varied.
b Fin orientation varied.
c Hole size and row orientation varied.
d No data are presented for this test as no periodic vibration was observed.

FIG. 3
PLAIN CYLINDER
DOUBLE AMPLITUDE & VIBRATION FREQUENCY VS SPRING STIFFNESS
MODEL I

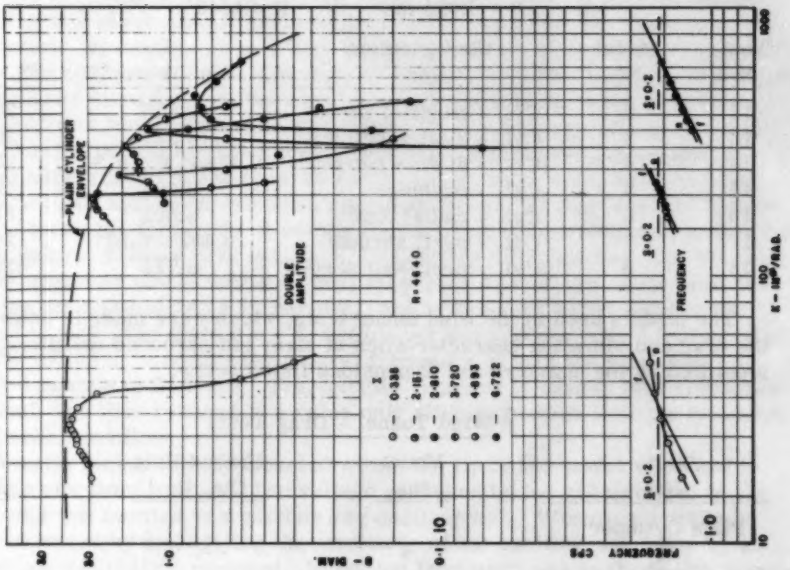

FIG. 2
PLAIN CYLINDER VIBRATION FREQUENCY & AMPLITUDE VS. VELOCITY

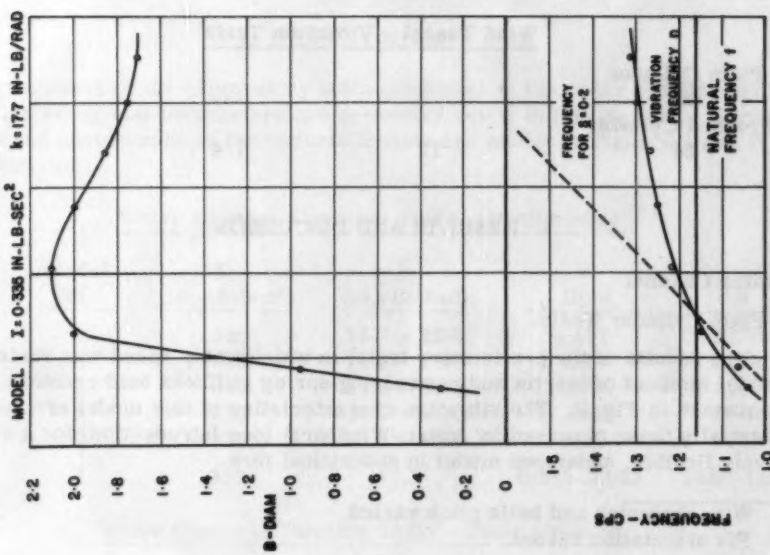

The results of subsequent tests, made to explore cylinder behaviour over a broader range of cylinder flexibility are presented in Fig. 3. It can be seen that large amplitudes persisted as flexibility decreased until a critical value was reached, beyond which amplitude diminished rapidly. The region of relatively small amplitudes is particularly significant in connection with the present investigation because stacks of current design are likely to fail if the tip double amplitude exceeds half a diameter.

Fig. 3 also shows the effect of flexibility on vibration frequency. As stiffness increases the frequency of vibration departs further from the values predicted by a constant Strouhal number of 0.20 until, at a stiffness corresponding to a double amplitude of 0.8 diameter, the curve of vibration frequency is virtually coincident with the curve of natural frequency.

Modified Cylinder Tests.

The various profile modifications tested are shown in Figs. 1, A and B. The wires parallel to the cylinder axis and the radially projecting fins were selected as profile modifications which might fix the stagnation and separation points and hence weaken the strength of the discharged vortices. It was thought that wire helixes and concentric bushings might prevent the formation of continuous vortices of full cylinder length—wire helixes forcing flow separation to occur at different azimuth angles in adjacent cross sections, and bushings causing vortices to be discharged at different frequencies from adjacent sections of different diameter. A perforated shroud was tested as a vortex suppression device because it was thought that the shroud would break up the flow into a large number of small vortices with the result of minimizing the periodic asymmetry of flow about the cylinder.

The variation of vibration amplitude and frequency for these profile modifications over a wide range of cylinder flexibility is presented in Figs. 4 and 5. It will be noted that the shroud proved to be the most effective suppressor at all stiffnesses, and for comparison purposes the envelopes of shrouded cylinder and plain cylinder amplitudes are presented with the results of the less effective suppressors in Fig. 4. The following behaviour was exhibited by the less effective suppressors: the parallel wires and radial fins possessed only unidirectional effectiveness and hence would not prove to be satisfactory suppressors in a stack application. The most beneficial helical configuration was not sufficiently effective to merit further consideration. The curve of amplitude versus stiffness for the cylinder with the bushings rose above the plain cylinder envelope, and attained an amplitude which might be expected of a plain cylinder with a diameter intermediate between those of the basic cylinder and the bushings.

Fig. 5 shows that the shroud was effective in suppressing vibration at all stiffnesses. It can be seen that the shroud became increasingly effective as stiffness increased. The application of a shroud to a cylinder which vibrated with a double amplitude of two diameters reduced amplitude by about 50 per cent, while double amplitudes of 0.7 diameter were reduced by 97 per cent. The effectiveness of suppressing small amplitude vibration is particularly promising because double amplitudes of the order of half a diameter have led to full scale stack failure.

The explanation of the effectiveness of the shroud can be readily deduced from a comparison of Figs. C and D. It will be seen that the individual vortices streaming in rows from the shrouded cylinder are smaller and much more closely spaced (hence are discharged at a higher frequency) than those shed by the plain cylinder. Comparison of these figures also indicates that

the spacing of the large vortices discharged from the plain cylinder was approximately that of the large vortices formed far behind the shrouded cylinder by the coalescence of the small, closely spaced vortices. As the vibration frequencies of the plain and shrouded cylinders were approximately the same, it is apparent that what little vibration was experienced by the shrouded cylinder must have been caused by the large vortices in the Karman street formed several diameters downstream. Their influence on the flow adjacent to the cylinder was small because the tangential velocity which characterizes vortex motion is inversely proportional to the distance from the center of the vortex.

The effects of varying the size and arrangement of the holes in the shroud were superficially investigated. Fig. 5 indicates that the shroud became slightly more effective as the hole size was increased while porosity was held constant. Rows of holes parallel and perpendicular to the cylinder axis proved more beneficial than rows inclined at 45 degrees. The application of the shroud to the lower half of the immersed length of the cylinder resulted in amplitude reductions of much less than one-half that effected by the full shroud.

Vibration frequency characteristics have been omitted from the discussion of the results of profile modifications because the variation of frequency with stiffness followed the same pattern as that described for the plain cylinder, i.e. as stiffness increased the vibration frequency of the modified models approached the natural frequency. This can be seen in a particular instance by comparison of the frequency curves of the shrouded cylinder in Fig. 5 with those of the plain cylinder in Fig. 3.

Wind Tunnel

Drag Tests

Plain cylinder tests (Fig. 6) demonstrated that transition occurred between Reynolds numbers of 130,000 and 280,000. As the Reynolds number attained at maximum tunnel speed was 420,000, a considerable portion of the tunnel speed range was available for testing within the supercritical regime. The drag coefficients for the smooth cylinder were found to be consistent with previously published data (Ref. 11).

The results of the drag tests of the shrouded cylinders (Fig. 6) show that the drag coefficient for each of the shrouded configurations remained substantially constant throughout the explored range of Reynolds numbers at values intermediate between the sub and supercritical drag coefficients of the plain cylinder. Investigation into the effects of shroud hole size on drag coefficient indicated, as might have been expected, that smaller holes resulted in a larger drag coefficient when porosity remained constant. The drag coefficient was found to increase as the shroud gap was enlarged. As the coefficients were based on the projected area of the shroud, this means that the drag increased in greater proportion than the projected area.

It should be noted that constancy of drag coefficient implies that the nature of the flow about the shrouded cylinder also remained substantially unchanged within the range of Reynolds numbers explored. In view of the extent of that range, it appears reasonable to anticipate that a similar form of flow will characterize the Reynolds numbers at which full scale stack vibration occurs.

FIG. 4

INEFFECTIVE SUPPRESSORS
DOUBLE AMPLITUDE VS SPRING STIFFNESS
R = 4640

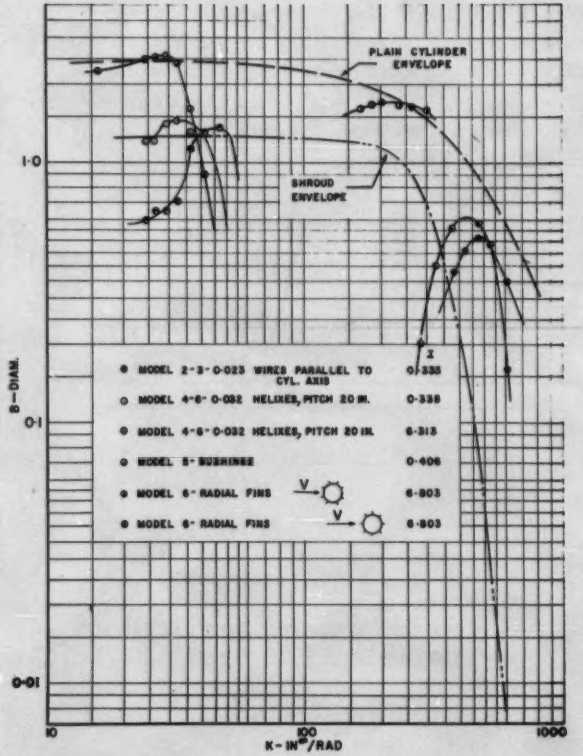

FIG. 5

SHROUDED CYLINDER
DOUBLE AMPLITUDE & VIBRATION FREQUENCY
VS. SPRING STIFFNESS
R = 4640

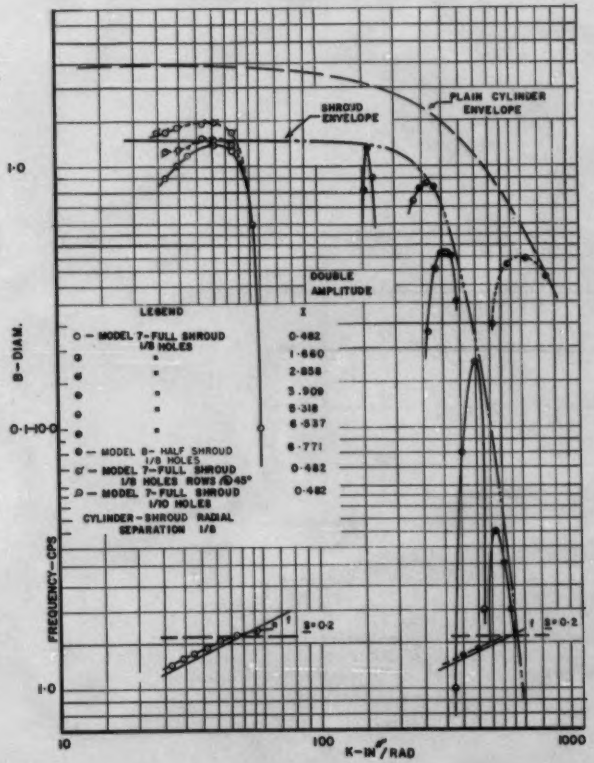

FIG. 6

CYLINDER DRAG COEFFICIENT VS. REYNOLDS NUMBER

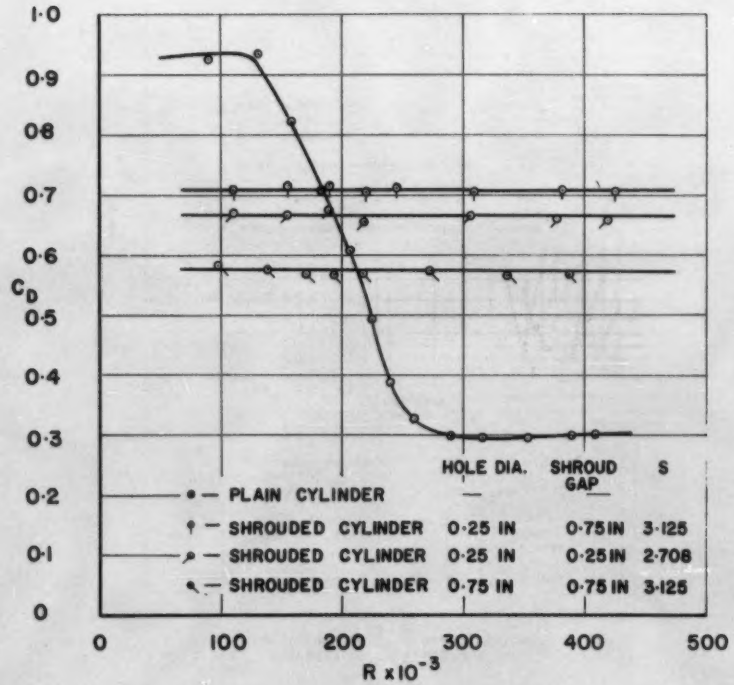

FIG. 7

PLAIN CYLINDER DRAG COEFFICIENT & TIP AMPLITUDE VS. DYNAMIC PRESSURE

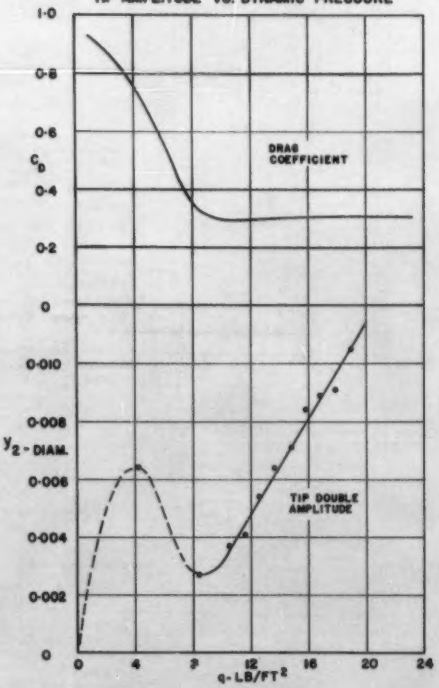

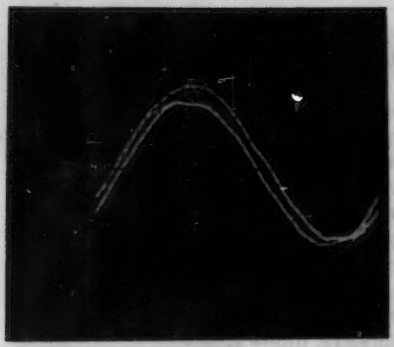

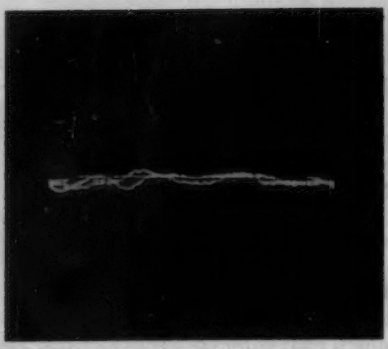

FIG. H
(TRANSITION REGIME)
(SEE FIG. 7)

PLAIN CYLINDER
$q = 5.25$ lb/ft^2
$f = 37.5$ cps
$n = 37.5$ cps

SHROUDED CYLINDER
$q = 5.25$ lb/ft^2
$f = 37$ cps

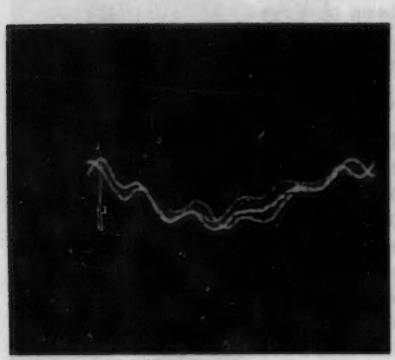

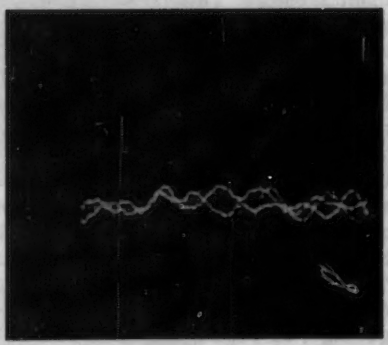

FIG. I
(LOW SUBCRITICAL)

PLAIN CYLINDER
$q = 10.5$ lb/ft^2
$f = 37.5$ cps
$n = 37.5$ cps

SHROUDED CYLINDER
$q = 10.5$ lb/ft^2
$f = 37$ cps

This leads to disproportionate indication of the amplitudes of high and low frequencies of vibration. As the secondary vibrations in these figures have frequencies about seven times those of the primaries, their relative amplitudes were actually little more than 1/50 of those indicated by the oscillograph trace.

Vibration Tests - Shrouded Cylinder.

Visual observation of the oscillograph trace revealed no identifiable periodic vibration of the shrouded model at any wind speed. (Wake pulsations could be felt by hand close behind the plain cylinder, but were not detected

Vibration Tests—Plain Cylinder.

At the low airspeeds which correspond to subcritical Reynolds numbers, the plain cylinder exhibited no appreciable vibration.

In the transition and supercritical regimes, irregular vibration was interspersed with short intervals of periodic oscillation, and the frequency of this regular vibration was always equal to the natural frequency of the cylinder. The fraction of time occupied by regular oscillation was greater in the transition region than at supercritical Reynolds numbers, but the duration of periodic behavior was never more than half the total time.

The variation of amplitude with dynamic pressure is presented in Fig. 7.* The large response to wind excitation which occurred in the transition range is believed to be a consequence of the inherent instability of flow separation which characterizes this regime. It also appears likely that this instability was amplified by the transverse motion of the cylinder. The amplitude of vibration diminished as transition was completed, but grew continuously thereafter as speeds increased in the supercritical regime.

At all airspeeds, the frequency of the only distinguishable periodic vibration was the natural frequency of the cylinder. It will be recalled that similar reluctance to vibrate at frequencies other than the natural frequency was noted in connection with the water channel tests of relatively stiff plain cylinder models. This phenomenon has also been observed by various investigators dealing with a variety of structures subject to wind induced oscillation: tall concrete and steel stacks (Refs. 12 and 13); suspension bridges (Refs. 14 and 15); and suspended pipe lines (Refs. 9 and 16). The records of Pagon (Ref. 13) also indicate that stack vibration is characterized by the same intermittency of irregular and periodic oscillation as that displayed by the wind tunnel model in the present investigation. Moreover, the reports of Omori and Pagon indicate that, contrary to current opinion, large amplitudes are attained by smokestacks at Strouhal numbers considerably less than 0.2 and thus further the belief held by the author that stack vibration at transitional and supercritical Reynolds numbers is a self excited phenomenon. That is, the spasmodic occurrence of large amplitude vibration, at only the natural frequency, appears to have no other explanation than the "self triggering", or regulating, influence of the cylinder's occasionally excited motion at natural frequency upon the otherwise aperiodic discharge of vortices. The fact that the wind speeds observed (or estimated) during some large amplitude stack vibrations were such that the values of the corresponding Strouhal numbers were approximately 0.2 is now believed to be entirely coincidental.

Because of the intermittent character of vibration, photographic records (Figs. H to K) were made to confirm visual observations. This was accomplished by taking an instantaneous photograph (approximately 1/25 sec.) at the moment a regular wave form appeared on the oscillograph screen. The persistence of periodic vibration for an appreciable interval of time is apparent in the similarly obtained time exposures (approximately one second) which are reproduced in Figs. J and K. To preclude misinterpretation of these oscillograms, attention is drawn to the fact that the output of an inertia pickup is proportional to the amplitude and the square of vibration frequency.

* Drag coefficient is also plotted in Fig. 7 for convenient reference. It should be noted that C_D is plotted against dynamic pressure in this chart, whereas in Fig. 6 Reynolds number was the abscissa.

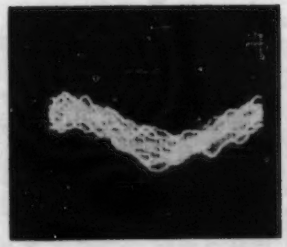

PLAIN CYLINDER
(TIME EXPOSURE)
$q = 15.75\ lb/ft^2$
$f = 37.5$ cps
$n = 37.5$ cps

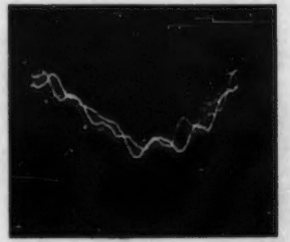

FIG. J
(SUPERCRITICAL)
PLAIN CYLINDER
$q = 15.75\ lb/ft^2$
$f = 37.5$ cps
$n = 37.5$ cps

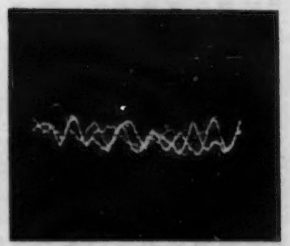

SHROUDED CYLINDER
$q = 15.75\ lb/ft^2$
$f = 37.5$ cps

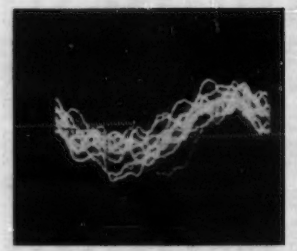

PLAIN CYLINDER
(TIME EXPOSURE)
$q = 18.90\ lb/ft^2$
$f = 37.5$ cps
$n = 37.5$ cps

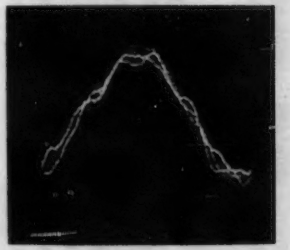

FIG. K
(SUPERCRITICAL)
PLAIN CYLINDER
$q = 18.90\ lb/ft^2$
$f = 37.5$ cps
$n = 37.5$ cps

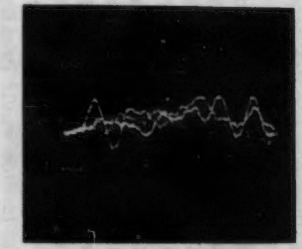

SHROUDED CYLINDER
$q = 18.90\ lb/ft^2$
$f = 37.5$ cps

within four diameters downstream of the shrouded model.) Oscillograms were made to confirm visual observations and these, reproduced in Fig. H show the effectiveness of the shroud in suppressing vibration in the transition regime. Figs. I, J, and K illustrate similar effectiveness at speeds in the supercritical region.

The present experiments have demonstrated the effectiveness of the shroud as a vibration suppressor at supercritical Reynolds numbers under only one set of conditions, i.e. those which correspond to a very stiff cylinder which, without a shroud, oscillated with small amplitudes. While it is obviously desirable to obtain proof of the effectiveness of the shroud in suppressing large amplitude vibration at supercritical Reynolds numbers, the difficulty of providing a sufficiently flexible model with which such Reynolds numbers could be attained in the Stanford tunnel prevented such tests. However, it is inferred from the results obtained that the action of the shroud during incipient stages of periodic motion would greatly inhibit the development of large amplitudes of vibration. Moreover, subcritical data from the water channel and the drag characteristics of the shrouded configuration appear to justify the expectation of comparable effectiveness when applied to more flexible cylinders.

CONCLUSIONS

The following conclusions are drawn from this study of the vibration of circular cylinders, which was directed primarily toward solution of the problem of smokestack vibration:

1. The general characteristics of the vibration of circular cylinders in fluid streams (in the absence of compressibility effects) may be described as follows:

At subcritical Reynolds numbers continuous, periodic vibration occurs, the characteristics of which are controlled by the conflict between the tendency of the cylinder to vibrate at its natural frequency and the tendency of a stationary cylinder to discharge vortices—and thus force vibration—at a rate proportional to fluid velocity (i.e. vibration characterized by a constant Strouhal number). The resulting vibration occurs within a limited range of fluid velocity—the range diminishing as cylinder flexibility is decreased. Vibration frequency lies between the natural frequency and that corresponding to a constant Strouhal number, approaching the natural frequency as cylinder flexibility is reduced. The relatively large and nearly uniform maximum amplitudes characterizing a wide range of low stiffness diminish rapidly as flexibility is reduced below a certain critical value.

As a consequency of the aperiodic shedding of vortices by a rigid cylinder in the transitional and supercritical flow regimes, the tendency to vibrate at a frequency proportional to velocity disappears and periodic vibration of a flexible cylinder occurs only at the natural frequency. However, regular periodic vibration is not continuous at these speeds; it occurs only spasmodically and irregular vibration of comparatively small amplitude occupies the remainder of the time. The amplitude of periodic vibration is relatively large in the transition range (due to the instability of flow separation), but diminishes upon entrance into the supercritical regime, and increases continuously to very large values with further increase of speed.

2. Profile modifications which consisted of wires parallel to the cylinder axis, helical wires, spaced concentric bushings, and radial fins were relatively ineffective in suppressing vibration in the subcritical flow regime.

3. The enclosure of a plain cylinder within a concentric perforated shroud proved effective in suppressing vibration at subcritical, transitional and supercritical Reynolds numbers. At subcritical Reynolds numbers the shroud became increasingly effective as cylinder flexibility decreased, reducing plain cylinder vibration amplitudes of the order of two diameters by 50 per cent, and amplitudes of 0.7 diameter by 97 per cent. The shroud virtually eliminated periodic vibration of a stiff model at transitional and supercritical Reynolds numbers.

4. It is believed that if a full scale stack were equipped with a perforated shroud it would be substantially immune to wind-induced vibration because:

(a) the demonstrated absence of scale effect upon the drag coefficients of shrouded cylinder models warrants the expectation of closely similar flow at the very large Reynolds numbers characteristic of stacks; and

(b) the proven effectiveness of the shroud as a suppressor of small amplitude vibration makes it reasonable to expect that the shroud would inhibit the attainment of large amplitudes, particularly under conditions of only spasmodic excitation.

REFERENCES

1. Dickey, W. L.: The Problems of Civil and Structural Design of Steam Electric Plants for the Pacific Gas and Electric Company in Central California. ASCE Convention Preprint #72, March, 1953.

2. Strouhal, V.: Uber eine besondere Art der Tonerregung. Ann. Phys. Chem., N.F., Bd 5, Heft 10, Oct. 1878, pp. 216-251.

3. Von Karman, Th. and Rubach, H.: Uber den Mechanismus des Flüssigkeits und Luftwiderstandes. Phys. Z. Bd 13, Heft 2, Jan. 15, 1912.

4. Roshko, A.: On the Development of Turbulent Wakes From Vortex Streets. NACA T.N. 2913, 1953.

5. Relf, E.F. and Simmons, L.F.G.: Frequency of Eddies Generated by Motion of a Cylinder Through Fluid. British A.R.C. R. and M. 917, 1924.

6. Dryden, H.L. and Heald, R.H.: Investigation of Turbulence in Wind Tunnels by a Study of the Flow About Cylinders. NACA T.R. 231, 1925.

7. Meier-Windhorst, A.: Flatterschwingungen von Zylindern im gleichmassigem Flüssigkeitsstrom. Mitt. des Hydraulischen Institute der Technischen Hochschule München, Heft 9, Munich, 1939.

8. Frank, W.: Stromungserregte Schornsteinschwingungen Archiv. F. Warmewirtschaft und Dampfkesselwesen, Vol. 22, issue 2, Feb. 1941.

9. Baird, R. C.: Wind-Induced Vibration of a Pipe-Line Suspension Bridge, and its Cure. ASME Trans., August, 1955, Vol. 77, No. 6.

10. Dickey, W.L. and Woodruff, G.B.: The Vibration of Steel Stacks. A.S.C.E. Proceedings Separate No. 540, November, 1954.

11. Weiselberger, C.: Further Information on the Laws of Fluid Resistance. NACA T.N. 121, 1922.

12. Omori: Wind Pressure on Tall Chimneys. Engineering, Vol. 106, 1918, pp. 334-36.

13. Pagon, W.W.: Wind Design by Aerodynamic Principles. Eng. News Record, July, 1934.

14. Farquharson, F.B., Smith, F.C., and Vincent, G.S.: Aerodynamic Stability of Suspension Bridges. University of Washington Engineering Experiment Station Bulletin No. 116.

15. Aerodynamic Stability of Suspension Bridges, Progress Report of the Advisory Board on the Investigation of Suspension Bridges - A.S.C.E. Separate No. 144, August, 1952.

16. Steinman, D.B.: Pipeline Bridge Stabilized with Diagonal Rope Stays. Civil Engineering, Vol. 22, No. 3, March, 1952.

Journal of the
ENGINEERING MECHANICS DIVISION
Proceedings of the American Society of Civil Engineers

SOME OBSERVATIONS ON OPEN CHANNEL FLOW AT SMALL REYNOLDS NUMBERS

Lorenz G. Straub,[1] M. ASCE, Edward Silberman[2]
and Herbert C. Nelson,[3] Associate Members, ASCE

(Proc. Paper 1031)

SYNOPSIS

This paper is confined to a summarization and correlation of the results of a number of theses studies on open channel flow in the range of Reynolds numbers below about 4×10^4. Hydraulic diameter is used as the length parameter in Reynolds number. Smooth laminar-, smooth turbulent-, rough laminar-, and rough turbulent-flow are considered separately, as is transition from laminar to turbulent flow in smooth channels.

The results indicate that at these small Reynolds numbers, smooth channel flow, both laminar and turbulent, is quantitatively similar to smooth pipe flow. Rough channel flow is probably qualitatively similar to rough pipe and rough plate flow, but there is no adequate method available to correlate rough flows in the small Reynolds number range. Channel shape is important in laminar flow, but its entire effect may be determined theoretically. There is only a negligibly small channel shape effect in smooth, turbulent flow and a somewhat more pronounced effect in rough, turbulent flow. Transition generally occurs at slightly higher Reynolds numbers in channels than in pipes, the exact effect depending on shape.

INTRODUCTION

During the past 25 years a large number of more or less related experimental studies have been made at the University of Minnesota on the hydraulics of flow in open and closed conduits. Much of the experimental work has been directed particularly toward establishing physical relationships of flow at small Reynolds numbers. Among these studies were a number of graduate

Note: Discussion open until December 1, 1956. Paper 1031 is part of the copyrighted Journal of the Engineering Mechanics Division of the American Society of Civil Engineers, Vol. 82, No. EM 3, July, 1956.

1. Director, St. Anthony Falls Hydr. Lab., Univ. of Minnesota, Minneapolis, Minn.
2. Associate Prof., St. Anthony Falls Hydr. Lab., Univ. of Minnesota, Minneapolis, Minn.
3. Hydr. Eng., Kimberly-Clark Corp., Neenah, Wisc.

theses concerned with steady, uniform flow in open channels in the laminar, transitional, and lower turbulent regions. This paper is limited to summarization and the presentation of a synthesis of the results of these studies which were conducted at the St. Anthony Falls Hydraulic Laboratory.(1-7)

This paper concerns only flows with the Froude number less than unity—that is, subcritical flow—and at high Weber numbers—that is, where capillary effects do not have significant influence upon the flow pattern. Furthermore, the treatment is confined to that part of the channel length where the boundary layer is fully developed—that is, where the velocity profiles over the reach of channel considered are essentially constant.

For the purpose of this paper the experimental studies naturally group themselves into two categories: (a) smooth channels, and (b) rough channels. There is the further classification into laminar flow, transition from laminar to turbulent flow, and turbulent flow. Therefore, in the following discussions an analytical presentation is given for each type of flow, followed immediately by a discussion of the experimental results pertaining to that flow for various channel shapes. Thus far, the most extensive experimental studies at the St. Anthony Falls Laboratory have been with smooth channels; therefore, this category is given primary consideration. However, flow in rough channels at low Reynolds numbers has also received attention in the test program and the results are here discussed, although much further research in this area is yet to be accomplished.

Notation

The notation used in this paper is defined where first introduced and is tabulated in Appendix A of this report. A Cartesian coordinate system is used in the algebraic treatment with the positive z-axis oriented in the direction of flow, the y-z plane vertical, and the origin at the free surface. The velocity at any point in the channel is w and the mean velocity is $\overline{w}$. The slope, s, is taken as positive when the channel inclination is downward in the direction of flow.

Channel friction is evaluated by using the Darcy-Weisbach friction factor, f, defined by the equation

$$S = \frac{f}{4R} \cdot \frac{\overline{w}^2}{2g}$$

where 4R is the hydraulic diameter, R being the hydraulic radius, or channel cross-sectional area divided by its wetted perimeter, and g is the acceleration of gravity. The friction factor is related to the Chezy "C" and Manning "n" by

$$C^2 = \frac{8g}{f}$$

$$n^2 = \frac{(1.486)^2}{8g} \cdot f R^{1/3}$$

Experimental Setup

Several experimental setups were used in the theses studies. However, they were basically the same as regards scale of the tests, system of circulation of the liquid mediums, and the instrumentation.

Figure 1 is typical of the apparatus. Channels of rectangular, fixed 90-degree triangular, variable triangular, and circular-arc cross sections were used. The test channels were formed from either a single rolled structural shape or, for the triangular channel of adjustable central angle, from two structural channels back to back with a sheet of rubber cemented across the pair of flanges at the vertex. The rectangular channel was 15 ft long and the others were either 20 or 22 ft long. The channels were all perfectly straight (probably within 0.01 in.), untwisted, and glossy smooth. The triangular channel of fixed vertex measured closely 90.7 degrees. The central angle of the channel of controllable shape could be closely set by screw adjustment arranged at four sections in the length of the channel. In general, an exceptionally high degree of precision in shape and control was possible.

A pumped recirculating system was used and included a low level reservoir, as well as a smaller head reservoir from which the channel was fed. The channels were all provided with bell-mouthed entrances which were removable. The discharge through the channel was measured by intercepting the flow in a weighing tank over measured intervals normally of several minutes duration. Both water and kerosene were used in the experiments and the temperature was controlled so as to hold the viscosity constant for each test.

Each channel was provided with three piezometer wells spaced at 5-ft intervals along its length. In the case of the rectangular channel, the piezometer wells were at distances of 2, 7, and 12 ft from the end of the bell-mouthed entrance; for the other channels the wells were either 7, 12, and 17 ft; or 8, 13, and 18 ft from the entrance. The fluid surface elevations in the wells could be measured to 0.001 in. by micrometer-fitted point gages. These gages were also used to set the channel slope and measure the depth of flow. In establishing flow in the channel, the tail gate was so adjusted that the depths measured at the last two piezometer taps, at least, were identical within 0.001 inch. (As will be noted subsequently, even this procedure was not sufficient to insure uniform flow at the highest Reynolds numbers of laminar flow because of the developing boundary layer. For most experimental runs, however, uniform flow was obtained.)

Velocity data (e.g., shown in Fig. 3 for flow at the 12-ft piezometer well) were obtained with a fine Pitot tube, the velocity head being measured in an adjacent well and referred to the piezometer well for the reference pressures. The tube could be traversed vertically and laterally by micrometer screw adjustment; the position was recorded to 0.01 inch. Surface velocity observations were made on floating particles of sufficient thickness to avoid inhibition by surface tension phenomena.

Smooth Channels—Laminar Flow

Theory

The Navier-Stokes equations [8] are applicable. With the stipulations previously stated, the pressure at the free surface is zero (atmospheric),

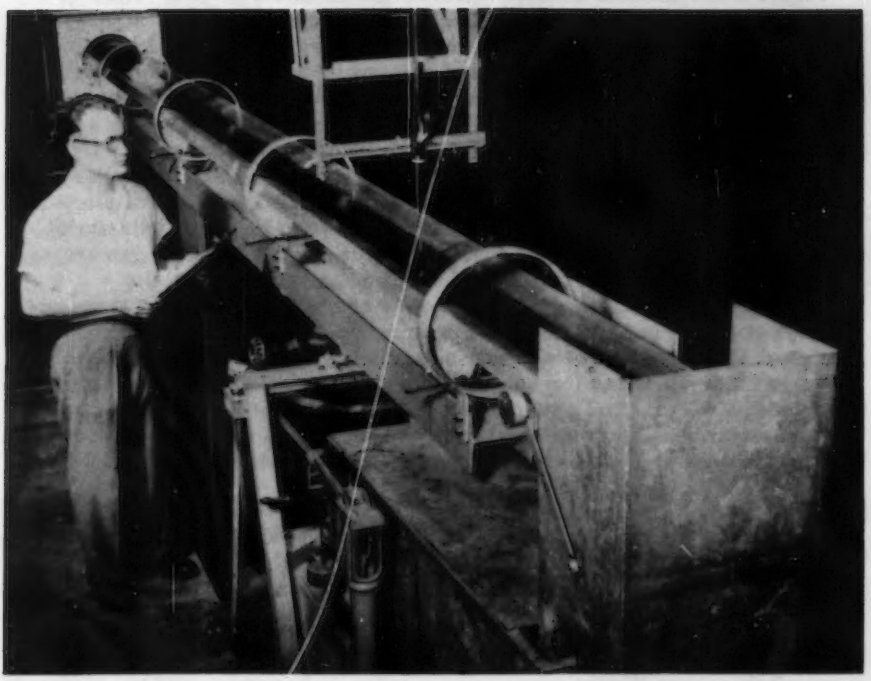

Fig. 1 – General View of Experimental Channel

the x- and y-components of the velocity are everywhere zero, and the z-component, w, is not a function of z. Hence, the Navier-Stokes equations reduce to

$$p+\rho gy = 0 \tag{1}$$

$$\frac{\partial^2 w}{\partial x^2}+\frac{\partial^2 w}{\partial y^2} = -\frac{gS}{\nu} \tag{2}$$

where p is the pressure, ρ is the density and ν is the kinematic viscosity of the liquid, and the external force is due to gravity and has the components per unit mass $Y \approx -g$ in the y-direction, and $Z \approx gS$ in the z-direction. Equation (1) shows that the pressure distribution is hydrostatic, leaving Eq. (2) to be solved for w when the appropriate boundary conditions are given. The solution of Eq. (2) is a two-dimensional problem in the x-y plane.

Equation (2) is a form of Poisson's equation and is applicable to such other problems as the determination of the streamlines for fluid enclosed by a rotating cylindrical boundary and the stress due to torsion of a cylindrical shaft. Analytical solutions can be obtained whenever the given cross section can be mapped conformally on the interior of a circle and approximate solutions can be obtained by numerical and other methods for any boundary configuration.[9]

The boundary conditions on Eq. (2) are

(a) $w = 0$ on all solid boundaries

(b) $\frac{\partial w}{\partial y} \approx 0$ at $y = 0$ (at the free surface)

The approximation sign is used in condition (b) because the presence of the atmosphere at the liquid surface results in a small drag and a non-zero value of the derivative. In solving Eq. (2), the derivative is made equal to zero; the influence of the resulting approximation may be estimated by comparison with experimental data. Several useful solutions of Eq. (2) are given in Appendix B. (These solutions are the same, of course, as for closed conduits obtained by reflecting the solid boundary in the free surface.)

Once Eq. (2) has been solved, the mean velocity $\overline{w}$ is given by

$$\overline{w} = \frac{1}{A}\iint w\, dx\, dy \tag{3}$$

where A is the cross-sectional area of the channel and the integral is taken over the entire cross section. Values of $\overline{w}$ for several channel shapes are also given in Appendix B.

The equation defining the friction factor may be written

$$f = \frac{K}{Re} \tag{4}$$

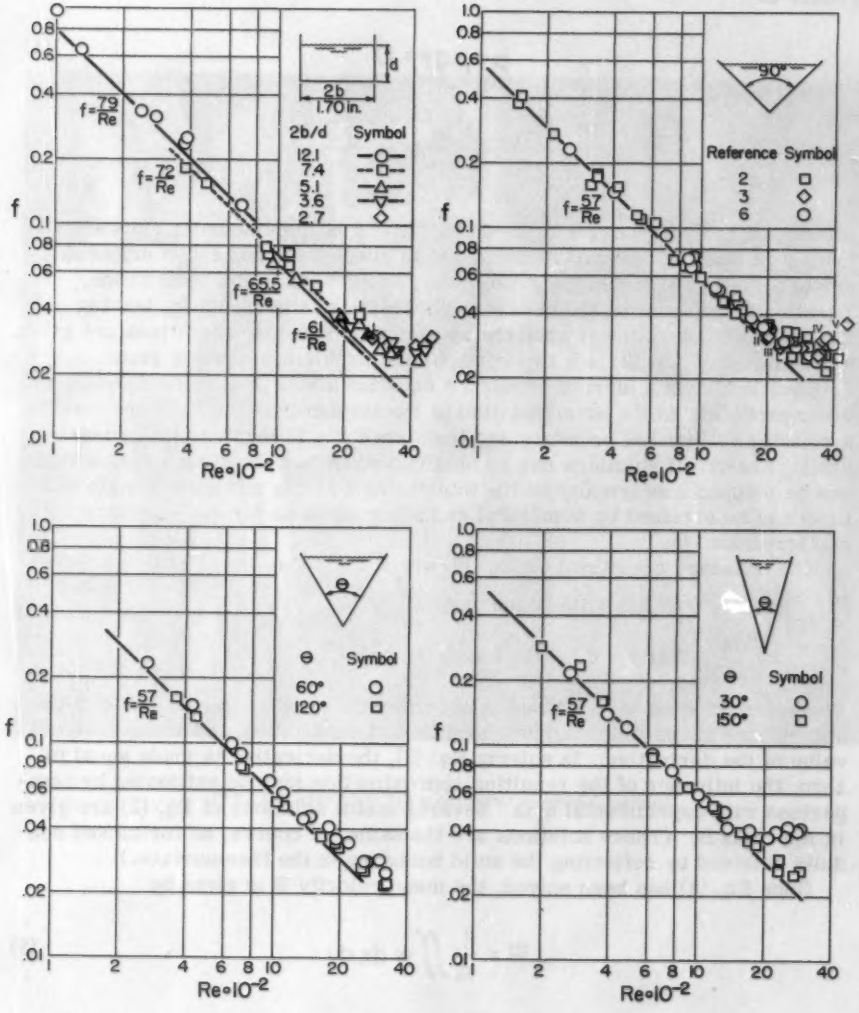

Fig. 2 - Friction Factor for Smooth, Laminar Flow

where Re is the Reynolds number given by

$$Re = \frac{4R\overline{w}}{\nu} \tag{5}$$

and

$$K = \frac{32gSR^2}{\nu\,\overline{w}} \tag{6}$$

Since by Eqs. (2) and (3), $\overline{w}$ is proportional to gS/ν and has a specific value for each channel shape, K is a purely numerical coefficient dependent only on channel shape. Theoretical values of K for several channel shapes are also given in Appendix B. Equation (4) plots as a straight line of slope minus one on full logarithmic paper.

Experiment

Experimental data pertaining to Eq. (4) are plotted on four graphs in Fig. 2; one for rectangular channels, one for triangular channels with 90-degree vertex angle, one for triangular channels with 60- and 120-degree vertex angles, and one for triangular channels with 30- and 150-degree vertex angles. Equation (4), with applicable values of K taken from Appendix B, is also plotted on each of these figures. (The value of K used for the 30- and 150-degree channels is that for the 60-, 90-, and 120-degree channels since the value for the 30- and 150-degree channels has not been computed; this value would seem to be approximately correct in view of Appendix B.) Not shown are similar data for circular-arc and 45-degree vertex angle, triangular channels; these are not sufficiently different from the data shown to warrant another figure, grouping about the line f = 64/Re for the circular-arc channels and falling just below the line f = 57/Re for the triangular channel.

Experimental data pertaining to the solution of Eq. (2) for 90-degree triangular channels are given as velocity profiles in Fig. 3. The experimental points are compared with the theoretical results obtained from Appendix B-3. The experimental data correspond to the points marked I, II, and III on the graph for the 90-degree triangular channel in Figure 2.

(Even though the goal of the present research was to investigate fully developed flow, the lengths of the channels involved made it necessary to accept some data where the boundary layer was clearly still developing. The exact length of the developing laminar boundary layer in a channel is not known. In a circular pipe, the entrance length, in hydraulic diameters, is estimated to be less than a tenth of the Reynolds number.[10] Applying this criterion to the present experiments, it is found that all of the data below a Reynolds number of about 1500 are in fully developed flow; however, as the Reynolds number increases, more and more of the data become influenced by the entrance region, depending on the hydraulic diameter for each experiment. Hence, the gradual departure of the data from the theoretical curves in Fig. 2 at the higher Reynolds numbers is not to be attributed entirely to transition but may be a result of including part of the entrance region in the channel reach for which data were obtained.)

It may be concluded that the theoretical results given by Eqs. (2), (3), (4), and (6) give a good estimate of the actual values in fully developed laminar

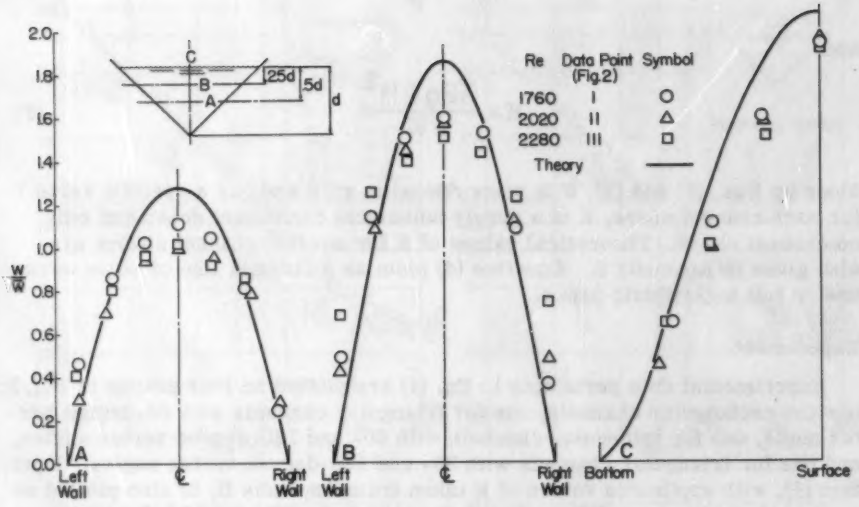

Fig. 3 - Velocity Profiles for Smooth, Laminar Flow

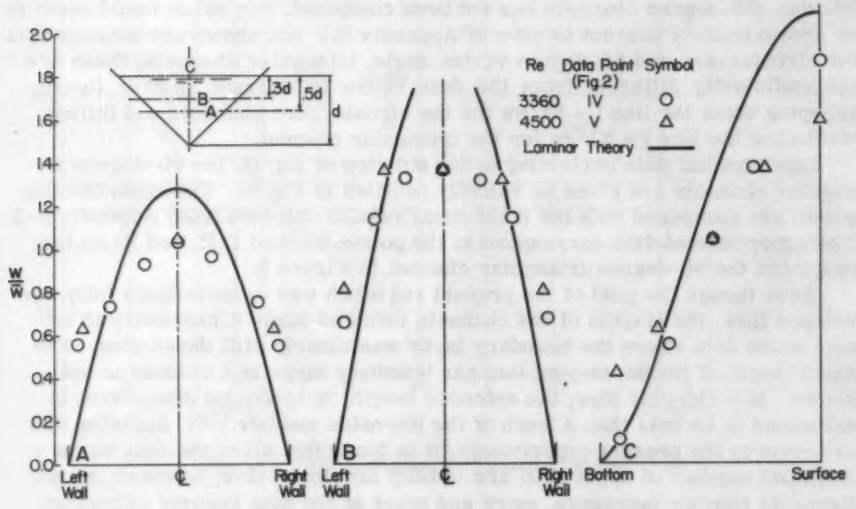

Fig. 4 - Velocity Profiles for Transition Region

flow in open channels. The entire effect of channel shape is given by these equations. The surface effect on the friction factor (which arises from assuming the velocity derivative at the surface is equal to zero and from neglecting surface tension) is minor.

Smooth Channels—Transition to Turbulence

For each of the data points represented in Fig. 2 for the rectangular and 90-degree triangular channels, the observer noted whether the flow appeared to be clearly laminar, clearly turbulent, or some of each. The observation for laminar flow was usually made by observing reflections of a long, straight object aligned with the channel in the liquid surface—an unbroken reflection was taken to indicate pure laminar flow. The data point of highest Reynolds number for which the flow appeared clearly laminar, is indicated by a letter "L" on the symbol for that point.

The solid symbol in Fig. 2 (rectangular channel, $2b/d = 5.1$ at $Re = 2550$) represents data obtained with the bell-mouthed entrance removed. Apparently, the removal of the bell mouth, and thereby the disturbance of the flow at the entrance, did not influence the character of the flow. Had the flow been in a transitional rather than laminar regime, a measurable effect would ordinarily have been expected.

Figure 4 shows velocity profiles corresponding to the data points marked IV and V in the transitional region of Fig. 2 for the 90-degree triangular channel. These are compared with the profiles from laminar theory already shown in Fig. 3. Data point IV is very closely the same as the previously shown laminar flow data, with a slight tendency toward increased velocity nearest the wall. On the other hand, point V shows clearly the higher velocity near the wall characteristic of a turbulent boundary layer.

To determine the Reynolds number of transition unequivocally, it would be necessary to prepare diagrams like those in Fig. 2, from data obtained with sufficient entry length. Transition would then be marked where the experimental data departed from the theoretical line of slope minus one. From the present observations, it appears that there is a shape effect on the Reynolds number of transition. Values in Table I, which follows this section, are estimated from Fig. 2 and from similar figures not presented herein.

For the triangular channels, many more data were available at the 90-degree vertex angle than for the other angles. If equally representative data were available for all channels, it is possible that estimated transitional Reynolds numbers might be lower for the channels of vertex angle different from 90-degrees.

Although the experimental channels were isolation mounted to prevent direct vibration by the pumping equipment, it is believed that there was still enough disturbance present to cause transition at the lowest possible Reynolds number. The values given below are therefore judged indicative of the lower Reynolds number of transition. This appraisal is supported by the solid data point in Fig. 2 already referred to.

Table I

TRANSITION REYNOLDS NUMBER

Rectangular Channel

Depth Ratio	2b/d = 7.4	2b/d = 5.1	2b/d = 3.6	2b/d = 2.7
Transition Re	2350+	3100	3600	2650

Triangular Channel

Vertex Angle	30°	45°	60°	90°	120°	150°
Transition Re	2000	2300	2700	2350	3150	2800

Circular-Arc Channel

Semicircular Arc:	Transition Re = 2200

Smooth Channels—Turbulent Flow

Theory

In the absence of a complete theory of turbulent flow, the value of the Darcy-Weisbach friction factor for open channels can only be estimated on a semi-empirical basis from earlier work on pipes. Such estimates have been made by Keulegan[11] and the subject is discussed by Rouse.[12] Keulegan made use of the logarithmic turbulent velocity profile, assuming this to be adequately descriptive at the velocity everywhere except in the laminar sub-layer; his results are equivalent to

$$\frac{1}{\sqrt{f}} = 2.03 \log \mathrm{Re}\sqrt{f} - 0.99 \qquad (7a)$$

for an average rectangular channel, and to

$$\frac{1}{\sqrt{f}} = 2.03 \log \mathrm{Pe}\sqrt{f} - 0.9 \qquad (7b)$$

for a 90-degree triangular channel, the shape factor being included in the last term. Equation (7b) is identical with the result for a smooth, circular pipe which is usually modified to

$$\frac{1}{\sqrt{f}} = 2 \log \mathrm{Re}\sqrt{f} - 0.8 \qquad (7c)$$

to conform better with experimental results.

For the present purposes where only small Reynolds numbers are involved, a power law profile is adequate and easier to handle than a logarithmic profile. Again, the profile is assumed to be adequately representative of the velocity throughout the channel. The appropriate profile along a normal to a straight wall is

$$\frac{w}{w_*} = B\left(\frac{h w_*}{\nu}\right)^m \tag{8}$$

where $w_* = \sqrt{\tau_0/\rho}$ is the friction velocity, τ_0 is the wall friction per unit area where the normal joins the wall, h is the distance from the wall and B and m are constants. For the smooth, circular pipe, Blasius gives the experimental result

$$f = \frac{0.316}{Re^{1/4}} \tag{9a}$$

where the Reynolds number is based on pipe diameter. Equation (9a) corresponds to B = 8.6, m = 1/7 in Eq. (8). Equation (9a) will also apply to a semicircular channel if there are no secondary currents. For a very wide channel the profile, Eq. (8), with B = 8.6 and m = 1/7 will yield

$$f = \frac{0.333}{Re^{1/4}} \tag{9b}$$

If the velocity profile is taken along a line other than a normal to a wall, Eq. (8) will no longer apply directly. For example, for the vertical profile along the line of symmetry of a 90-degree triangular channel, the velocity at any point P is given by Eq. (8) with $h = y/\sqrt{2}$. However, w_* varies from the vertex to the free surface. If $\bar{w}_*$ is the mean friction velocity defined by

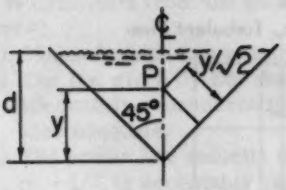

$$\bar{w}_* = \sqrt{\bar{\tau}_0/\rho} = \sqrt{RgS}$$

$$\frac{w_*}{\bar{w}_*} = F\left(\frac{y}{d}\right) \approx \left(\frac{Gy}{d}\right)^p \text{, roughly}$$

where G and p are empirical constants which measure the distribution of friction velocity along the wall. Using the above relation and with b = 8.6, m = 1/7, the profile along the line of symmetry of a 90-degree triangular channel is

$$\frac{w}{\bar{w}_*} = 8.2\left(\frac{G\nu}{d\bar{w}_*}\right)^{8p/7}\left(\frac{y\bar{w}_*}{\nu}\right)^{(1+8p)/7} \tag{10}$$

Experiment

In Fig. 5, experimental data for various rectangular and triangular channels in the lower turbulent Reynolds number range are presented as graphs of friction factor versus Reynolds number. Equation (9a) is plotted for comparative purposes on all of the graphs and Eq. (9b) is also plotted on one of them. Similar data obtained for circular-arc channels and for 45-degree

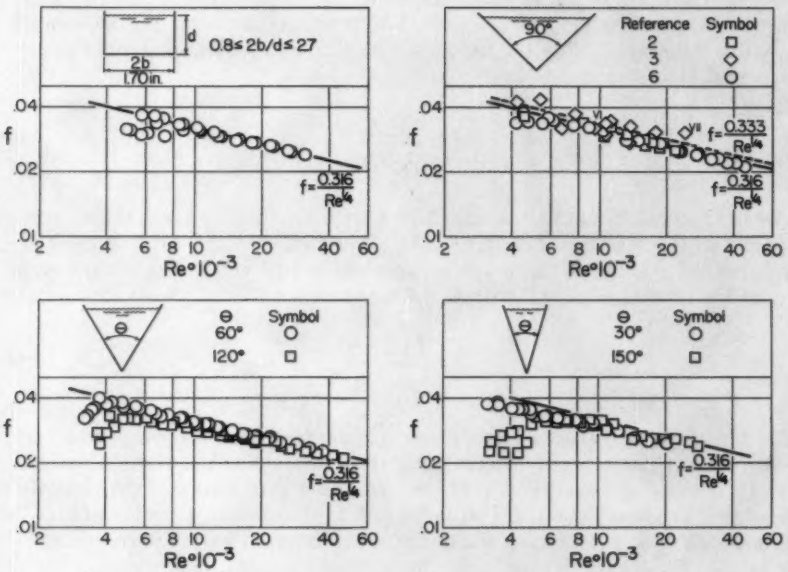

Fig. 5 – Friction Factor for Smooth, Turbulent Flow

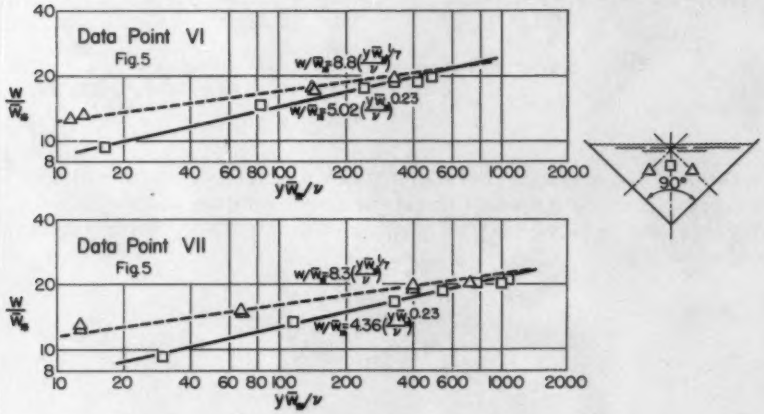

Fig. 6 – Velocity Profiles for Smooth, Turbulent Flow

triangular channels are not shown in the figures. For comparison Keulegan[11] gives the equivalent of

$$f = \frac{0.325}{Re^{1/4}}$$

as the mean line of all of Bazins' data on smooth rectangular channels. The data in Fig. 5 could be represented equally well by Eqs. (7a) and (7b) for the rectangular and triangular channels, respectively.

In Fig. 6, velocity profiles are shown for two of the data points for the 90-degree triangular channel. Profiles both normal to the wall and along the line of symmetry are plotted on full logarithmic paper to facilitate comparison with Eqs. (8) and (10). The experimental data yield m = 1/7 and p = 0.076; B = 8.3 and 8.8 for the two separate graphs, but if the two sets of data were superimposed on one graph, B = 8.6 would adequately describe the average line through the data along the normals; G = 1.14 or 1.36 for the two graphs. (It is to be noted that the least accurate data in these experiments is the measurement of the slope. This measurement enters directly into the computation of $\overline{w}_*$ so that the coefficients B and G, as determined in Fig. 6 are less accurate than the exponents, m and p.)

It is believed that the entrance length problem in the turbulent-flow region was minor. In smooth pipes with disturbed entrance conditions at a Reynolds number of the order of 10^4, only 12 diameters are required theoretically for the wall friction to become equal to its value in fully developed flow.[13] Furthermore, the velocity profiles shown in Fig. 6 are characteristic of fully developed turbulent flow.

It is concluded from the data in Figs. 5 and 6 that at these small Reynolds numbers:

(a) Channel shape has relatively little influence on frictional loss.
(b) The law given by Eq. (9a) for the friction factor for smooth pipes is adequately representative of all smooth channels. Equation (7c) is also adequate.
(c) The power law velocity distribution given by Eq. (8) with $B \approx 8.6$ and m = 1/7 is acceptably representative of the true velocity distribution except near the free surface.

Rough Channels—Laminar Flow

Theory

Following a familiar line of reasoning for rough pipes,[14] the velocity in a 90-degree triangular channel at a distance from the wall equivalent to the roughness height, k, is approximately (from Appendix B-3),

$$w_k = 10 \frac{k}{d} \overline{w}$$

where d is the depth of liquid in the channel and $k/d << 1$. The relative roughness is then given by the tip Reynolds number of the roughness and is

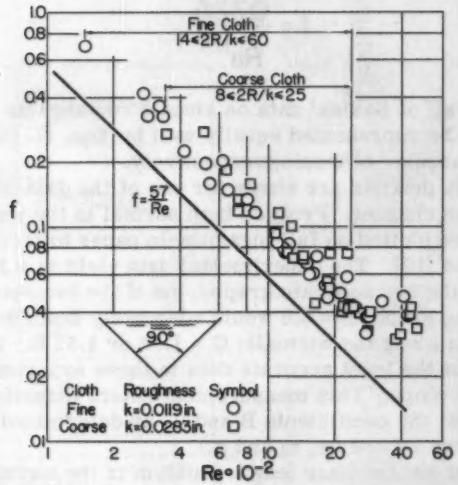

Fig. 7 - Friction Factor for Rough, Laminar Flow

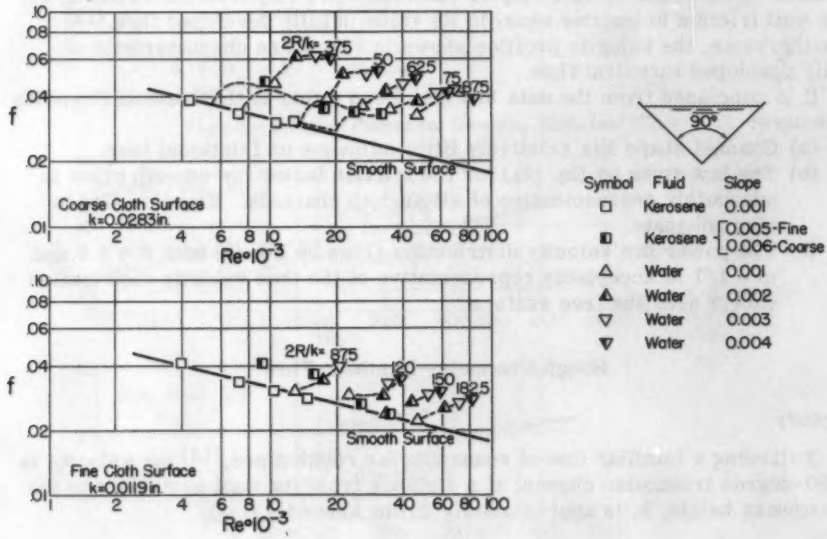

Fig. 8 - Friction Factor for Rough, Turbulent Flow Using Abrasive Cloth Roughness

$$Re_k = \frac{w_k k}{\nu} = 7.1\left(\frac{k}{d}\right)^2 \cdot \frac{4R\bar{w}}{\nu} = 7.1\left(\frac{k}{d}\right)^2 \cdot Re$$

assuming that the presence of the roughness does not affect the flow. There is, presumably, some critical value of the tip-roughness Reynolds number below which the laminar flow is practically undisturbed by the wakes of the roughness elements. Calling this critical value Re_{kc},

$$k < \left(\frac{Re_{kc}}{7.1\,Re}\right)^{1/2} \cdot d, \quad \text{or} \quad \frac{2R}{k} > \left(\frac{3.55\,Re}{Re_{kc}}\right)^{1/2} \tag{11}$$

in order for the laminar flow to be uninfluenced by the roughness. The critical roughness Reynolds number must depend on the shape and spacing of the roughness elements.

If the roughness height is greater than the value given by Eq. (11), the friction factor can be expected to be larger than the calculated value for laminar flow, and the velocity profile near the wall can be expected to be shifted away from the wall. No theoretical method is available for computing the magnitude of these effects; not only the roughness height, but also its shape and spacing will enter into the result.

Experiment

A series of experiments were conducted in the 90-degree triangular channel previously described, using rough surfaces. The surfaces were prepared by cementing abrasive cloth to the smooth channel walls. Sharp-edged particles constituted the abrasive material. Two grades of cloth were used; specifications are contained in the following table.

Table II

DESCRIPTIVE TABULATION OF ROUGH SURFACES

Grade of Cloth	Range of Grain Diameter Inches	Approximate Mean Diameter Inches	Approximate Mean Spacing Inches
Fine	0.0105–0.0132	0.0119	0.0144
Coarse	0.026–0.0307	0.0283	0.0386

Results of the experiments at Reynolds numbers below 5000 are given in Fig. 7 as a plot of friction factor versus Reynolds number. The channel bottom is taken at the base of the roughness elements in calculating the data. Velocity profiles were not measured. The theoretical result for laminar flow in smooth, 90-degree triangular channels is shown for comparison by the heavy line in Fig. 7. There is little doubt that the roughness of the type used has influenced the laminar flow.

If the friction factor and Reynolds number for the data in Fig. 7 are recalculated, taking the channel bottom at the tips of the roughness elements,

the data are brought closer to the theoretical line, but the fine cloth data lie generally above the coarse cloth data.

(It should be noted that some of the divergence of the experimental data in Fig. 7 might be attributable to a too short entry length, as was the case in Fig. 2. The entry length for these rough channel data was 11 ft; this corresponds to a range of from 80 hydraulic diameters at some of the high Reynolds numbers to 400 hydraulic diameters at the smaller Reynolds numbers. There is, thus, some possible effect of entry length especially for Reynolds numbers above 2000.)

It is concluded from Eq. (11) that the critical-roughness Reynolds number is less than two for the roughness used herein. This value is of smaller order than has previously been assumed for uniform sand roughness in pipes.[14]

Rough Channels—Turbulent Flow

Theory

No completely satisfactory theory for rough, turbulent flow exists, even for pipes. It has become common practice to describe a rough surface by the height k, or nominal height k_s, of the roughness particles. Although this practice facilitates correlating friction loss data in special cases, it must be used with caution in dealing with arbitrarily rough surfaces. Even when using surfaces roughened artificially in systematic pattern, generally more than a single linear dimension is required to describe the roughness geometrically; equations or formulas for friction loss which contain only the single roughness parameter k or k_s cannot, therefore, be expected to be generally valid under all conditions. Although formulas involving two or more linear roughness measures have been proposed (by Morris,[15] for example) and even appear to be verified by some of the experimental data which follow, these formulas have not been sufficiently tested to warrant publication as recognized theory.

The most satisfactory investigation of rough surfaces to date has been that of Nikuradse for closely packed, uniform sand grains in pipes. Here, the one linear dimension k does suffice to measure the roughness because of the uniform shape and close packing of the grains. When the surface is sufficiently rough, Nikuradse's data are represented by[16]

$$\frac{1}{\sqrt{f}} - 2\log\frac{2R}{k} = 1.74 \qquad (12)$$

This equation represents the well-known flow regime where the friction factor has become independent of the Reynolds number and depends only on the relative roughness of 2R/k. Based on Keulegan's analysis,[11] the above equation may also be applied directly to a 90-degree triangular channel. Since this paper is primarily concerned with flow at small Reynolds numbers, Eq. (12) represents a limiting case, and this only for roughness of the type studied by Nikuradse.

For surfaces other than those composed of uniform sand grains, it is common practice to replace k in Eq. (12) by k_s, the nominal roughness size; k_s is determined empirically for each surface from experimental data in

order to make Eq. (12) valid. (It is sometimes necessary to go to extremely high Reynolds numbers to accomplish this, and then the region of constant friction factor may be approached either from below or from above.)

Between the region of applicability of Eq. (12) for rough flow and Eq. (7c) for smooth flow, there exists a flow regime where both viscosity and roughness influence the friction factor. It is this regime that is mainly involved in the present paper. Except for Nikuradse's data on uniform sand-grain roughness in pipes, satisfactory correlation of data in this region has not been attained. It can be expected that the relation between the friction factor and Reynolds number will depend on many factors, such as the form of the roughness, its average size, the average spacing of the separate elements and their relative orientation, and of course, on the viscosity and velocity. As a matter of fact, the relative roughness size can no longer be expressed as a function of the channel size only, but must be measured with respect to the thickness of the laminar sublayer of the flow. Thus, for uniform sand grains, the relative roughness can be expressed as[16]

$$\frac{k}{\nu/\bar{v}_*} = \frac{Re\sqrt{f}}{2R/k} \qquad (13)$$

This parameter, when plotted against the left side of Eq. (12) does correlate Nikuradse's uniform sand-grain data. The resulting experimental curve becomes asymptotic to Eq. (12) when the relative roughness given by Eq. (13) is equal to about 400 and to Eq. (7c) when the relative roughness is about 16.

For other types of roughness, the substitution of k_s for k in the definition of relative roughness, as is sometimes done, can hardly be expected to produce the same correlation as for uniform sand grains, except in fortuitous circumstances.

Experiment

Two sets of experiments with rough surfaces in triangular channels have been completed. Both of these involved measurements of bulk-flow quantities only, and not of velocity profiles. One set was part of the study already introduced in the section "Rough Channels—Laminar Flow," using abrasive cloths as the surface roughness. Typical data from these experiments are shown in Fig. 8 as graphs of friction factor versus Reynolds numbers. Depths have been taken to the bottom of the roughness elements in these graphs. The lines of constant 2R/k have been drawn on the graphs considering unplotted as well as plotted data points.

The second set of experimental data was obtained in the triangular channel of variable cross section using strip roughness elements. The strip roughness elements of square cross section were laid completely across the channel walls with their long dimension normal to the flow direction. Three spacings along the channel were used. Typical experimental data are shown in Fig. 9 as graphs of friction factor versus Reynolds number for the 90-degree channels at the three different spacings. Other typical data, showing the effect of channel shape, are presented in Fig. 10. Depths have been taken to the tops of the strips in Figs. 9 and 10.

In general, the data presented in Figs. 8 to 10 have not yet reached sufficiently high Reynolds numbers for Eq. (12) to apply. Even those few data

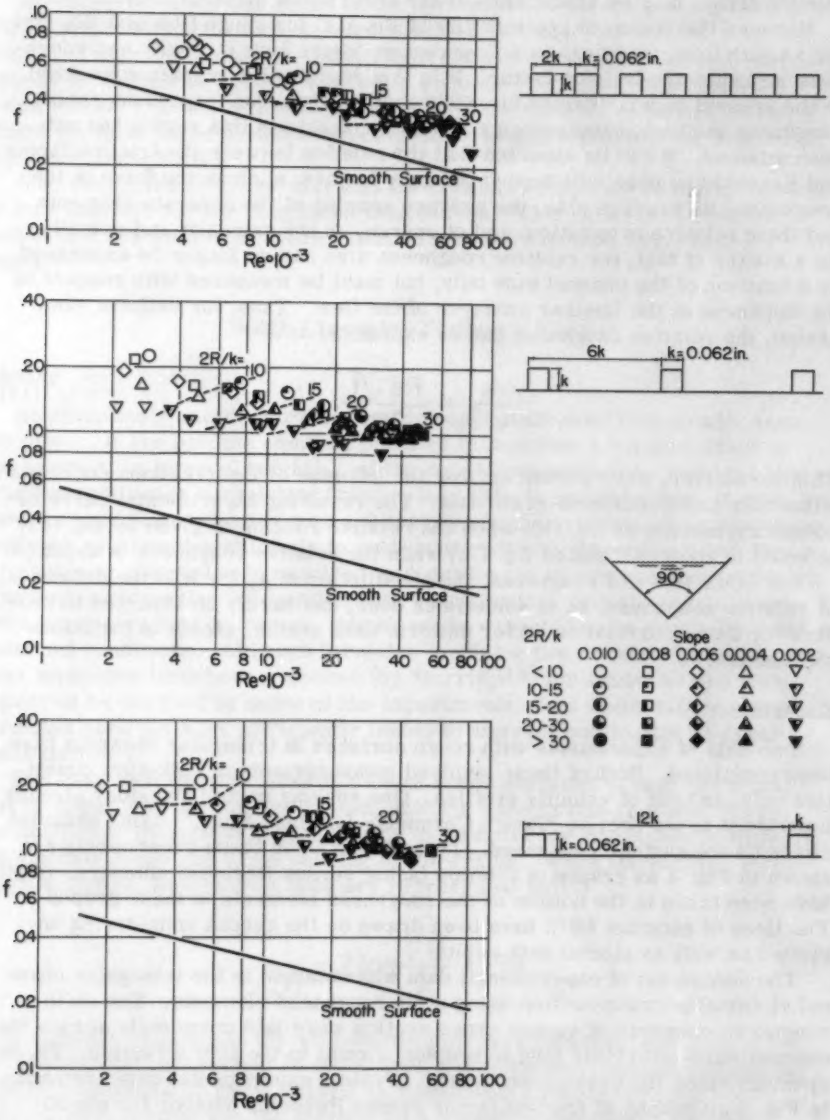

Fig. 9 – Friction Factor for Rough, Turbulent Flow Using Strip Roughness

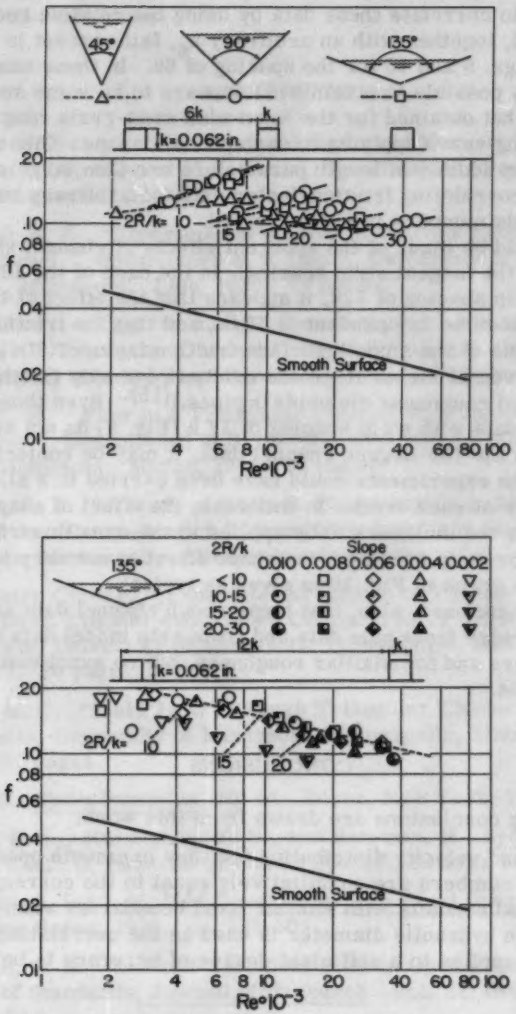

Fig. 10 – Friction Factor for Rough, Turbulent Flow as Influenced by Channel Shape

which appear to indicate that a constant friction factor may have been reached should be looked upon with caution because of the small number of data points involved.

Any attempt to correlate these data by using the relative roughness defined by Eq. (13), together with an arbitrary k_s, fails except in the cases of the graphs of Figs. 9 and 10 for the spacing of 6k. In these cases, by choosing $k_s = 6k$, it is possible to obtain what appears to be some sort of correlation similar to that obtained for the Nikuradse sand-grain roughness, a different correlating curve applying to each channel shape. Other methods of correlation using additional length parameters are also largely futile. Hence, the problem of correlating friction-factor data for arbitrary rough surfaces at small Reynolds numbers is still unsolved.

Mention should be made of the apparent effects of channel shape, especially as shown for the largest strip spacing. In the case of the 135-degree channel with strip spacing of 12k, it appears that the effect of the strips eventually will become independent of $2R/k$, and that the friction factor will become a multiple of the smooth surface friction factor. (Similar results have been observed at higher Reynolds numbers for ship roughness[17] and for widely spaced roughness elements in pipes.)[15] Even though the 90-degree channel data with strip spacing of 12 k (Fig. 9) do not appear to follow the same law as the 135-degree channel data, it may be conjectured that they would do so if the experiments could have been carried to a slightly higher Reynolds number at each depth. In that case, the effect of shape would be simply to change the multiples to be applied to the smooth surface curve.

At the smaller strip spacings, the shape effect is not very pronounced, and only the one graph in Fig. 10 is given as typical.

It might be mentioned, also, that these rough channel data are not too different in appearance from pipe data and from ship model data at similar Reynolds numbers and for similar roughness, but no exact comparison is obtainable, as yet.

CONCLUSIONS

The following conclusions are drawn from this work:

1. Friction and velocity distribution for flow in smooth open channels at small Reynolds numbers are quantitatively equal to the corresponding values for flow in closed conduits with similar fixed boundaries when the Reynolds number based on hydraulic diameter is used as the correlating parameter. This statement applies to a sufficient degree of accuracy to both laminar and turbulent flow.

2. Friction in rough channels may be similar to friction in rough pipes or on rough plates, but there being no suitable correlating parameter for rough flow available, even for pipes, it is not feasible to make a comparison at this time. There is great need for the development of a means to correlate rough flow data in the region where viscous influences are still important.

3. Shape of the channel does not have an important influence on friction for turbulent flow in smooth channels at small Reynolds numbers; it does have some effect on friction in rough channels. Shape is quite important for laminar flow. The entire effect of shape in laminar flow may be computed theoretically; some results are given in Appendix B.

4. The lower critical Reynolds number for transition between laminar and turbulent flow in smooth channels depends to some extent on channel shape. The value varies from 2000 to over 3000, being generally larger than the value for closed conduit flow.

REFERENCES

1. Silberman, Edward. "Experimental Studies of Viscous Flow in Open Channels." Unpublished M.S. thesis, University of Minnesota, Minneapolis, Minnesota. 1936. 51 pages.
2. Anderson, S. H. "Experimental Studies of Viscous Flow in a Triangular Open Channel." Unpublished M.S. thesis, University of Minnesota, Minneapolis, Minnesota. June, 1939. 71 pages.
3. Purdy, Harry. "Experimental Studies of Velocity Distribution at a Section in a 90° Triangular Channel." Unpublished M.S. thesis, University of Minnesota, Minneapolis, Minnesota. 1947. 108 pages.
4. Forns, J. M. "Flow in a Triangular Channel with Varied Boundary Roughness." Unpublished M.S. thesis, University of Minnesota, Minneapolis, Minnesota. March, 1948. 99 pages.
5. Donovan, D. K. "A Study of Viscous Flow in an Open Channel having a Circular Arc Cross-Section." Unpublished M.S. thesis, University of Minnesota, Minneapolis, Minnesota. September, 1949. 67 pages.
6. Feng, Peter Chi-Te. "Experimental Studies of Viscous Flow in a Triangular Open Channel with Varied Central Vertex Angle." Unpublished M.S. thesis, University of Minnesota, Minneapolis, Minnesota. December, 1952. 66 pages.
7. Nelson, H. C. "Fluid Flow in Rough Triangular Channels." Unpublished M.S. thesis, University of Minnesota, Minneapolis, Minnesota. March, 1953. 131 pages.
8. Lamb, H. Hydrodynamics, 6th ed., Dover, New York, 1945. p. 577 (Eq. 4).
9. Dryden, H. L., Murnaghan, F. D., and Bateman, H. Hydrodynamics, Part II, Chap. II, National Research Council, Bulletin No. 84. 1932.
10. Goldstein, S. (ed.) Modern Developments in Fluid Dynamics, Oxford, Clarendon Press, 1938. pp. 301-304.
11. Keulegan, G. H. "Laws of Turbulent Flow in Open Channels," U. S. Bureau of Standards, Journal of Research. Vol. 21, (December, 1938), pp. 707-741.
12. Rouse, H. Elementary Mechanics of Fluids, John Wiley and Sons, Inc. New York. 1946. pp. 214-216.
13. Holdhusen, J. S. "The Turbulent Boundary Layer in the Inlet Region of Smooth Pipes." Unpublished Ph.D. thesis, University of Minnesota, Minneapolis, Minnesota. February, 1951. 83 pages.
14. Goldstein, S. (ed.) Modern Developments in Fluid Dynamics, Oxford, Clarendon Press, 1938. p. 311.

15. Morris, H. M. "A New Concept of Flow in Rough Conduits," Ph.D. thesis, University of Minnesota, Minneapolis, Minnesota. October, 1950. 151 pages. Also, in ASCE Proc. separate No. 390. January, 1954. 31 pages.

16. Rouse, H. Elementary Mechanics of Fluids, John Wiley and Sons, Inc. New York. 1946. pp. 205-206.

17. Proceedings, Seventh International Congress on Ship Hydrodynamics, Goteborg, Sweden, 1955. 333 pages. Part II, "Friction and Turbulence Stimulation," pp. 55-128.

18. Nuttal, H. "Flow of a Viscous Incompressible Fluid: Expressions for a Uniform Triangular Duct." Engineering, Vol. 178, No. 4623, pp. 299-300. September 3, 1954.

19. Synge, J. L. "Flow of Viscous Liquid Through Pipes and Channels." Proceedings of Symposia in Applied Mathematics. Vol. IV, 1953. pp. 141-165.

APPENDIX A

LIST OF SYMBOLS

A	Cross-sectional area of channel.
b	Half-width of channel.
B	Constant coefficient in power low velocity distribution.
C	Chezy's C.
d	Depth of water in channel.
f	Darcy-Weisbach friction factor.
G	Constant.
g	Acceleration of gravity.
h	Distance measured normally to a wall.
k	Height of roughness element.
k_s	Equivalent sand roughness height.
K	Parameter in $f = K/Re$.
m	Exponent in power low velocity distribution.
n	Manning's n.
p	Exponent.
R	Hydraulic radius.
Re	Reynolds number = $4R\,\overline{w}/\nu$.
S	Channel and energy slope.
w	Local velocity parallel to channel axis.

$\overline{w}$	Mean velocity parallel to channel axis.
w_k	Velocity at distance k from wall (at tips of roughness elements).
w_*	Friction velocity = $\sqrt{\tau_o/\rho}$
$\overline{w}_*$	Mean friction velocity over channel walls.
x, y, z	Coordinate axes—z parallel to flow direction, yz plane vertical with origin at free surface.
ν	Kinematic viscosity of liquid.
ρ	Density of liquid.
τ_o	Wall shear stress.
$\overline{\tau}_o$	Mean shear stress over channel walls.

APPENDIX B

FLOW PARAMETERS FOR SEVERAL OPEN CHANNEL SHAPES

Analytically Derived Solutions

1. Semicircular Channel

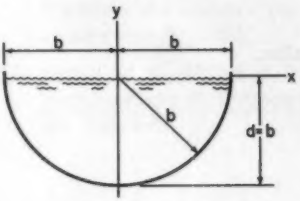

$$w = \frac{gS}{4\nu} b^2 \left(1 - \frac{x^2}{b^2} - \frac{y^2}{b^2}\right)$$

$$\bar{w} = \frac{gS}{8\nu} b^2$$

$$K = 64$$

2. Rectangular Channel

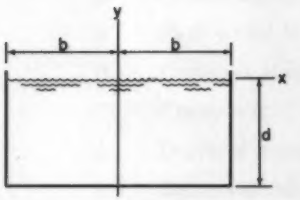

$$w = \frac{gS}{2\nu} d^2 \left(1 - \frac{y^2}{d^2} - \frac{32}{\pi^3} \sum_{n=0}^{\infty} \frac{(-1)^n}{(2n+1)^3} \frac{\cosh \frac{2n+1}{2} \frac{\pi x}{d}}{\frac{2n+1}{2} \frac{\pi b}{d}} \cos \frac{2n+1}{2} \frac{\pi y}{d}\right)$$

$$\bar{w} = \frac{gS}{3\nu} d^2 \left(1 - \frac{192}{\pi^5} \frac{d}{b} \sum_{n=0}^{\infty} \frac{1}{(2n+1)^5} \tanh \frac{2n+1}{2} \frac{\pi b}{d}\right)$$

$$K = \frac{96}{\left(1 + \frac{b}{d}\right)^2} \frac{1}{1 - \frac{192}{\pi^5} \frac{d}{b} \sum_{n=0}^{\infty} \frac{1}{(2n+1)^5} \tanh \frac{2n+1}{2} \frac{\pi b}{d}}$$

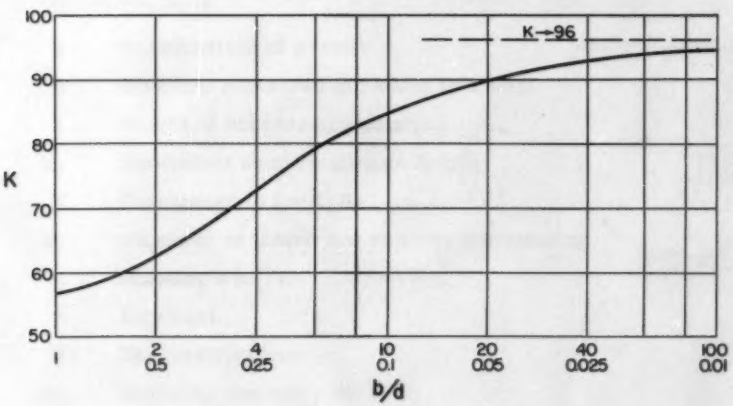

3. 90-Degree Triangular Channel (Symmetrical)

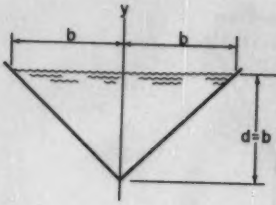

$$w = \frac{gS}{4\nu} d^2 \left(1 - \frac{(x+y)^2}{d^2} - \frac{32}{\pi^3} \sum_{n=0}^{\infty} \frac{(-1)^n}{(2n+1)^3} \frac{\cosh \frac{2n+1}{2} \frac{\pi(x-y)}{d}}{\cosh \frac{(2n+1)}{2} \pi} \cos \frac{2n+1}{2} \frac{\pi(x+y)}{d}\right)$$

$$\bar{w} = \frac{gS}{1422\nu} d^2$$

$$K = 56.9$$

4. 60-Degree Triangular Channel (Vertical Leg)

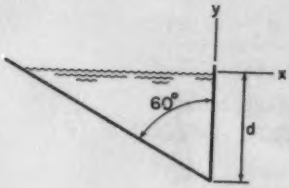

$$w = \frac{\sqrt{3}gS}{12\nu} x d \left(\frac{x^2}{d^2} + 2\sqrt{3}\frac{x}{d} + 3 - 3\frac{y^2}{d^2}\right)$$

$$\bar{w} = \frac{gS}{20\nu} d^2$$

$$K = 53\tfrac{1}{3}$$

5. Elliptical Channel

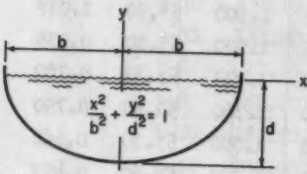

$$w = \frac{gS}{2\nu} \frac{b^2 d^2}{b^2 + d^2} \left(1 - \frac{x^2}{b^2} - \frac{y^2}{d^2}\right)$$

$$\bar{w} = \frac{gS}{4\nu} \frac{b^2 d^2}{b^2 + d^2}$$

$$K = \frac{128\left(1 + \frac{b^2}{d^2}\right)}{\left(1 + \frac{b^2}{d^2}\right)\left[1 + \frac{1}{4}\left(\frac{b-d}{b+d}\right)^2 + \frac{1}{64}\left(\frac{b-d}{b+d}\right)^4 + \frac{1}{256}\left(\frac{b-d}{b+d}\right)^6 + \cdots\right]}$$

6. Edge or Bottom of Triangular Channel

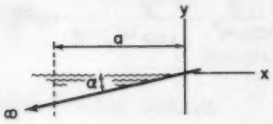

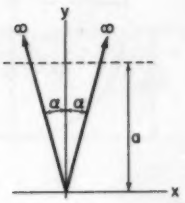

$$w = \frac{gS}{2\nu}\,\frac{x^2\tan^2\alpha - y^2}{1-\tan^2\alpha}$$

$$\bar{w} = \frac{gS}{6\nu}\,\frac{\sin^2\alpha}{\cos 2\alpha}\,a^2$$

$$K = 48\cos 2\alpha$$

$\alpha < \frac{\pi}{4}$

Numerical Solutions

7. Triangular Channel (Vertical Leg)

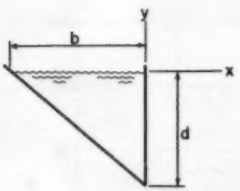

$$\bar{w} \approx \frac{qgS}{81\nu}\,\frac{b^3}{d}$$

Values of K and $q^{2!}$

b/d	K	q	b/d	K	q
0.577	50.3	4.837	1.500	53.50	1.027
0.650	50.5	4.095	1.580	53.20	0.935
0.750	50.9	3.347	1.732	53.33	0.780
0.830	51.6	2.850	1.760	53.50	0.750
1.000	52.6	2.113	1.880	53.10	0.662
1.110	53.4	1.752	2.000	53.60	0.497
1.200	54.0	1.520	2.500	54.20	0.285
1.300	54.0	1.320	3.000	55.40	0.225

8. 60-Degree Triangular Channel (Symmetrical)

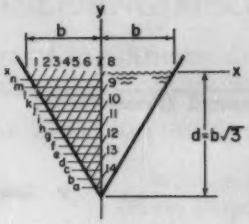

$$w = \frac{gS}{6000\nu} b^2 H$$

$$\bar{w} \approx \frac{gS}{94\nu} b^2$$

$$K \approx 56.6$$

Values of H determined by relaxation
(H = 0 at all boundary points)

Pt	H	Pt	H	Pt	H
b-14	18.22	i-10	231.50	m-5	229.25
c-13	34.33	j-6	95.11	m-6	280.00
d-12	48.22	j-7	169.55	m-7	314.75
d-13	64.44	j-8	223.00	m-8	332.25
e-11	60.67	j-9	255.25	n-2	74.88
e-12	91.11	j-10	266.00	n-3	149.00
f-10	71.67	k-5	95.67	n-4	215.50
f-11	114.55	k-6	173.00	n-5	270.50
f-12	128.77	k-7	232.00	n-6	311.50
g-9	80.55	k-8	271.50	n-7	336.75
g-10	134.22	k-9	291.50	n-8	345.25
g-11	161.00	ℓ-4	94.00	x-1	51.22
h-8	87.44	ℓ-5	171.55	x-2	121.55
h-9	150.00	ℓ-6	234.25	x-3	190.00
h-10	187.50	ℓ-7	280.00	x-4	249.75
h-11	200.00	ℓ-8	307.75	x-5	297.25
i-7	92.22	ℓ-9	317.25	x-6	330.00
i-8	161.77	m-3	87.00	x-7	346.75
i-9	208.25	m-4	164.33		

9. 120-Degree Triangular Channel (Symmetrical)

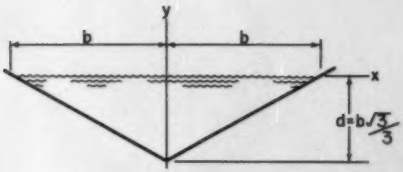

w: Same as 8, above.

$\overline{w} \approx \frac{gS}{9.4\nu} d^2$

$K \approx 56.6$

10. Trapezoidal Channel with 60-Degree Sides

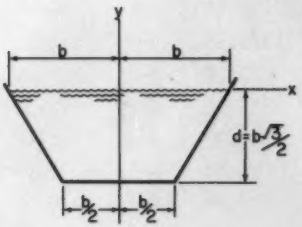

w: Footnote 22

$\overline{w} \approx \frac{8gS}{5\nu} b^2$

$K = 60$

Journal of the
ENGINEERING MECHANICS DIVISION
Proceedings of the American Society of Civil Engineers

LATERAL BRACING FORCES ON BEAMS AND COLUMNS

William Zuk*
(Proc. Paper 1032)

SUMMARY

Slender beams and columns are generally braced against buckling to increase their strength. Yet little is known about the magnitude of the bracing force. Its magnitude is usually assumed to be some small value based on engineering judgment.

It is thus the purpose of this paper to derive quantitatively the amounts of bracing force required for eight representative cases of beams and columns. Some of the cases are solved exactly by the direct solution of the basic differential equations, while others are solved approximately by energy methods. In all cases, the behavior is assumed elastic.

Several numerical examples are included which show that the order of magnitude of these bracing forces is small and falls within a limited range.

INTRODUCTION

In the professional practice of structural engineering, there often arise situations where it is difficult to decide whether or not adequate lateral support exists. Some examples of questionable lateral support are the following.

(a) If a beam has welded or clipped to its top flange a light gage metal deck, is this flexible decking adequate to provide lateral support?
(b) If a tie rod is attached to the web of a beam at its neutral axis, is the rod effective as a lateral support?
(c) If a column is embedded in a masonry wall which has a large opening several feet away, is there sufficient masonry between the column and the opening to act as a lateral support?

Heretofore, the designer relied on experience or "rules of thumb" to provide such information. Although this paper is not attempting to offer a

Note: Discussion open until December 1, 1956. Paper 1032 is part of the copyrighted Journal of the Engineering Mechanics Division of the American Society of Civil Engineers, Vol. 82, No. EM 3, July, 1956.

* Associate Prof. of Civ. Eng., Univ. of Virginia, Charlottesville, Va.; formerly Instructor and Graduate Student, Dept. of Struct. Eng., Cornell Univ., Ithaca, N. Y.

complete answer to the question of lateral bracing, it is attempting by the analysis of eight typical cases, to determine a general relationship of the applied force or moment on the member to the lateral bracing force.

Theory shows that prior to buckling, beams or columns which are truly straight exert no force whatsoever on the lateral bracing. Only members with initial crookedness or initial eccentricities of load cause such lateral forces. Thus in all cases to be considered, the member will be assumed initially crooked. Since in reality all members do possess some imperfection, this condition is in no sense a limitation. The analysis, however, will be limited to elastic materials and "small deflections".

Typical Cases

CASE I—Column with a concentric axial load and an immovable point support at mid-height.

Referring to Figure 1, the differential equations of equilibrium are as follows:

Between $x = 0$ and $x = L/2$

$$B_1 \frac{d^2y}{dx^2} = - P (y_0 + y_1) + \frac{Fx}{2}$$

Between $x = L/2$ and $x = L$

$$B_1 \frac{d^2y}{dx^2} = - P (y + y_2) + \frac{Fx}{2} - F (x - L/2)$$

where y_1 and y_2 are additional deflections due to P,

y_0 is the initial crookedness assumed as " $a \sin \frac{x}{L}$ ",

and $B_1 = EI$. (Flexural Rigidity)

The boundary and continuity conditions are as follows:

at $x = 0$, $y_1 = 0$, $\frac{d^2y_1}{dx^2} = 0$

at $x = L/2$, $y_1 = y_2 = 0$, $\frac{d\,y_1}{dx} = \frac{d\,y_2}{dx}$

at $x = L$, $y_2 = 0$, $\frac{d^2y_2}{dx^2} = 0$

The solution of these differential equations yields the following:

$$F = \frac{2p^3 L^2 a \left[1 + \cos pL + 2 \sin^2 \frac{pL}{2} \right]}{(\pi^2 - p^2L^2) \left[\frac{2 \tan \frac{pL}{2}}{B_1 p^2} - \frac{L}{2B_1 p} - \frac{L \cos p\,L}{2B_1 p} - \frac{L \sin^2 \frac{pL}{2}}{B_1 p} \right]} \qquad (1.1)$$

where $p = \frac{P}{B_1}$

The expression (1.1) is of course too complex for general use. However,

if the critical elastic buckling load $P = \frac{4\pi^2 B_1}{L^2}$ is substituted, the expression reduces to

$$F \max = \frac{64\pi^2 B_1 a}{3L^3} \tag{1.2}$$

It is noted that the lateral force is a direct function of the initial crookedness "a".

CASE II—Column with a concentric axial load and a continuous immovable lateral support.

Refer to Figure 2. Since the support is rigid, no bending moments in the column are involved. Thus the forces on an element of the column are as shown in Figure 2a. From equilibrium, $-P\frac{d^2y_0}{dx^2}\,dx = f\,dx$, where "f" is the lateral force per unit length. Thus $f = -P\frac{d^2y_0}{dx^2}$

Assuming $y_0 = a \sin\frac{\pi x}{L}$, $f = \frac{\pi^2}{L^2}$ Pa $\sin\frac{\pi x}{L}$ (2.1)

The maximum unit lateral force is at the center and is equal to

$$f_1 = \frac{\pi^2 Pa}{L^2} \tag{2.2}$$

However, it can be shown that for another shape of initial crookedness, such as $y_0 = \frac{4a}{L^2}(xL - x^2)$ which satisfies the boundary conditions, the lateral force is a constant, namely $f = \frac{8Pa}{L^2}$.

However, here again in each case, the lateral force is a direct function of the magnitude of the initial crookedness at the center.

CASE III—Column with a concentric axial load and an elastic lateral support at mid-height.

Refer to figure 3. This case has been solved by Winter, Green, and Cuykendall[1] and is given here only for comparison and completeness. It has been demonstrated in Ref. (1) that the initial crookedness "a" in columns elastically braced as in this case, may be multiplied by the factor $\frac{1}{1-\mu}$ to obtain the total deflection.

The quantity $$\mu = \frac{P}{P(\text{critical})}$$

Thus $$\delta = a\,\frac{\mu}{1-\mu} \text{ and } F = k_1 a\,\frac{\mu}{1-\mu} \tag{3.1}$$

where k_1 is the elastic spring constant, and the initial crookedness is affine with the buckling mode.

It is then only necessary to know the critical buckling load of the elastically supported column to obtain the lateral force. The approximate value of

$$P(cr) = \frac{\pi^2 B_1}{L^2} + \frac{3}{16} k_1 L \tag{3.2}$$

This critical value applies, however, only for values of the spring constant not exceeding $\frac{16\pi^2 B_1}{L^3}$ (3.3)

Thus within this limitation

$$F = \frac{16\, a\, k_1\, PL^2}{16\pi^2 B_1 + 3k_1 L^3 - 16PL^2} \tag{3.4}$$

In connection with the application of (3.4), several limitations should be mentioned. First, the equation is not valid when "P" approaches "$P_{(cr.)}$", as the deflection and the lateral force would then become infinite. Secondly, the spring constant k_1 must be smaller than the critical value determined by (3.1). If the spring constant exceeds this critical value, the column will buckle as in curve (3) rather than (2) in figure 3. For this case, the lateral force may be determined approximately by utilizing the results of Case I, as follows.

Let $a_1 = a + \frac{F}{k_1}$, where a_1 is the total deflection at center of the column. Since in expression (1.2), "F" varies linearily with the lateral position of the bracing force, "a_1" as defined may be substituted for "a" as it appears in (1.2). The small approximation involved is that "a" in (1.2) is due to a no stress condition; whereas in this case, "a_1", is partly due to the elastic stresses. However, it can be demonstrated that the error is small and always on the safe side.

Letting $\psi = \frac{64\pi^2 B_1}{3L^2}$

$$F_{max} = a\, \frac{\psi}{1 - \frac{\psi}{k_1}} \tag{3.5}$$

It is seen that for the same applied load, the effect of the elastic support is to increase the value of the lateral force over that of the immovable support.

CASE IV—Column with a concentric axial load and a continuous elastic support.

Refer to figure 4.

Reasoning as in Case III, the maximum lateral force per unit length,

$$f_1 = k_1\, a_n\, \frac{\mu}{1 - \mu} \tag{4.1}$$

where "a_n" is the largest initial crookedness affine with the buckling mode.

Again as in Case III, it is only necessary to determine the critical buckling load. This is known to be[2]

$$P_{(cr.)} = \frac{\pi^2 B_1}{L^2} \left(n^2 + \frac{k_1 L^4}{n^2 \pi^4 B_1} \right) \tag{4.2}$$

where "n" is determined from

$$\frac{k_1 L^4}{\pi^4 B_1} = n^2 (n + 1)^2 \tag{4.3}$$

Substituting (4.2) into (4.1)

$$f_1 = \frac{\pi^2 n^2 k_1 a_n\, PL^2}{\pi^4 n^4 B_1 + k_1 L^4 - \pi^2 n^2 PL^2} \tag{4.4}$$

A detailed discussion of this case and other cases where the elastic brace is applied at several discreet points along the column will be found in references (1) and (10), and therefore not discussed here.

CASE V—Bisymmetrical I-beam with equal end moments and a fixed lateral point support applied at any elevation at the mid-span.

Refer to figure 5. The differential equations of equilibrium of lateral bending and twist respectively are as follows. These equations are consistent in form, limitation, and sign convention with those of Timoshenko.(2)

Between $z = 0$ and $z = L/2$

$$B_1 \frac{d^2u_1}{dz^2} = (\beta_0 + \beta_1)^m - \frac{F}{2} z$$

$$C \frac{d^2\beta_1}{dz^2} - C_w \frac{d^3\beta_1}{dz^3} = - M\left(\frac{du_0}{dz} + \frac{du_1}{dz}\right) + \frac{Fh}{2}$$

Between $z = L/2$ and $z = L$

$$B_1 \frac{d^2u_2}{dz^2} = (\beta_0 + \beta_2)\, M - \frac{Fz}{2} + F\left(z - \frac{L}{2}\right)$$

$$C \frac{d\beta_2}{dz} - C_w \frac{d^3\beta_2}{dz^3} = - M\left(\frac{du_0}{dz} + \frac{du_2}{dz}\right) + \frac{Fh}{2} - Fh$$

where C = Torsional Rigidity

C_w = Warping stiffness $\dfrac{B_1 h_t^2}{4}$

β_0 = Initial twist angle = $b \sin \dfrac{\pi z}{L}$

u_0 = Initial lateral displacement = $- a \sin \dfrac{\pi z}{L}$

Boundary and continuity conditions are as follows:

at $z = 0$, $u_1 = 0$, $\beta_1 = 0$, $\dfrac{d^2u_1}{dz^2} = 0$

at $z = L/2$, $u_1 = u_2$, $\beta_1 = \beta_2$, $\dfrac{du_1}{dz} = \dfrac{du_2}{dz}$, $u_1 = h\beta_1$

at $z = L$, $u_2 = 0$, $\beta_2 = 0$, $\dfrac{d^2u_2}{dz^2} = 0$

The solution of this set of differential equations yields the following:

$$F = \frac{4aM^2L^2 - 4k_2M(hML^2 + CL^2 + \pi^2C_w)}{L^2(2k_3 \tan \frac{\alpha L}{2} + MhL + CL)} \tag{5.1}$$

where

$$k_2 = \frac{M^2bL^4 + Ma\pi^4B_1L^2}{\pi^4B_1C_w + C\pi^2B_1L^2 - M^2L^4}$$

$$k_3 = \frac{Mh\alpha^2C_w - C\alpha^2C_w + h^2M^2 - C^2}{\alpha\,(C + \alpha^2C_w)}$$

$$\alpha = \left\{\frac{1}{2}\left[\left(\frac{C}{C_w}\right)^2 + \frac{4M^2}{B_1C_w}\right]^{1/2} - \frac{C}{2C_w}\right\}^{1/2}$$

Expression (5.1) may be simplified to some extent by assuming no initial twist (b = 0), a buckling mode of two half waves ($\alpha = \frac{2\pi}{L}$), the lateral brace at the compression flange ($h = +\frac{h_t}{2}$), the maximum crookedness as allowed by AISC specifications (a = L/1000), for steel (E = 30 x 10^6 psi), and for the maximum buckling moment

$$M_{(cr.)} = \frac{2\pi}{L^2}\left[B_1(4\pi^2 C_w + CL^2)\right]^{1/2}$$

For these conditions

$$F_{max} = \frac{153 \times 10^6 h_t^2 I_y^2}{L^2}\left(\frac{30.8 I_y h_t^2 + KL^2}{1520 I_y^2 h_t^3 + 55.2 I_y KL^2 h_t^2 + K^2 L^4}\right) \qquad (5.2)$$

where K is the torsional constant involved in the torsional rigidity $C = \frac{KE}{2(1+m)}$ and m is Poisson's ratio. K for most rolled sections may be found in reference (5).

CASE VI—I-beam with equal end moments and a continuous fixed lateral support at any constant elevation along the entire beam.

Refer to figure 6. Using the same coordinate system and notation as in Case V, the differential equations of lateral bending and twist respectively are as follows:

$$B_1 \frac{d^2u_1}{dz^2} = (\beta_0 + \beta_1) M + \int_0^z f\,(z - \zeta)\,d\zeta - z\int_0^{\frac{L}{2}} f\,d\zeta$$

$$C\frac{d\beta_1}{dz} - C_w \frac{d^3\beta_1}{dz^3} = -M\left(\frac{du_0}{dz} + \frac{du_1}{dz}\right) + h\int_0^{\frac{L}{2}} f\,d\zeta - h\int_0^z f\,d\zeta$$

where ζ is an auxiliary variable representing z.
Assuming u_0, β_0, and the boundary conditions the same as in Case V except that $u_1 = h\beta_1$ for all values of z, the solution of this set of differential-integral equations is as follows:

$$f = \frac{\pi^2 M^2 aL^2 + \pi^4 MahB_1 = \pi^4 MbCw + \pi^2 MbCL^2 + \pi^2 M^2 bhL^2}{\pi^2 C_w L^2 + CL^4 + \pi^2 h^2 B_1 L^2 + 2MhL^4} \sin\frac{\pi z}{L} \qquad (6.1)$$

To maximize and reduce (6.1) consider as in Case V, b = 0, $h = +\frac{h_t}{2}$, a = 1/1000, E = 30 x 10^6 psi. Since for continuous rigid bracing on the compression side of the centroid of the section, the beam will not buckle (assuming the support strength adequate) the maximum moment may be taken as the yield strength of the material times the section modulus of the beam (assumed as $33{,}000 \times \frac{2I_x}{h_t}$)

$$f_{1\,max} = \frac{660\, I_y}{h_t^2 L}\left(\frac{22{,}700\, I_x h_t^2 + I_y L^2}{2270\, I_y h_t^2 + 192KL^2 + I_x L^2}\right) \qquad (6.2)$$

CASE VII—I-beam with equal end moments and an elastic point support against lateral movement applied at the center.

Refer to figure 7. For initially crooked beams with no lateral restraint, H. Nylander [3] has demonstrated that the initial crookedness is amplified by the factor $\frac{1}{1-\mu_1}$ where $\mu_1 = \frac{M}{M(critical)}$

Thus $u_c\ (z = \frac{L}{2}) = a\ \frac{\mu_1}{1 - \mu_1}$

By analogy with elastically braced columns, as in Case III, the lateral force at the support

$$F = k_1\, a\, \frac{\mu_1}{1 - \mu_1} \tag{7.1}$$

It is thus only necessary to obtain the critical buckling moment, which will be done by the Rayleigh-Ritz energy method.

This is expressed as $\partial (U-W) = 0$ (7.2)

where "U" is the internal strain energy and

"W" is the external work

The energy expressions may be found in Reference (4) as

$$U = \frac{\beta_1}{2} \int_0^L \left(\frac{d^2u_1}{dz^2}\right)^2 dz + \frac{C_w}{2} \int_0^L \left(\frac{d^2\beta_1}{dz^2}\right)^2 dz + \frac{C}{2} \int_0^L \left(\frac{d\beta_1}{dz}\right)^2 dz$$

which represents the sum of the lateral bending, warping, and twisting energies respectively.

$$W = 2M\phi - \frac{k_1 u_c^2}{2}$$

where ϕ is the rotation of the end sections.

The quantity u_1 will be taken as $\sum_{n=1,3,5}^{\infty} a_n \sin \frac{n\pi z}{L}$ and β_1 may be determined from the equilibrium equation

$$\frac{d^2u_1}{dz^2} = \frac{\beta_1 M}{B_1} + \frac{k_1 u_c z}{2}$$

Thus $\beta_1 = -\frac{\pi^2 B_1}{L^2 M} \sum_{n=1,3,5}^{\infty} n^2 a_n \sin \frac{n\pi z}{L} - \frac{k_1 z}{2M} \sum_{n=1,3,5}^{\infty} a_n \sin \frac{n\pi}{2}$ (7.3)

Utilizing these basic relations, the equation (7.2) reduces to the form,

$$1 = \sum_{n=1,3,5}^{\infty} \frac{4k_1 L^7 M^2_{(cr.)} + C\, k_1^2\, L_8}{2\pi^4 B_1 n^4 L^4 M^2_{(cr.)} - 2\pi^8 C_w B_1^2 n^8 - 2\pi^6 C B_1^2 n^6 L^2}$$

Due to the presence of the high powers of "n" in the denominator, this is a very rapidly converging series with the second term about 5% the first.

Thus taking only the first term to obtain a working value,

$$M_{(cr.)} = \left[\frac{2\pi^8 C_w B_1^2 + 2\pi^6 C L^2 B_1^2 + C L^8 k_1^2}{2L^4(\pi^4 B_1 + 2L^3 k_1)}\right]^{1/2} \tag{7.4}$$

Thus $$F \simeq k_1 a \frac{\frac{M}{M_{(cr.)}}}{1 - \frac{M}{M_{(cr.)}}} = k_1 a \frac{M}{M_{(cr.)} - M} \qquad (7.5)$$

where $M_{(cr.)}$ may be obtained from (7.3).

As in Case III, there is a limiting value of k_1 for which expression (7.5) is no longer applicable. This limiting value represents the critical value of the spring constant at which the beam configuration changes from one half wave to two half waves. To obtain this value, equate the critical moment as from (7.3) or (7.4) to $M_{(cr.)} = \frac{2\pi}{L^2}\left[B_1(4\pi^2 C_w + CL^2)\right]^{1/2}$ which is the buckling moment of a laterally unsupported beam of half the original length.

As trial computations for standard building frames will show, the spring constant for ordinary construction generally exceeds this critical value, so that the results of this case do not have great practical application.

For the more numerous cases in which the spring constant exceeds this critical value, an approximate analysis as used in connection with Case III can be made.

The result is $F_{max} = a \frac{\psi_1}{1 - \frac{\psi_1}{k_1}}$ where

$$\psi_1 = \frac{1024\pi^6 B_1 C_w^2 + 256\pi^4 B_1 C_w C L^2}{15\pi^2 C_w C L^5 + 3C^2 L^7}$$

CASE VIII—I-beam with equal end moments and a continuous elastic line support against lateral moment applied along the entire length of beam.

Refer to figure 8. The basic approach used here is the same as in Case VII, with the maximum lateral force per unit length.

$$f_1 = k_1 a_n \frac{\mu_1}{1 - \mu_1} \qquad (8.1)$$

The critical moment will again be found by use of the energy method. Assume

$$u_1 = \sum_{n=1,2,3}^{\infty} a_n \sin \frac{n\pi z}{L}$$

The quantity β_1 is found from equilibrium to be

$$\sum_{n=1,2,3}^{\infty} \left(\frac{k_1 L^2}{\pi^2 M_n^2} - \frac{\pi^2 B_1 n^2}{L^2 M} \right) a_n \sin \frac{n\pi z}{L}$$

The resulting expression for the critical buckling moment in this case is in closed form

$$M_{(cr.)} = (\pi^4 B_1 n^4 + k_1 L^4) \left[\frac{\pi^2 C_w n^2 + CL^2}{\pi^6 B_1 n^6 L^4 + 3\pi^2 n^2 L^8 k_1} \right]^{1/2} \qquad (8.2)$$

The general method of determining "n", the number of half waves into which the beam buckles, is to set

$$M_{(cr.)}(\text{for } m = n) = M_{(cr.)}(\text{for } n = n + 1)$$

This relation represents the transition from one buckling mode to another and enables one to determine k_1 at which the transition will occur. A direct solution leads to a very high order algebraic equation, and it is thus suggested that the easiest way of determining this critical value of k_1 is by a numerical method.

Thus from (8.1), $$f_1 = k_1 a_n \frac{M}{M_{(cr.)} - M} \qquad (8.3)$$

where $M_{(cr.)}$ may be obtained from (8.2).

Numerical Examples

Although simplified expressions for the maximum lateral force have been determined for the several typical cases, they still lack the unity required for specification or design purposes. Except for the crookedness factor "a", there appear to be no obvious basic parameters relating columns and beams with fixed and flexible supports. A sample numerical analysis is thus presented in Table 1 to show that some overall relation does appear possible. For this example a 10WF33 steel beam, twenty feet long, with an initial crookedness of 1/1000 is selected as a basis of comparison. In most cases, the load or moment used is the critical buckling value. The buckling value is taken as an upper limit, even though yielding may take place at a lower value. These computations seem to strongly indicate that the maximum lateral force is a relatively small value, generally falling within an upper limit of about 2% of the applied load on columns, or the compression flange force on beams. The only exceptions are beams where the bracing is at the centroid of the section, rather than at the compression flange. It is intuitively obvious (and it can also be shown by theory) that beam bracing is most effective when applied on the compression side of the beam.

It can also be shown that if a brace is applied at $h = -\frac{1}{\pi\sqrt{B_1}}\left[\pi^2 C_w + CL^2\right]^{1/2}$ (the lateral rotational axis of the beam) the brace is completely ineffective.

There are some test results which give a further indication regarding the magnitude of the lateral bracing force. In 1942 a series of column tests on light gage steel sections were performed at Cornell University in connection with elastic wall bracing.(1) The results are in very good agreement with the theory as discussed in Case III and IV.

Unfortunately, no test information on the lateral bracing forces for bi-symmetrical beams seems to be available at the present time.

Although Cases I, III, V, and VII considered in this paper deal only with a single brace at the center of the column or beam, it may be deduced that a column or beam supported by more than one brace will induce into each brace a lateral force of about 2% of the total applied load or compression flange force.

As an example, consider a column with three evenly spaced immovable supports as in Fig. 9. It is obvious from the figure that since each segment AC and CE represent Case I, for design purposes the force on each brace

may also be taken as 2% of "P". Note that the support forces may act in either direction perpendicular to the buckling axis of the column, dependent on the direction of the initial crookedness.

Several other numerical examples of common elastic building frames have been analyzed, although not presented here as the details are not too vital. However, the conclusions in each case show that the equivalent elastic spring stiffness is greatly in excess of that required to serve as effective bracing. The limitation as to the use of elastic bracing seems to be in the development of excessive stress and deflections in these bracings.(11)

This paper has thus far dealt only with the cases of lateral supports positioned between the ends of the member. It is perhaps unnecessary to point out that these "interior" support forces create lateral forces (also torques in the case of beams) at the ends of the members. However, once the values of the interior forces are known, the values at the end may be determined by simple statics.

Lateral forces may be exerted at the ends of members even if no interior supports or support forces are present. Such end forces would be present if the member were erected out of plumb or if the load were eccentric, or if the end support were elastic. Consider as an example Fig. 10, a column erected out of plumb and/or with an eccentric load (whose combined eccentricity is represented by δ_0), and with either a pinned or elastic end support.

From equilibrium of moments, $P(\delta_0 + \delta) - FL = 0$

Thus
$$F = \frac{Pk_1\delta_0}{k_1L - P} \qquad (9.1)$$

For pinned end, $k_1 = \infty$, so $F = \frac{P\delta_0}{L}$

The AISC specifications allow a maximum value of $\frac{\delta_0}{L} = \frac{1}{500}$. Thus for immovable ends, $F_{max} = 0.2\%\ P$.

For the general case of elastic support, the minimum value of "k_1" required for stability of the column is determined by setting the denominator of (9.1) equal to zero.

Thus $k_{1min} = \frac{P}{L}$

To limit "δ" to a practical value, consider $k_1 = 3/2\ k_1$ min.
Thus for this case of elastic support $F_{max} = 0.6\%\ P$

It is again seen that the lateral forces on the ends of members are also small. It should be remembered, however, that the lateral forces at the ends due to the effect above may act in conjunction with the lateral end forces due to the "interior" support forces.

CONCLUSIONS

In professional engineering practice, the value of the bracing force is generally assumed as 2% of the applied load for axially compressed columns, and as 2% of the compression flange force for beams (references (7), (8), (9)). No structure designed by this rule has to the writer's knowledge been known to fail; and nothing in this paper seems to negate the usefulness of such a rule. On the contrary, the theoretical analysis strongly seems to support it. However, before final acceptance of this rule as a specification, it may be

desirable to investigate numerically many more cases than described in this paper; and also by full scale tests to validate the results here presented, and to define the limits of applicability to certain borderline cases such as light gage beams, trusses, or open web joists.

ACKNOWLEDGMENT

The writer wishes to acknowledge the cooperation of Dr. G. Winter and Professor P. Bijlaard of the Structural Engineering Department of Cornell University in conjunction with the development of the author's doctoral dissertation[11] upon which this paper is based.

REFERENCES

1. Winter, Green and Cuykendall, Light Gage Steel Columns in Wall-Braced Panels, Cornell Univ. Engr. Exper. Station Bulletin #35, Part 2, October 1947.
2. S. Timoshenko, Theory of Elastic Stability, McGraw-Hill Book Co.
3. H. Nylander, Torsional and Lateral Buckling of Eccentrically Compressed I and T Columns, Trans. Royal Inst. of Tech., Sweden, 1949.
4. G. Winter, Lateral Stability of Unsymmetrical I Beams and Trusses in Bending, Trans. ASCE, 1943.
5. Bethlehem Steel Company, Torsional Stresses in Structural Beams, Booklet S-57.
6. G. Winter, Strength of Slender Beams, Trans. ASCE, Vol. 109, 1944.
7. C. M. Throop, Suggestions for Safe Lateral Bracing Design, Engr. News Record, Feb. 6, 1947.
8. E. E. Seelye, Data Book for Civil Engineers, Vol. I, pg. 1-72.
9. Detroit Steel Products, Lateral Bracing, Reference Bulletin, Aug. 18, 1953.
10. G. G. Green, Lateral Buckling of Elastically Braced Columns, Ph.D. Thesis, Cornell Univ. 1948.
11. W. Zuk, Lateral Support Forces on Beams and Columns, Ph.D. Thesis, Cornell Univ., Ithaca, N. Y., Feb. 1955.

TABLE 1

Bracing Force Values

Case	"F" as % "P"	Conditions
I	0.53	"P" based on buckling value
II	0.63*	"P" taken same as Case I
III	2.00	"k_1" taken as limiting value. "P" taken as 0.8 P(cr.) to limit deflection to $\frac{L}{200}$
IV	1.80*	"k_1" taken as limiting value. "P" taken as 0.8 P
Case	**"F" as % $\frac{M}{h_t}$**	**Conditions**
V	0.75	Lateral brace at compression flange. "M" based on buckling moment
	2.04	Lateral brace at centroid of cross section. "M" based on buckling moment
VI	0.54**	Lateral brace at compression flange. "M" taken same as Case V
	2.35**	Lateral brace at centroid of section. "M" taken same as Case V
VII	0.82	Lateral brace at centroid. "M" based on 0.8 $M_{(cr.)}$. "k_1" taken as limiting value.
VIII	0.20**	Lateral brace at centroid. "M" based on 0.8$M_{(cr.)}$. "k_1" taken as limiting value.

*$F = \int f \, d \, x$
**$F = \int f \, d \, z$

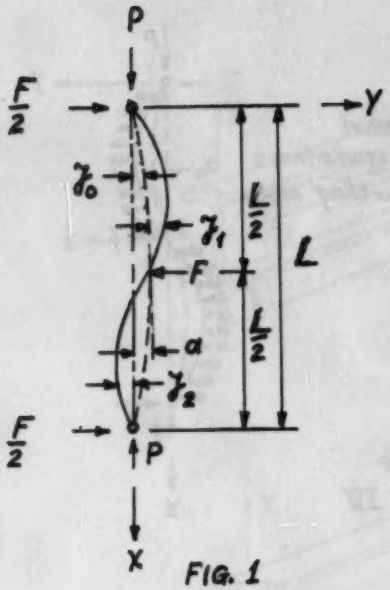

FIG. 1
CASE I

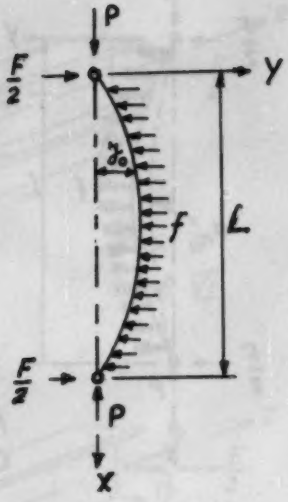

FIG. 2
CASE II

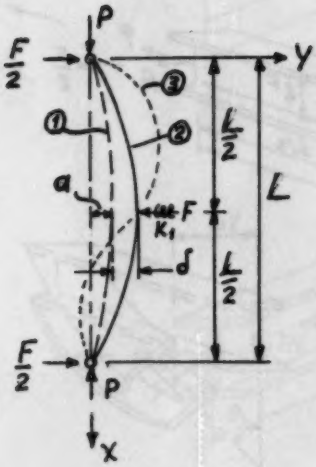

FIG. 3
CASE III

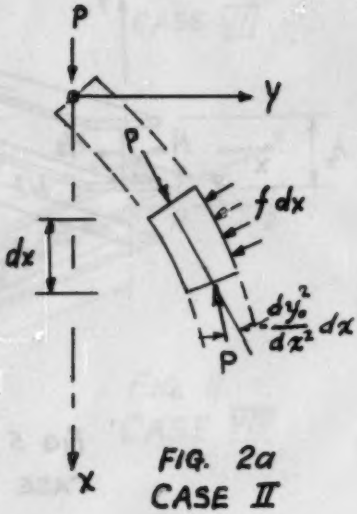

FIG. 2a
CASE II

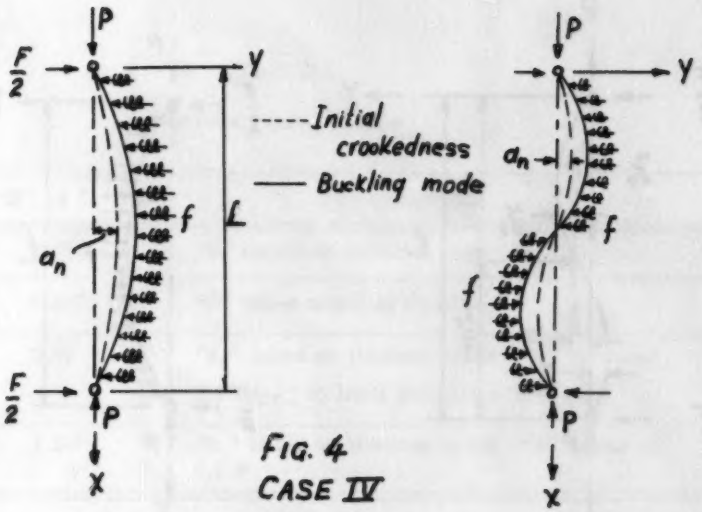

FIG. 4
CASE IV

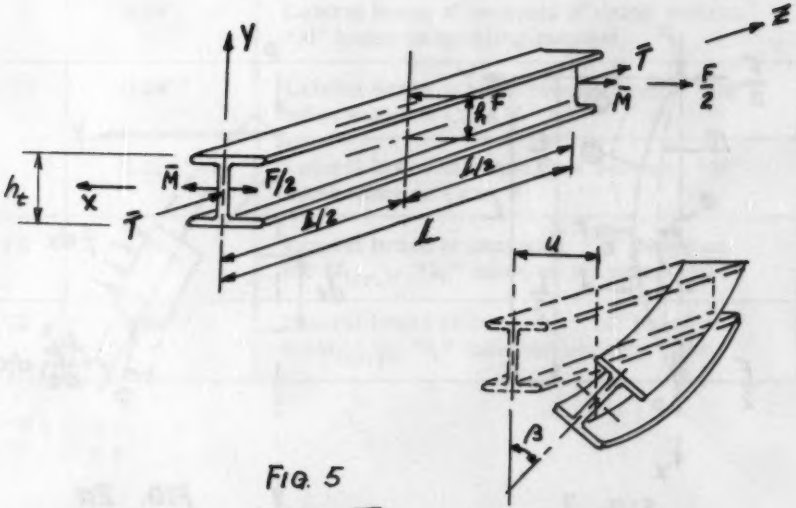

FIG. 5
CASE V

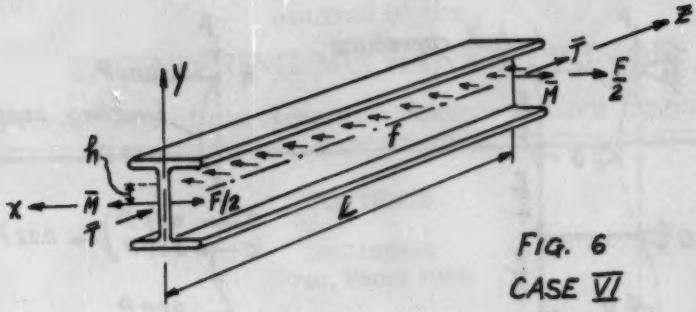

FIG. 6
CASE VI

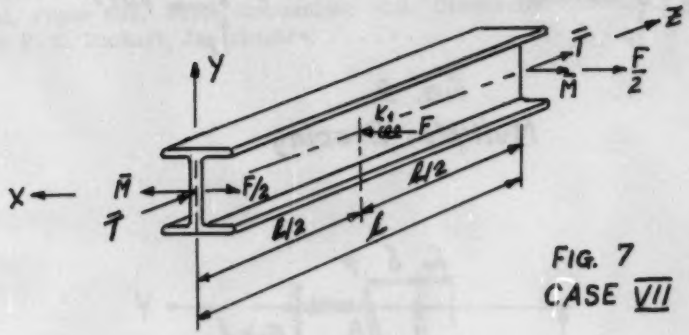

FIG. 7
CASE VII

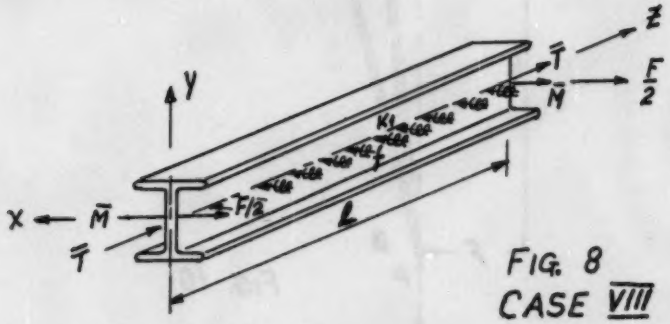

FIG. 8
CASE VIII

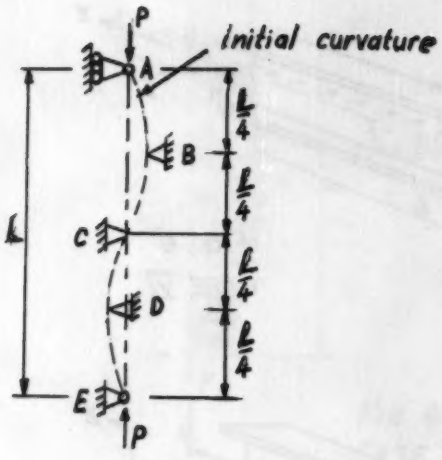

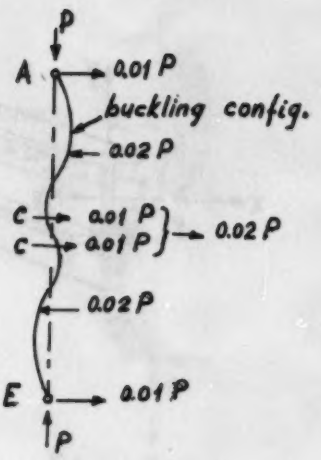

FIG. 9
Multiple Bracing

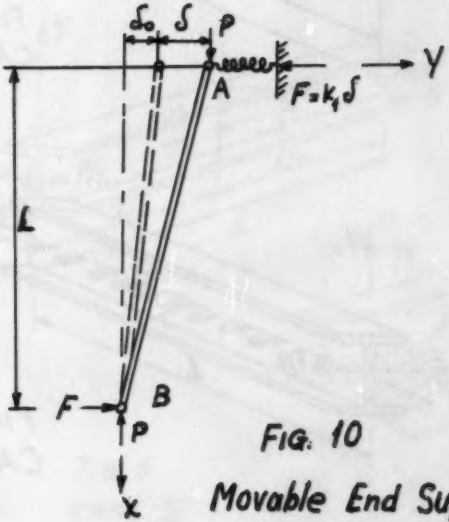

FIG. 10
Movable End Support

Journal of the
ENGINEERING MECHANICS DIVISION
Proceedings of the American Society of Civil Engineers

CONTENTS

DISCUSSION
(Proc. Paper 1033)

Page

Analysis for Sheet Pile Retaining Walls, by F. E. Richart, Jr.
(Proc. Paper 694. Prior discussion: 819. Discussion closed)
by F. E. Richart, Jr. (closure) 1033-3

Note: Paper 1033 is part of the copyrighted Journal of the Engineering Mechanics Division of the American Society of Civil Engineers, Vol. 82, No. EM 3, July, 1956.

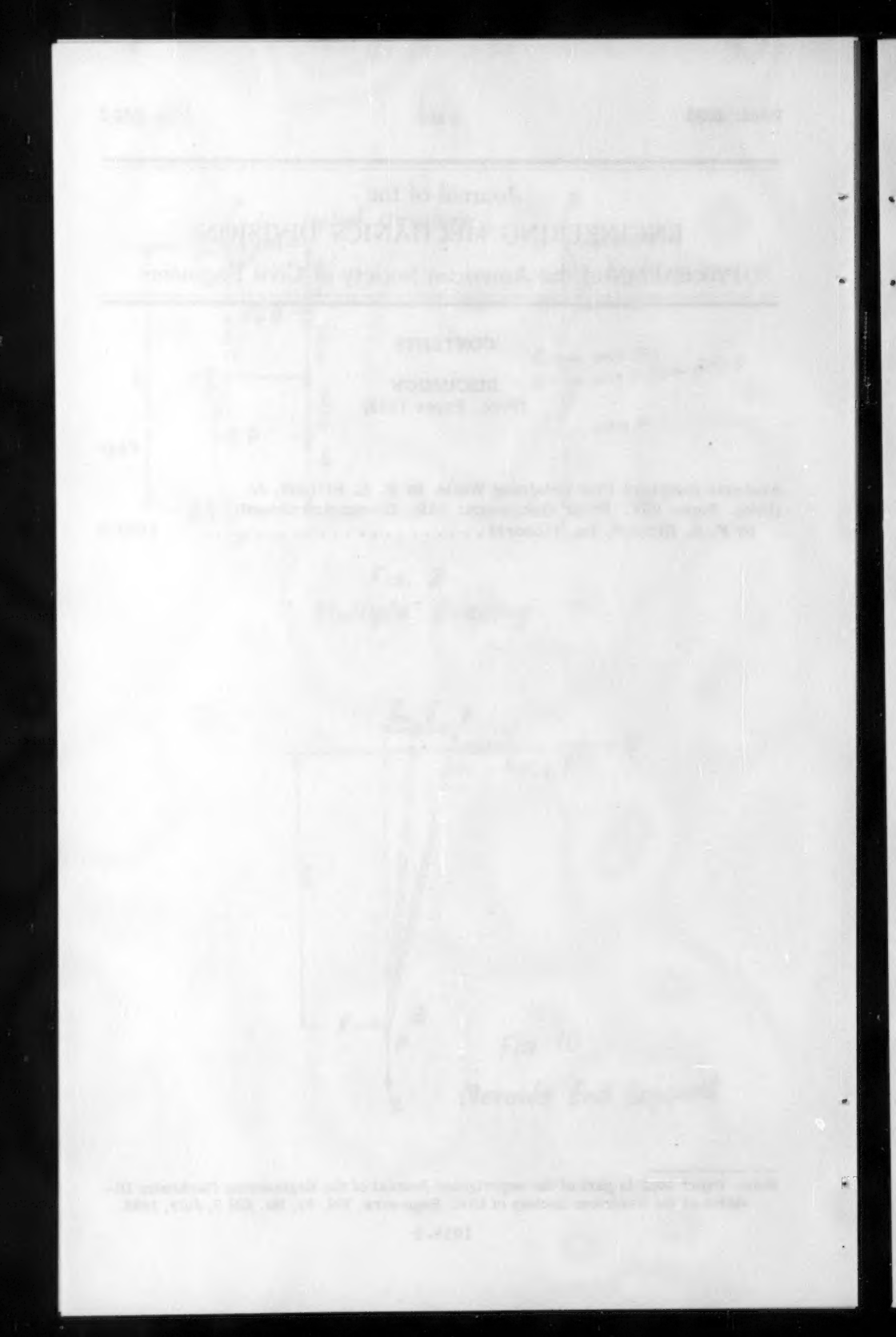

Discussion of "ANALYSIS FOR SHEET PILE RETAINING WALLS"

by F. E. Richart, Jr.
(Proc. Paper 694)

F. E. RICHART, JR.,* A.M. ASCE.—The writer appreciates Mr. Rowe's comments and criticisms and recognizes that he has conducted extensive studies of the behavior of sheet piles. However, his three excellent papers (references 14, 15 and 16) appeared in print during the time interval between the submission of the subject paper (May, 1954) and its publication as ASCE Proceedings Separate No. 694 (May, 1955). Consequently, the writer did not have the benefit of Mr. Rowe's investigations prior to the time the paper was accepted.

Mr. Rowe's tests[3] on model anchored sheet pile walls were made with sand of uniform density below the dredge line and with sand of uniform density (but not necessarily the same as that below the dredge line) or water pressure above the dredge line, as he pointed out in his discussion. Unfortunately, the writer's statement did not make this completely clear, but it was intended to point out that in Mr. Rowe's tests the material above the dredge line was of uniform density. His mathematical analysis of the problem[14] also tied in the loading above the dredge line to the analytical solution for the structural behavior of the wall.

By comparing the maximum bending moment and the tie rod loads obtained from the mathematical analysis with those obtained from the "free earth support" procedure, Mr. Rowe was able to establish curves for use in design. These curves show the "reductions" below the free earth support values for maximum moment and tie rod load which are associated with the soil stiffness modulus and the significant dimensions of the wall installation. Thus his procedure is established as a correction to the values obtained by the free earth support method, and by this consideration he can take care of a layered backfill consisting of several different materials. However, as he has indicated, for conditions in which the sand is stiff with respect to the pile, Mr. Rowe's procedure for the moment reduction would tend to err to low values, which would require that the design procedure include a check on the distribution of soil pressures to determine whether or not they conform to reality.

The procedure described by the writer is based on a mathematical analysis which considers separately the load and structural behavior of the wall above the dredge line from that below the dredge line. By use of the numerical procedure, the load and moment acting on the wall are determined in a continuous manner from the top of the wall to the dredge line. Table IV illustrates this procedure as it applies to Example B (Fig. 10). Thus, the load (V_S) and the bending moment (M_S) due to the soil above the dredge line are given.

---

* Associate Prof. of Civ. Eng., Univ. of Florida, Gainesville, Fla.

16. "A Stress-Strain Theory for Cohesionless Soil With Applications to Earth Pressure at Rest and Moving Walls," By P. W. Rowe, Geotechnique, Vol. 4, No. 2, page 70, June, 1954.

These values are used in the computation by the "free earth support" method and in Table II.

By continuing the computations to a depth of 0.1H below the dredge line, the moment and shear values lead directly to an analysis by the "equivalent beam" method, while a continuation of the computations to a greater depth provides the basis for an analysis by the "elastic line" method. When the computations are extended below the dredge line, it is necessary to include the passive pressure in computing the load on the wall at any depth. Thus by arranging the computations in the form indicated in Table IV, one sheet pile installation may be analyzed by several of the conventional procedures with only a small amount of work beyond that needed to determine the load due to the backfill and surcharge.

The value "C" was chosen by the writer to represent the value of the coefficient of subgrade reaction at the depth, D, to which the pile extends below the dredge line. This is a convenient point at which to identify the mechanical behavior of the soil in the neighborhood of a sheet pile installation. It was not the intent of the paper to include rules or procedures for establishing numerical values for the soil stiffness quantities, but rather to investigate analytically the importance of variations in this parameter upon the structural behavior of a sheet pile wall.

In the conclusion it was emphasized that as more reliable values of the soil properties become available, they should be adopted. Professor K. Terzaghi[17] has recently contributed an outstanding study of the coefficients of subgrade reaction and has established numerical values which may be used for design. For sheet piles he has designated as 1_h (tons/ft.^{3}) the constant of horizontal subgrade reaction with free earth support, depth of sheet pile penetration D (value for $\frac{z}{D} = 1$). The term 1_h may be substituted directly for m (soil stiffness modulus) in Mr. Rowe's analysis, or for C (coefficient of compressibility) in the subject paper. The writer agrees that the terminology used to define C could be confusing and that either of the other two is preferable.

The use of the procedure described by Eq. (19), implies that the soil behavior is not significantly affected by the movement of the wall. This is approximately true only if the soil is stiff with respect to the flexibility of the pile. In such cases the degree of fixity at the dredge line (which permits the moment reduction) depends to a lesser degree on the depth of penetration than upon the relative stiffnesses of pile and subsoil, as was pointed out by Mr. Rowe.

If the pile has a small depth of penetration and has a flexural rigidity which is very large with respect to the stiffness of the subsoil, then the depth of penetration has an important effect upon the subsoil stiffness. For this case, the value of the constant, 1_h, is equal to the soil stiffness at the tip of the pile. Thus at a given depth below the dredge level the resistance offered by the soil, as a result of a unit horizontal displacement, varies inversely as the total depth of pile penetration. The use of this concept for conditions in which the pile is less than infinitely stiff with respect to the subsoil will lead to a conservative design, that is, computed bending moments larger than those which actually occur.

17. "Evaluation of Coefficients of Subgrade Reaction," by K. Terzaghi, Geotechnique, Vol. V, No. 4, December, 1955, pages 297-326.

The numerical values of 1_h given by Professor Terzaghi[17] are considerably lower than the values of m indicated by Mr. Rowe in Table III. For dense sands, log 1_h = 4.60 for dry or moist sand, and log 1_h = 4.41 for submerged sand as contrasted to log m = 6.10 as given in Table III. Since numerical values for subsoil stiffnesses are being established for design purposes at the present time, it is suggested that reference 17 and the accompanying discussions, as well as references 14 and 16, be used for the selection of the appropriate soil stiffness modulus to be used in the analysis of sheet pile walls.

After the soil constant has been established, its value may be used in place of the symbol C in the equations and graphs included in the subject paper during the analysis of a sheet pile installation which was designed on the basis of the "free earth support" or "equivalent beam method." If only the maximum bending moment in the wall, and the tie rod load are desired, then very likely Mr. Rowe's design curves would involve less effort in obtaining these values. However, for a more detailed analysis of a given installation, the writer feels that it is logical to consider the behavior of the wall above and below the dredge line, separately, and that the diagrams included in the paper should be of appreciable value in studying the structural behavior of the embedded pile length.

TABLE IV. - NUMERICAL COMPUTATION FOR MOMENT, SHEAR AND DEFLECTION

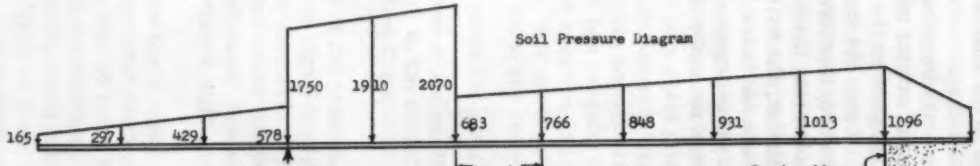

															Common Terms	Units
Elevation		+12	+8	+4	0	-4	-8	-12	-16	-20	-24	-28	-32			ft.
Pressure	= p	-165	-297	-429	-578	-1750	-1910	-2070	-683	-766	-848	-931	-1013	-1096	-429		lb/ft^2
Equivalent Concentrated force	= $\bar{p}$	-627	-1782	-2591	-1585	-5410	-11,460	-6650	-2132	-4595	-5089	-5585	-6079	-3205	-2621	-1954	$\frac{h}{6}$	lb/ft
Shear	= V	(0)	-627	-2409	-5000	-11,995	-23,455	-31,637	-36,232	-41,321	-46,906	-52.985	(-56190) -58810		(-60765)	$\frac{h}{6}$	lb/ft
Moment	= M	0	-627	-3036	-8036	-20,031	-43,486	-75,123	-111,355	-152,676	-199,582	-252,567	-311,377			$\frac{h^2}{6}$	$\frac{ft\,lb}{ft}$ (or, $\frac{in\,lb}{in}$)
	M	0	-1.672	-8.096	-21.43	-53.42	-115.96	-200.33	-296.95	-407.14	-532.22	-673.51	-830.33			1000	in lb/in
Angle Change	$\alpha = \frac{-M}{EI}$	0	1.672	8.096	21.43	53.42	115.96	200.33	296.95	407.14	532.22	673.51	830.33			$\frac{1000}{EI}$	in^{-1}
Concentrated Angle Change	$\bar{\alpha}$	0.768	24.82	104.06	275.02	671.59	1413.35	2416.21	3576.97	4900.57	6402.85	3750.4				$\frac{1000h}{12EI}$	
Slope	= θ		-23536	-23511	-23407	-23130	-22460	-21050	-18630	-15050	-10150	-3750	(0)			$\frac{1000h}{12EI}$	
Deflection	= y				114,220	91090	68630	47580	28950	13900	3750	0				$\frac{1000h^2}{12EI}$	in

At the Dredge Line (EL - 28')

$M_s = 252,570 \frac{h^2}{6} = 673,500$ ft lb/ft

$V_s = 56,190 \frac{h}{6} = 37,460$ lb/ft = 3122 lb/in

For M = 0 at EL - 32', Ap = 25,950 lb/ft

$\left(A_p = \frac{M_{-32}}{32} = \frac{311,377}{32} \times \frac{(4)^2}{6} \right)$

Deflections of the Anchor Point for Cantilever above EL - 28'

$y_s = \frac{114,220\ h^2 \cdot 1000}{12EI} = 30.33$ in. Due to Soil Loads.

$y_{A_p} = \frac{Ap\ l^3}{3EI} = 0.01749$ Ap in. Due to Anchor Pull.

DIVISION ACTIVITIES

ENGINEERING MECHANICS DIVISION

Proceedings of the American Society of Civil Engineers

NEWSLETTER

July, 1956

Though the EMD Newsletter first appeared in December 1954 this issue marks its initial inclusion in the Journal of the Engineering Mechanics Division. It is hoped that this arrangement will prove advantageous by providing a permanent file of news items of interest to the Division.

Since EMD Newsletters must be prepared some five weeks before publication, announcements featuring some future conferences may appear after such meetings are held. Nevertheless, readers will at least learn of their existence and can write for the conference proceedings if they should be interested.

EARTHQUAKE ENGINEERING

A world conference on Earthquake Engineering was held at the University of California in Berkeley from June 12-16, 1956. Thirty-eight papers and two panel discussions were scheduled. The sessions included papers on (1) earthquake ground motions, (2) analysis of structural response to earthquakes, (3) development of aseismic construction throughout the world, (4) earthquake effects on soils and foundations, and (5) design of earthquake resistant structures.

The conference was sponsored by the University of California, the ASCE Structures Division and the Structural Engineers Association of California. Proceedings of the conference may be ordered from the Secretary of the Earthquake Engineering Research Institute, Mr. Karl V. Steinbrugge, Merchants Exchange Building, Room 1039, 465 California Street, San Francisco, California. The cost is $7.00 if ordered before or at the conference and $8.50 thereafter.

NINTH INTERNATIONAL CONGRESS OF APPLIED MECHANICS

The Ninth International Congress of Applied Mechanics will be held at the University of Brussels, Brussels, Belgium from September 5-13, 1956. Brochures of the conference may be obtained from the Secretary of the ASME, 29 West 39th Street, New York 18, New York.

Note: No. 1956-16 is part of the copyrighted Journal of the Engineering Mechanics Division of the American Society of Civil Engineers, Vol. 82, EM 3, July, 1956.

STRUCTURAL ENGINEERING CONFERENCE

The University of Kansas was host to a Structural Engineering Conference on May 3, 1956. Papers presented covered the field of plastic design for structural steel. The American Institute of Steel Construction and local steel fabricators were joint sponsors.

RESEARCH PRIZES

ASCE Research Prizes for 1956 of $100.00 each will be awarded on the recommendation of the ASCE Committee on Research. Nominations are being made by the several divisions of the Society. Prizes are awarded for research accomplished by members of the Society. Not more than five such awards may be made in any one year.

A-BOMB IN INDUSTRY CONFERENCE

A conference on the A-Bomb in Industry was held on November 17, 1955 in Chicago. Some EMD readers may not have known of this meeting and may be interested in obtaining a copy of the proceedings. These may be ordered from the Armour Research Foundation, 10 West 25th Street, Chicago 16, Illinois for $3.00 each. The subjects covered were: "The Need to Prepare" by Dr. R. L. Janes, Assistant Manager, Armour Research Foundation, "Operational Planning to Meet Disaster" by Mr. J. H. Redmond, Manager of Operations, Koppers Company, Inc., "Dispersion—A Vital Prescription for Survival" by Colonel Innis D. Harris, Deputy Assistant Director for Plans in Readiness, Office of Defense Mobilization, "Protecting the Existint Plant" by Mr. R. W. Sauer, Supervisor, Structural Analysis Section, Armour Research Foundation, "A Philosophy for Anti-Blast Structural Design" by Dr. N. M. Newmark, Research Professor of Civil Engineering, University of Illinois, and Mr. Samuel F. Clabaugh, Assistant Professor Military Science, University of Maryland, on "The Economics of Plant Protection."

BIRTHDAY GREETINGS

May 11, 1956 marked the seventy-fifth birthday of Theodore von Karman, member of ASCE since 1932 and an honorary member since 1949. Dr. von Karman is known for his many publications to the fields of aeronautical engineering and mechanics. He was educated at the Technical University of Budapest and the University of Goetingen. He came to the United States in 1930 and has been associated ever since then with the California Institute of Technology as Director of the Aeronautics Laboratory. He has served as consultant to many industries and the U. S. Air Force.

SEMINAR IN STATISTICAL METHODS

A seminar in Statistical Methods in Materials Research was held from June 24-29 at the Pennsylvania State University. The program consisted of a series of lectures by men from cooperating industries and the University who have made important contributions by applying statistical methods to problems in materials research. Information on the seminar may be obtained from Mr. T. Reed Ferguson, Extension Conference Center, The Pennsylvania State University, University Park, Pennsylvania.

EDITORIAL NOTE

A request in the February 1956 EMD Newsletter for information concerning special conferences related to mechanics being held or planned throughout the world met with some success. A few such notices are included in this issue. There must be many more in which EMD members would be interested. It is hoped that more information of this type will be supplied to the editor so that all of our membership will learn of such activities. The next issue goes to press October 15, 1956; information should reach the editor before September 1, 1956.

Dan H. Pletta, Editor

EMD Newsletter

V.P.I.

Blacksburg, Va.